STUDY OF QUASI-OPTICAL CIRCUIT TECHNIQUES IN VARACTOR MULTIPLIERS

by Jesse J. Taub and Gediminas P. Kurpis

Prepared by
CUTLER-HAMMER, INC.
Deer Park, Long Island, N. Y.
for Electronics Research Center

NATIONAL AERONAUTICS AND SPACE ADMINISTRATION • WASHINGTON, D. C. • NOVEMBER 1969

STUDY OF QUASI-OPTICAL CIRCUIT TECHNIQUES IN VARACTOR MULTIPLIERS

By Jesse J. Taub and Gediminas P. Kurpis

Prepared under Contract No. NAS 12-625 by
CUTLER-HAMMER, INC.
Deer Park, Long Island, N.Y.

for Electronics Research Center

NATIONAL AERONAUTICS AND SPACE ADMINISTRATION

For sale by the Clearinghouse for Federal Scientific and Technical Information
Springfield, Virginia 22151 – Price $3.00

TABLE OF CONTENTS

LIST OF ILLUSTRATIONS

STUDY OF QUASI-OPTICAL CIRCUIT TECHNIQUES IN VARACTOR MULTIPLIERS

By Jesse J. Taub and Gediminas P. Kurpis

AIL - a division of CUTLER-HAMMER
Deer Park, New York 11729

SUMMARY

Circuit techniques applicable to quasi-optical multipliers operating at millimeter wavelengths have been studied. Directional filters consisting of iterations of dielectric slabs have been theoretically and experimentally investigated. A theory that is in good agreement with experiment is presented together with a step-by-step design procedure. Three types of tuner circuits to be used as impedance matching devices have been theoretically analyzed for their range of matching and dissipation loss properties. The dissipation loss is low (less than 0.2 db) for all types. A tuner consisting of a variable susceptance with variable position is found to be the best of the types described. The problem of representing quasi-optical varactor mounts by suitable equivalent circuits is considered but its completion must await experimental work to be performed on a future program. The report concludes with a discussion of measurement techniques suitable for quasi-optical components.

INTRODUCTION

Objectives

The objectives of this contract are to study quasi-optical circuit techniques that are applicable to millimeter wavelength varactor multipliers. More specifically, four problem areas have been defined:

1. Directional filters for separation of fundamental and harmonic frequencies

2. Tuners for adjusting the fundamental and harmonic loads to the desired impedance levels
3. Equivalent circuits for quasi-optical varactor mounts
4. Measurement techniques applicable to the development and evaluation of multiplier circuits

The study of these problem areas was performed in accordance with the statement of work given in Appendix A.

Historical Background

The generation of CW millimeter wavelength power with fundamental solid-state oscillators has been limited to several milliwatts. The achievement of 10 mw at 88 GHz (reference 1) with bulk gallium arsenide and 100 mw at 100 GHz with avalanche diodes (reference 2) are representative of the current state of the art of fundamental oscillators. Solid-state oscillators yield output powers that drop at a rate of $(1/f)^2$. Thus, while 1 watt avalanche diode oscillators at 30 GHz are feasible (reference 3), only 250 mw of power is attainable at 60 GHz. If, for example, a 1-watt 30-GHz oscillator drove a frequency doubler having an efficiency higher than 25 percent, more 60-GHz power would be obtained than from a 60-GHz fundamental oscillator.

Recent advances (reference 4) in varactor diode fabrications have resulted in cutoff frequencies in the 800 GHz range with average capacitances of 0.15 pf and selfresonant frequencies of 70 GHz. Assuming no circuit losses, one can achieve doubler efficiencies (reference 5) for a 30-GHz input of 50 percent; tripling 30 GHz would yield an efficiency of 33 percent. Further advances in cutoff frequency to about 1500 GHz are possible which will result in efficiencies of 70 and 50 percent, respectively.

Unfortunately, the use of these diodes in standard-size millimeter waveguide results in significant circuit losses. The use of highly oversized (typically ten times larger than standard in each cross-section dimension) waveguide has been used previously to reduce circuit losses at millimeter

and submillimeter wavelengths (references 6 - 9). The dominant TE_{10} mode is preserved in the oversized guide. The effect of loss reduction from that of a standard-sized waveguide at 300 GHz illustrates the degree of loss reduction attainable.

A number of components using oversized waveguide have been previously studied (in varying degrees) using quasi-optical elements such as gratings, prisms, and dielectric plates (slabs); they have been described in references 6 - 9.

These components include:

- Double-prism attenuators or couplers
- Phase shifter using a double prism
- Tuner or impedance transformer using a double prism
- Directional and nondirectional filters using dielectric slabs
- Grating bandpass filters (nondirectional)
- Focused varistor mounts
- Bolometer mounts
- Ferrite isolator using Faraday rotation
- Tapers

This work serves as a good background because multiplier circuits contain some of these components. For example, a multiplier circuit using quasi-optical techniques would have the block diagram shown in Figure 1. The diplexing filter function is fulfilled by the directional filter and the varactor mount design is aided by the earlier work on focused varistor mounts. No previous tuner or measurement technique work had been performed.

General Considerations

The nature of the tasks as outlined in the statement of work were such that a detailed theoretical treatment of directional filters and tuners is

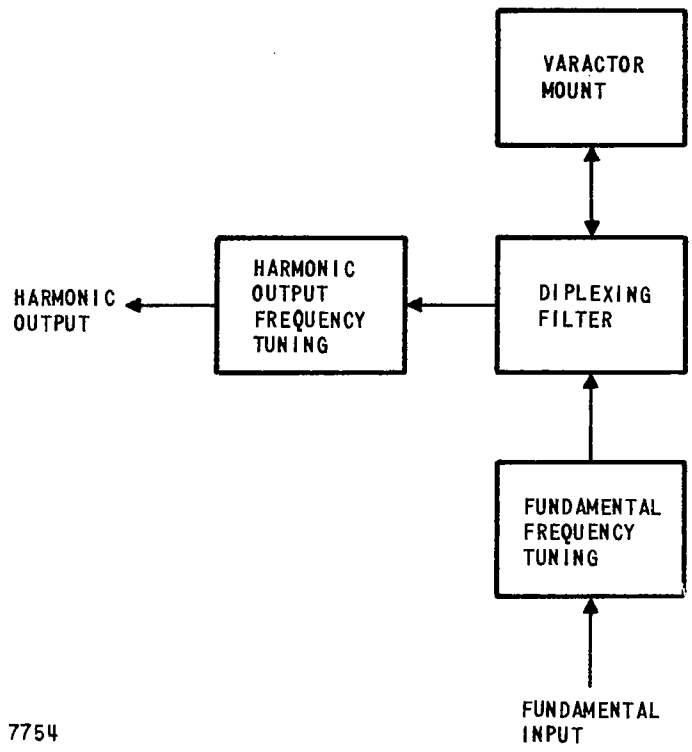

FIGURE 1. BASIC QUASI-OPTICAL MULTIPLIER BLOCK DIAGRAM

required. The nature of the work on matching and measurement techniques is more of a preliminary nature. The material presented in this report reflects this emphasis. The data given herein on directional filters should be sufficient for design purposes. The analysis of tuners has led to several possible tuner circuits that appear to be feasible. The work on mounts and measurements requires much additional experimental effort that should be performed on future programs.

DIRECTIONAL FILTERS

General

Quasi-optical directional filters can be realized by placing a frequency-sensitive transmission path at an angle θ to the axis of the incident wave; this is shown in Figure 2A. This medium should have an index of refraction n that is a function of x (the distance from the input interface). Such a device can, by properly choosing n(x), be made to have an output with desired passband/stopbands. Power that is not passed is reflected (except for incidental dissipation) to the complementary port. A typical characteristic is shown in Figure 3. This filter is matched at all frequencies and does not couple to the direction marked "isolated output."

In practice, it is easier to realize a varying index of refraction medium in the form of discrete changes created by a series of dielectric slabs separated by an air region. Furthermore, $\theta = 45^{o}$ is convenient because it places the four ports of interest in a cross arrangement. This circuit is shown in Figure 2B. Finally, placing this structure in an oversized rectangular waveguide (Figure 2C) yields the structure that is stressed herein.

Reference 9 developed a theory, based on the impedance concept, for analyzing the behavior of directional filters consisting of iterations of dielectric slabs separated by air sections of equal electrical length. The starting point in this program was to establish the degree of agreement between theory and experiment attainable over a range of frequencies (encompassing a full passband and a full stopband). The theory is then presented and detailed theoretical data is given. These results are used to develop a simple design procedure.

Other designs such as the low ripple and modified equal iteration types are also considered herein.

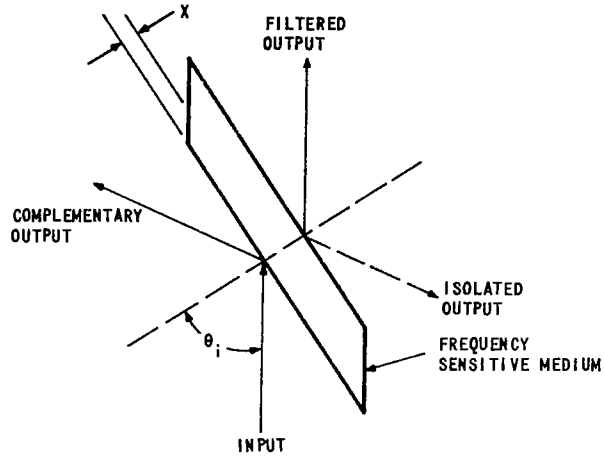

A. GENERAL

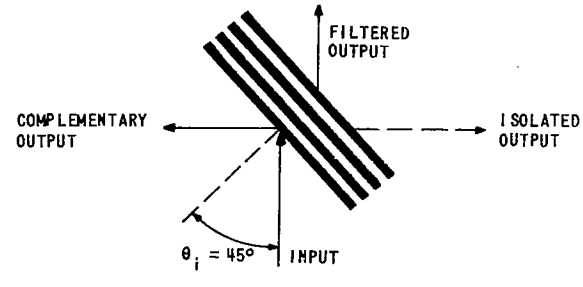

B. DIELECTRIC SLAB-AIR, $\theta_i = 45°$

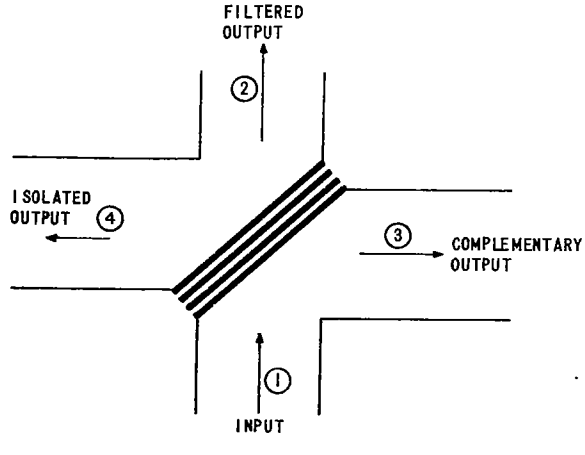

C. DIELECTRIC SLAB-AIR IN OVERSIZE WAVEGUIDE

7755

FIGURE 2. QUASI-OPTICAL DIRECTIONAL FILTERS

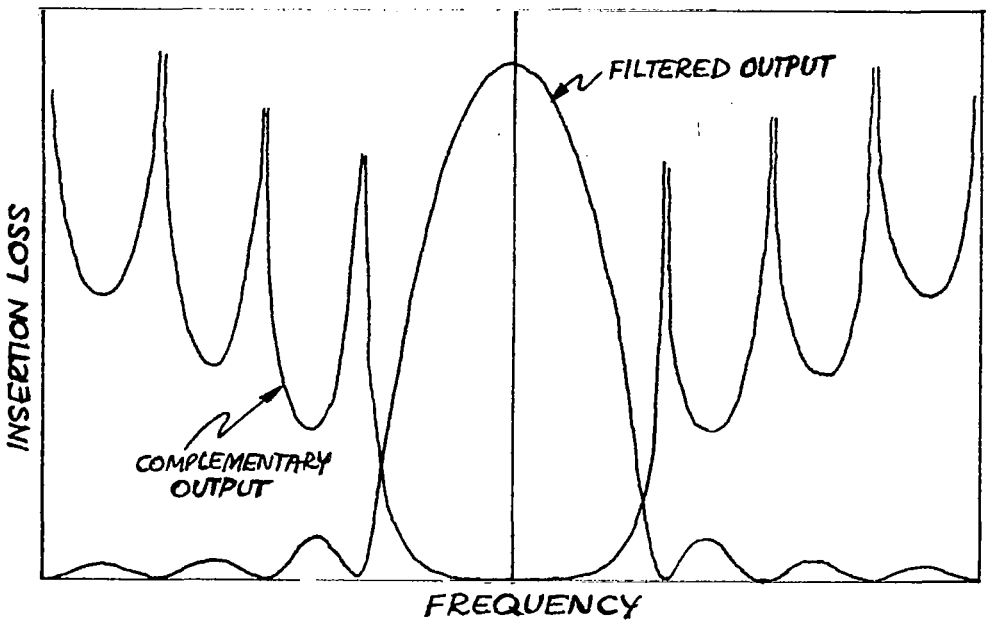

FIGURE 3. RESPONSE OF A TYPICAL DIRECTIONAL FILTER

Experimental Verification

Partial data on a filter consisting of iterations of four quartz slabs separated by uniform air spaces was available from reference 9. This showed the insertion loss versus frequency from 26 to 40 GHz as indicated in Figure 4A. This filter had a maximum measured insertion loss (port 1-port 2) of 28 db at 30 GHz and relatively low loss (2 db) at 40 GHz.

To be used in a frequency doubler this filter must have low loss at the second harmonic (60 GHz). Thus, additional measurements were made on this filter, which are included in Figure 4A. This supplement constitutes insertion loss from 40 - 49 GHz and 56 - 67 GHz. The data indicates that

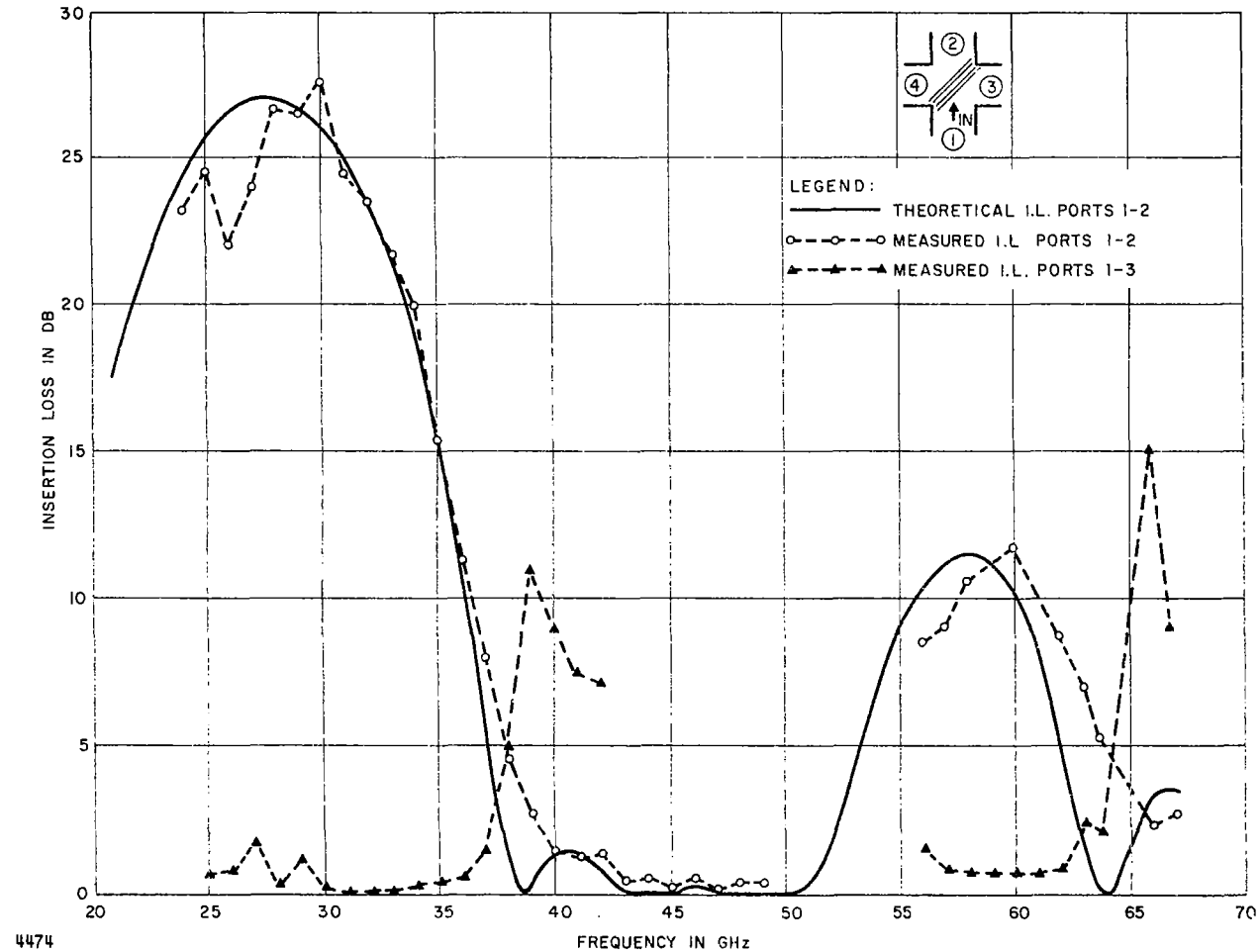

FIGURE 4A. INSERTION LOSS VS FREQUENCY OF A QUARTZ/AIR FOUR-ITERATION DIRECTIONAL FILTER ($\phi_\epsilon = 1.35\phi_0$)

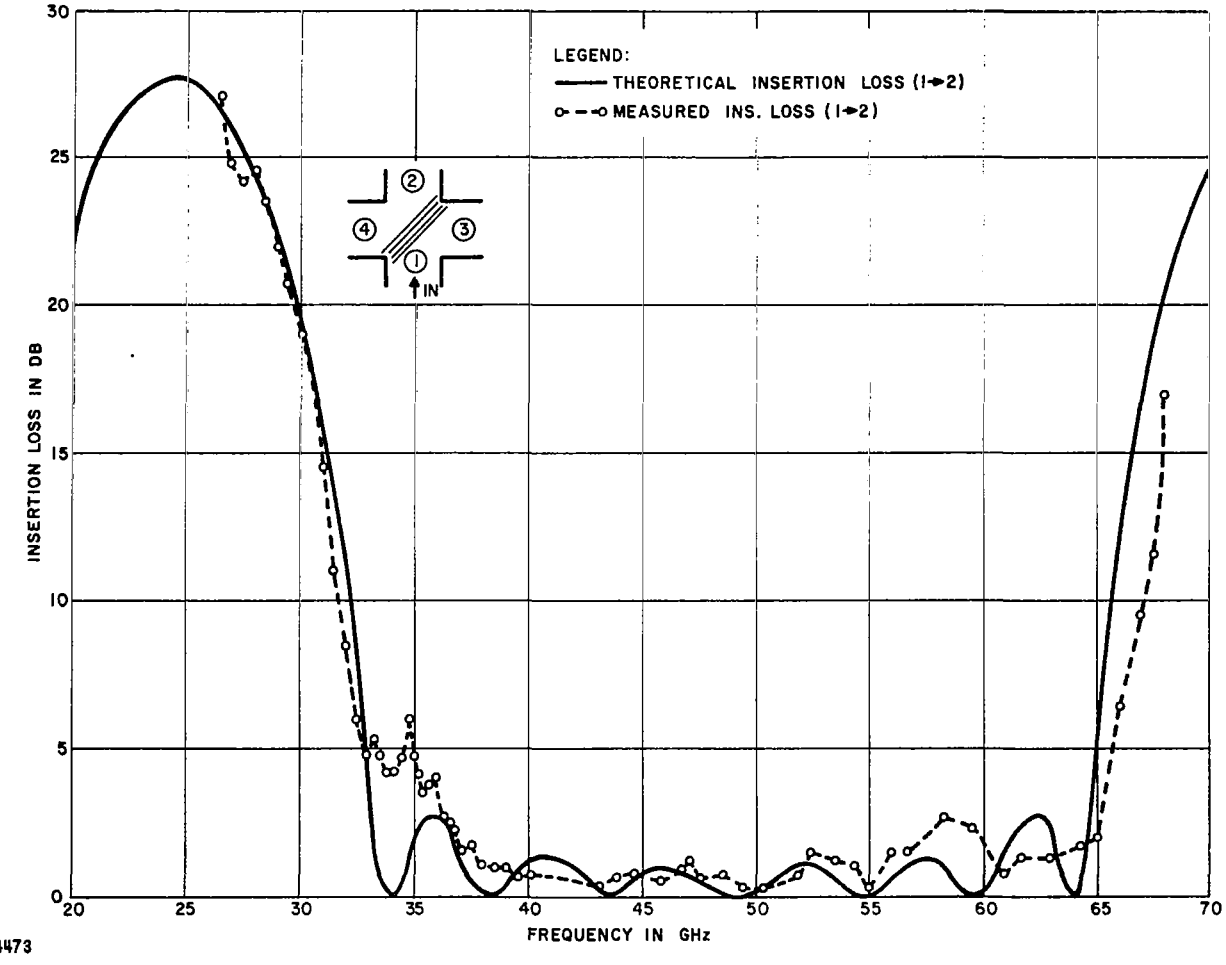

FIGURE 4B. INSERTION LOSS VS FREQUENCY OF A QUARTZ/AIR FOUR-ITERATION DIRECTIONAL FILTER ($\phi_e = \phi_o$)

the reference 9 filter is not useful for a doubler circuit application because of a high 12-db loss at 60 GHz, where low loss had been expected.

The data was particularly disappointing in that there appeared to be a lack of agreement with theory. Further investigation of the drawings for this filter indicated that the quartz slab thicknesses were designed to give maximum rejection ($\lambda/4$) at 24.5 GHz while the air sections were $\lambda/4$ at 33 GHz. This electrical length inequality produced high loss at 60 GHz; as a further check, the theoretical loss curve was computed and found to be in close agreement.

This length error was rectified by choosing the quartz and air spacings to both be $\lambda/4$ at 24.5 GHz, and a new filter was constructed. Its insertion loss versus frequency was measured and compared to the theoretical. Measurements were made from 26 to 68 GHz and the data is given in Figure 4B. The agreement with theory is within 2 db for most of the frequency range; additional measurement error at some frequencies existed because of higher mode excitation due to nonideal tapers.

The data was felt to be in sufficient agreement with the theory given in reference 1 to justify use of the theory in designing directional filters for a variety of responses.

Equal Iteration Filter

Design theory. --For completeness, the theoretical approach used in reference 9 is summarized in Appendix B. The theory computes the insertion loss of iterative layers of dielectric separated by another dielectric (usually air) as indicated in Figure 5; the insertion loss is defined as the ratio of the incident to transmitted power.

The results for the dissipationless case are:

$$L = 10 \log \frac{\left| P_n^2 Y^2 + 4 P_{n-1}^2 - 4 P_n P_{n-1} + P_n^2 X^2 \right|}{4} \text{ dB} \qquad (1)$$

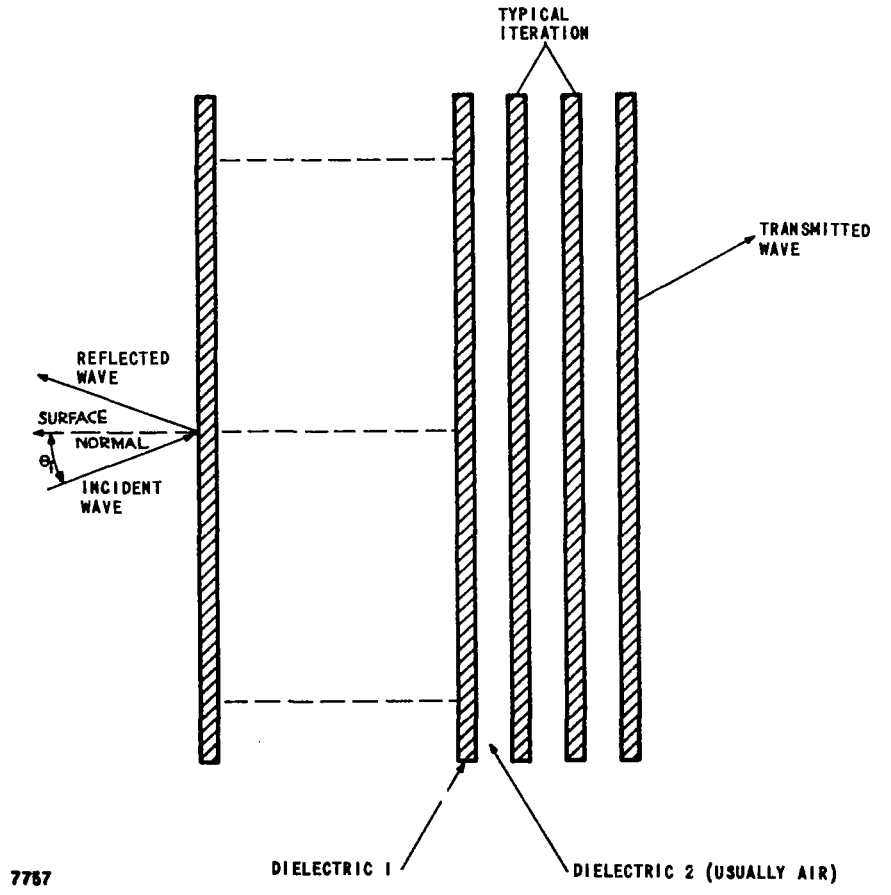

FIGURE 5. ITERATED DIELECTRIC SLABS WITH A LINEARLY POLARIZED WAVE, INCIDENT AT AN ANGLE θ_i, WHOSE ELECTRIC VECTOR IS PERPENDICULAR TO THE PLANE OF INCIDENCE

where

n = the number of iterations

P_n = Tchebycheff polynomial of the second kind (equations for P_n are given in Appendix B)

$$Y = 2\cos^2 \phi - (\sin^2 \phi)(Z + 1/Z) \tag{2}$$

$$X = (1/2 \sin 2\phi)(2 + Z + 1/Z) \tag{3}$$

ϕ = electrical path length of each dielectric slab or air separation (defined in Appendix B)*

Z = the wave impedance (normalized to $\epsilon_r = 1$) of each dielectric medium

$$= \frac{\cos \theta_i}{\left(\epsilon_r - \cos \theta_i\right)^{1/2}} \tag{4}$$

θ_i = angle of incidence (between the axis normal to the first slab surface plane and the direction of propagation)

ϵ_r = relative dielectric constant of each dielectric slab

Substituting the values of P_n from Appendix B gives the insertion loss as a function of electrical length for specific values of n. The results for

$1 \leq n \leq 6$ are:

For n = 1

$$L = 10 \log \frac{|Y^2 + X^2|}{4} \text{ db} \tag{5}$$

---

* In this design ϕ_ϵ (the electrical path length in dielectric) and ϕ_0 (the electrical path length in air) are equal, that is, $\phi_\epsilon = \phi_0 = \phi$.

For n = 2

$$L = 10 \log \frac{|Y^4 - 4Y^2 + X^2Y^2 + 4|}{4} \text{ db} \tag{6}$$

For n = 3

$$L = 10 \log \frac{|(Y^2 - 1)^2 Y^2 + 4Y^2 - 4(Y^2 - 1)Y^2 + (Y^2 - 1)X^2|}{4} \text{ db} \tag{7}$$

For n = 4

$$L = 10 \log \frac{|(Y^3 - 2Y)^2 Y^2 + 4(Y^2 - 1)^2 - 4(Y^3 - 2Y)(Y^3 - Y) + (Y^3 - 2Y)X^2|}{4} \text{ db} \tag{8}$$

For n = 5

$$L = 10 \log \frac{|(Y^4 - 3Y^2 + 1)Y^2 + 4(Y^3 - 2Y)^2 - 4(Y^4 - 3Y^2 + 1)(Y^4 - 2Y^2) + (Y^4 - 3Y^2 + 1)X^2|}{4} \text{ db} \tag{9}$$

For n = 6

$$L = 10 \log \frac{|(Y^5 - 4Y^3 + 3Y)^2 Y^2 + 4(Y^4 - 3Y^2 + 1)^2 - 4(Y^5 - 4Y^3 + 3Y)(Y^5 - 3Y^3 + Y) + (Y^5 - 4Y^3 + 3Y)^2 X^2|}{4} \text{ db} \tag{10}$$

Examination of these results indicates that L is a function of ϕ, ϵ_r, and θ_i. For the oversized waveguide directional filters a most convenient choice is $\theta_i = 45^\circ$. Thus, once θ_i is established, it is possible to compute L versus

ϕ with ϵ_r as a parameter. Curves or tables of these data can serve as tools in the design of directional filters for a variety of desired responses. It has been found that curves are sufficiently accurate and are more convenient to use; thus, the design procedures will be based on the use of curves.

Design considerations. --The insertion loss versus normalized frequency was computed on a GE time-sharing computer using an advanced basic programming language. The insertion loss (from port 1 to port 2) L_{12} versus $f(\phi)$ is plotted for 1 through 6 dielectric slabs in Figures 6 - 11.

Assuming, as theory predicts, perfect isolation between ports 1 and 4, no internal dissipation and no reflections at port 1, the insertion loss at the complementary output port, that is L_{13}, is obtainable from L_{12} by virtue of energy conservation: $P_{in} = P_{12} + P_{13}$ or $P_{in} = |L_{13} + L_{12}|$.

The L_{12} versus f curves in Figures 6 - 11 are obtained for $\theta_i = 45^o$ and $\epsilon_r = 2.5; 4.0; 10.0$, which correspond to Rexolite (or Polystyrene), quartz, and alumina (or beryllia) relative dielectric constants, respectively. The abscissae in the above figures were labeled as normalized frequency f, which is a linear function of $\phi_\epsilon = \phi_o = \phi$; the two are related as $\phi = \frac{\pi}{2}f$. The principal (or the first) insertion loss maximum occurs at $f = 1$ or $\phi = \frac{\pi}{2}$. Insertion loss is an even function about $\phi = \frac{\pi}{2}$ and is periodic within intervals of π in ϕ or 2 in f. The insertion loss peak increases monotonically with increasing ϵ_r. For example, if $n = 4$ and $\epsilon_r = 4$ (quartz slabs), the peak insertion loss is 28 db. Assuming it were used with a varactor connected at port 3, and $f = 1$ ($\phi = \frac{\pi}{2}$) were chosen to coincide with the fundamental frequency, virtually all of the power from port 1 will be coupled to port 3. Second harmonic energy will couple from port 3 to port 4 with almost zero db insertion loss. This is because $L_{34} = L_{12}$ and the second harmonic corresponds to $f = 2$ ($\phi = \pi$) which has the same loss as $\phi = f = 0$.

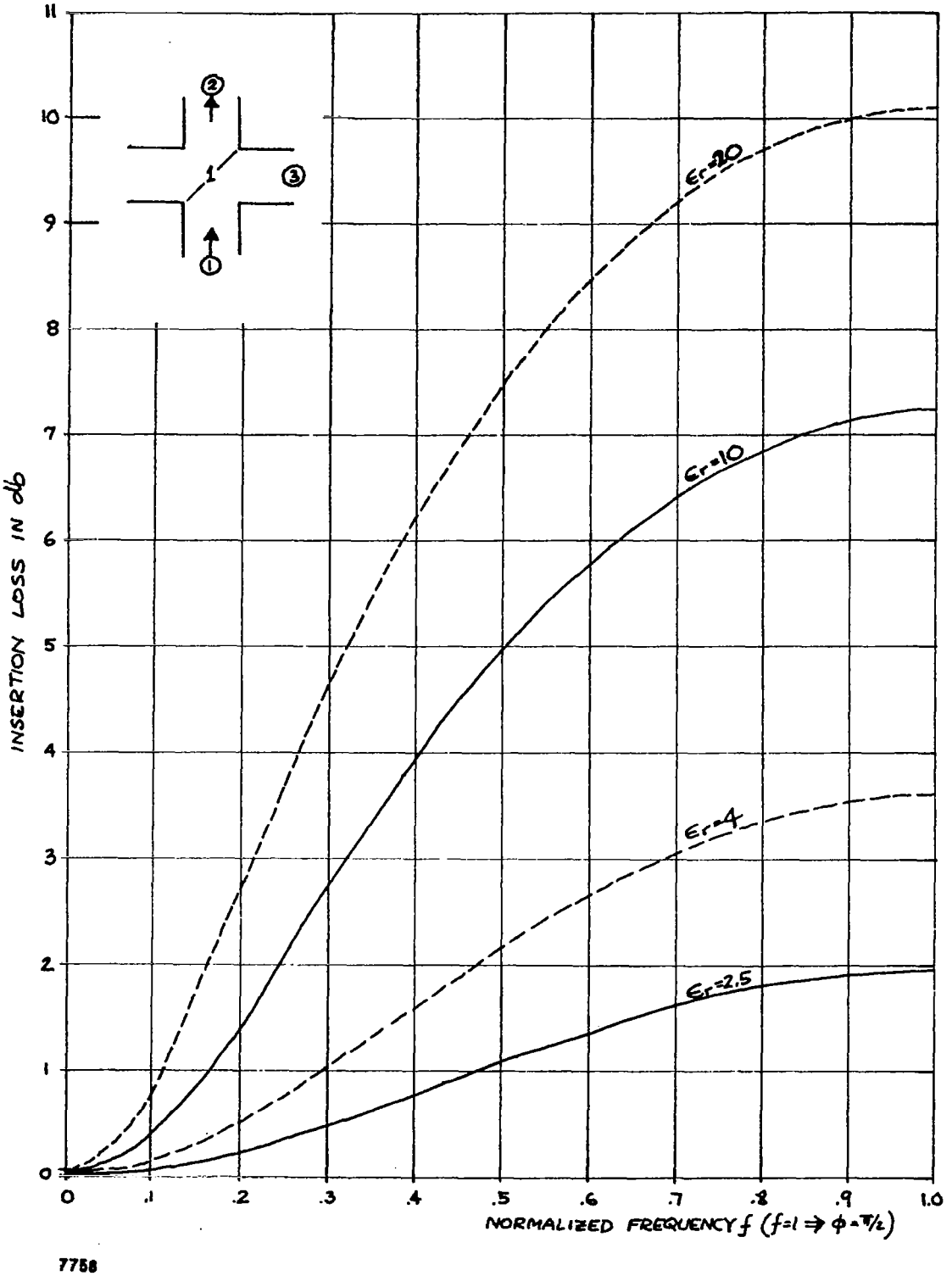

FIGURE 6. CHARACTERISTICS OF n = 1 FILTER

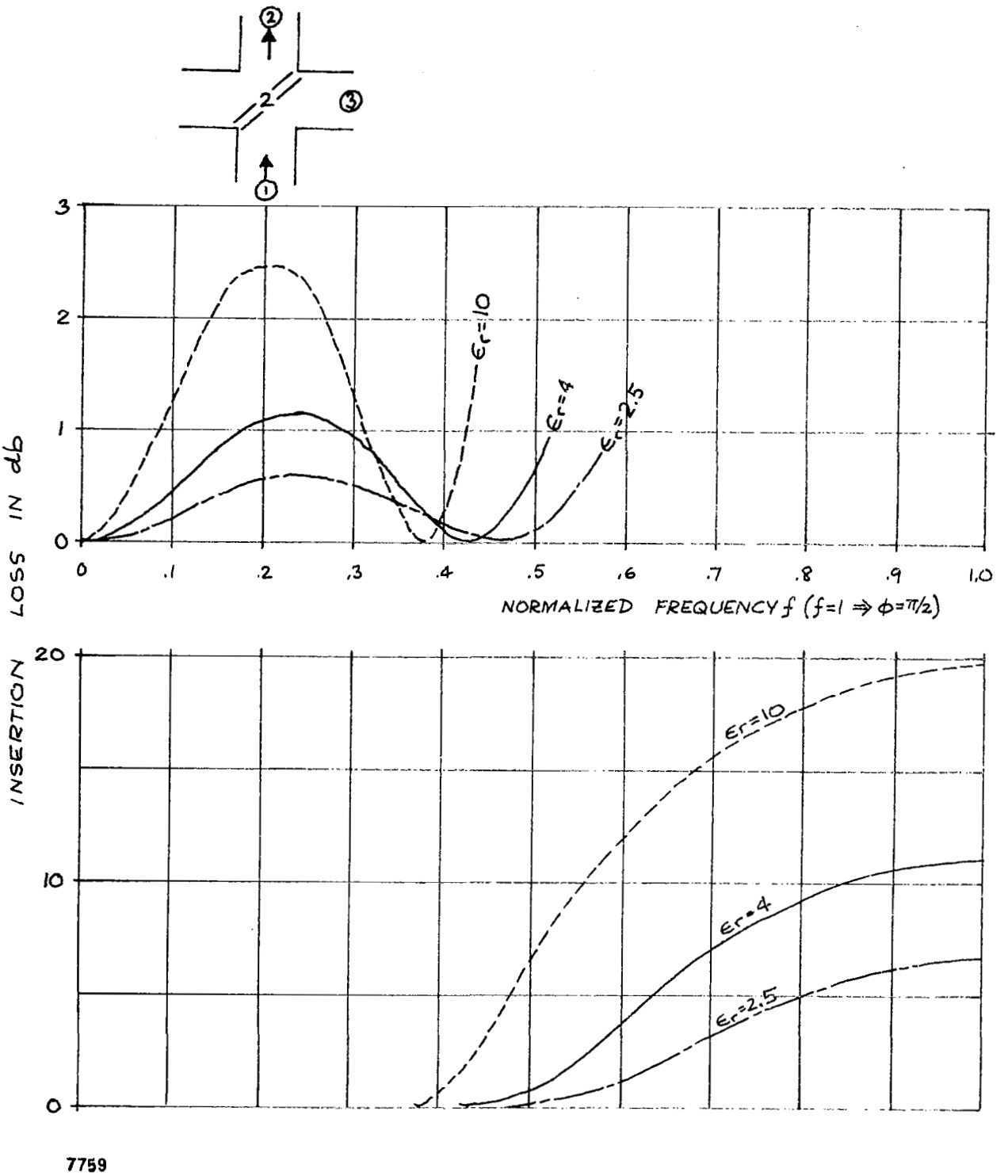

FIGURE 7. PASSBAND AND REJECTION BAND OF n = 2 FILTER

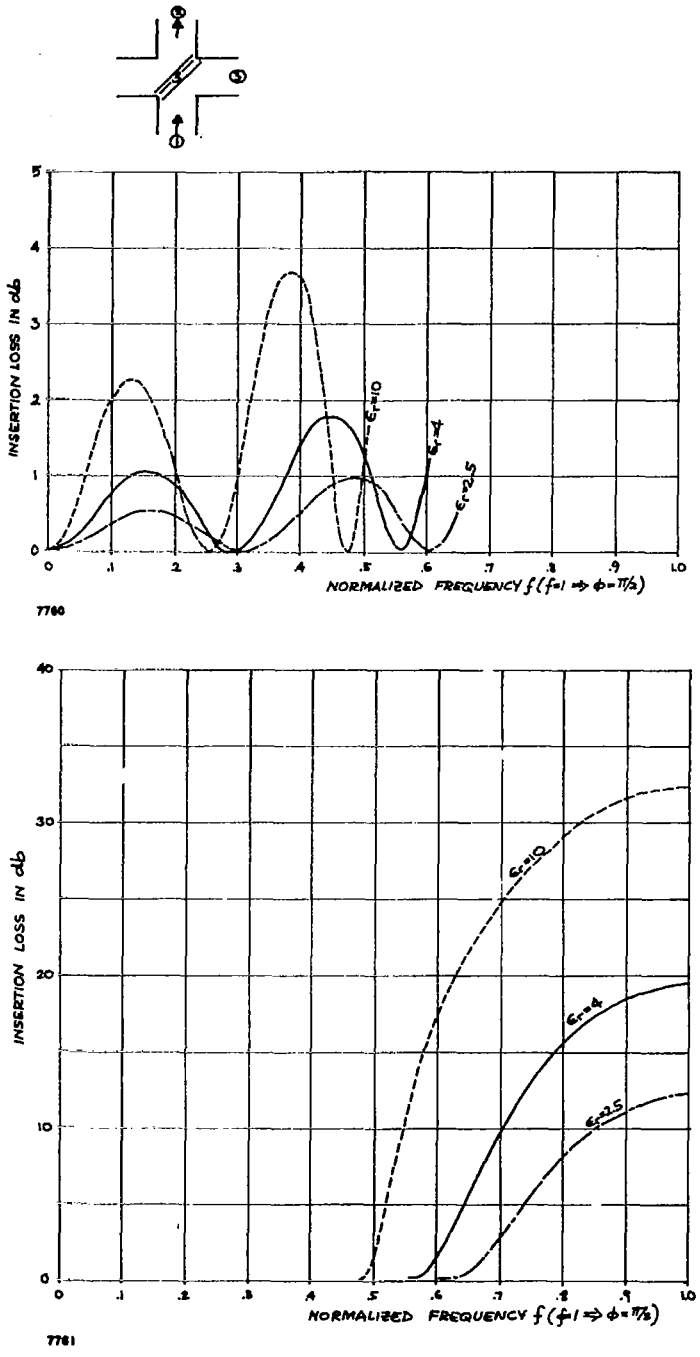

FIGURE 8. PASSBAND AND REJECTION BAND OF n = 3 FILTER

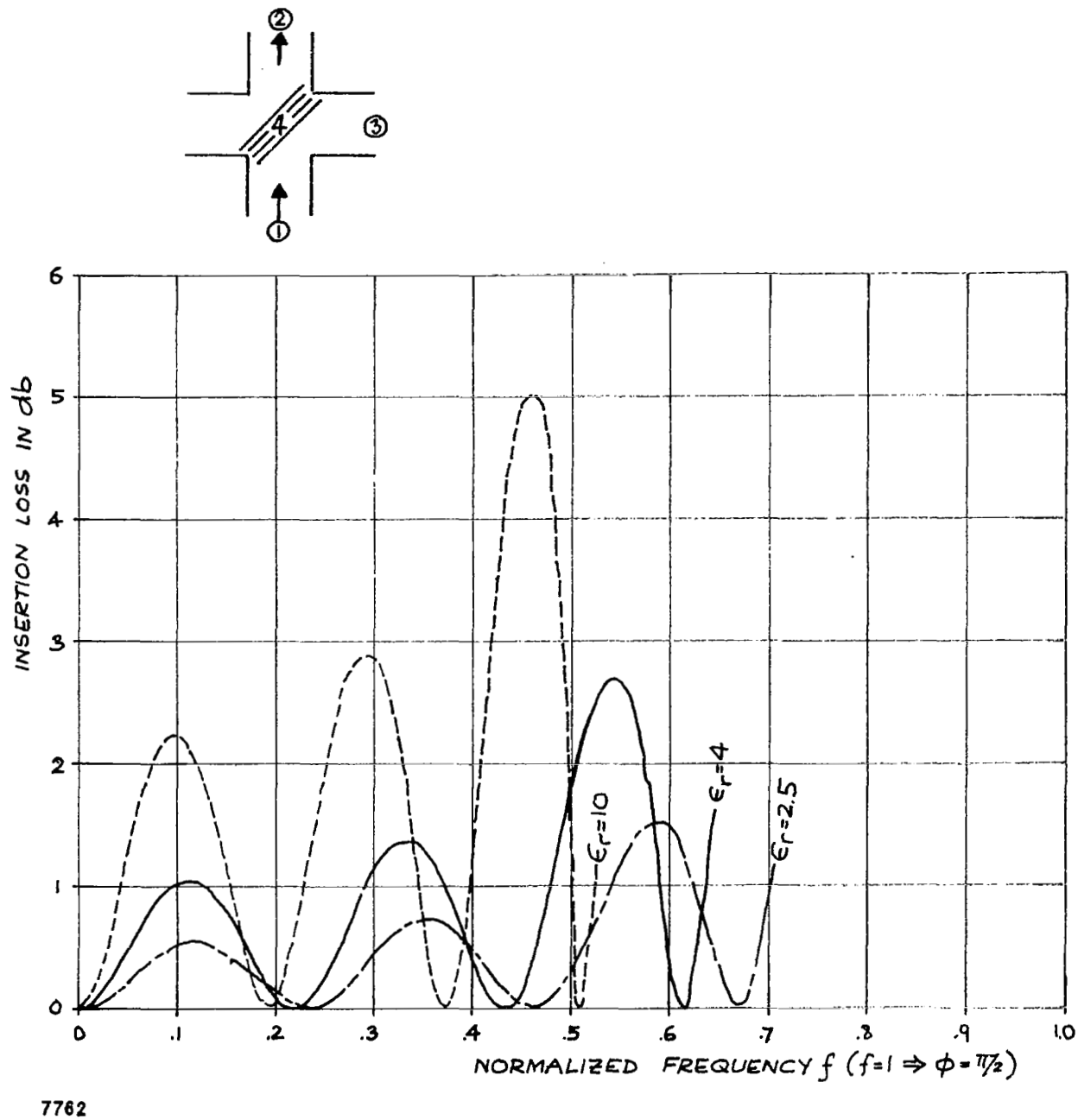

FIGURE 9A. PASSBAND REJECTION BAND OF n = 4 FILTER

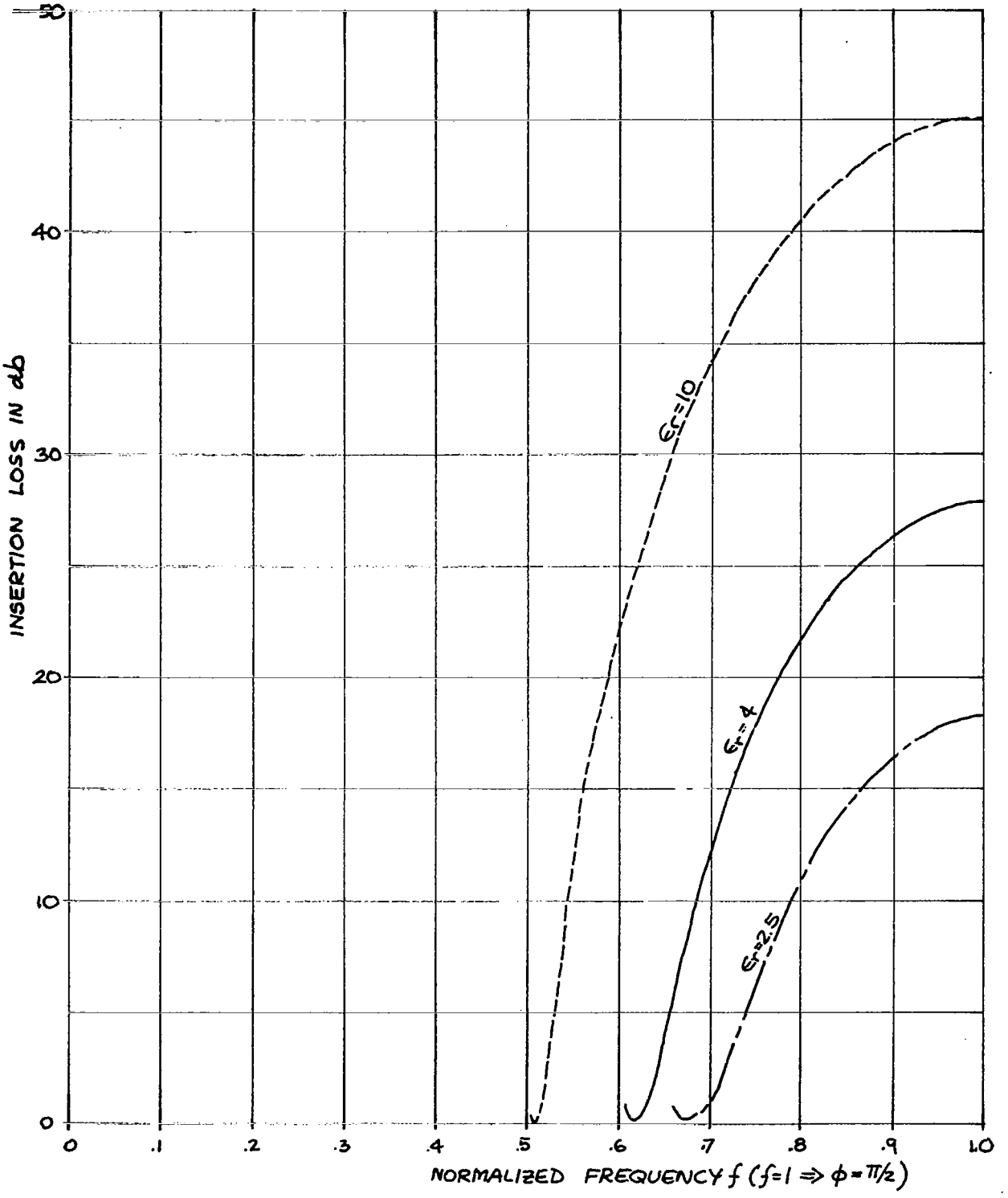

FIGURE 9B. PASSBAND AND REJECTION BAND OF n = 4 FILTER

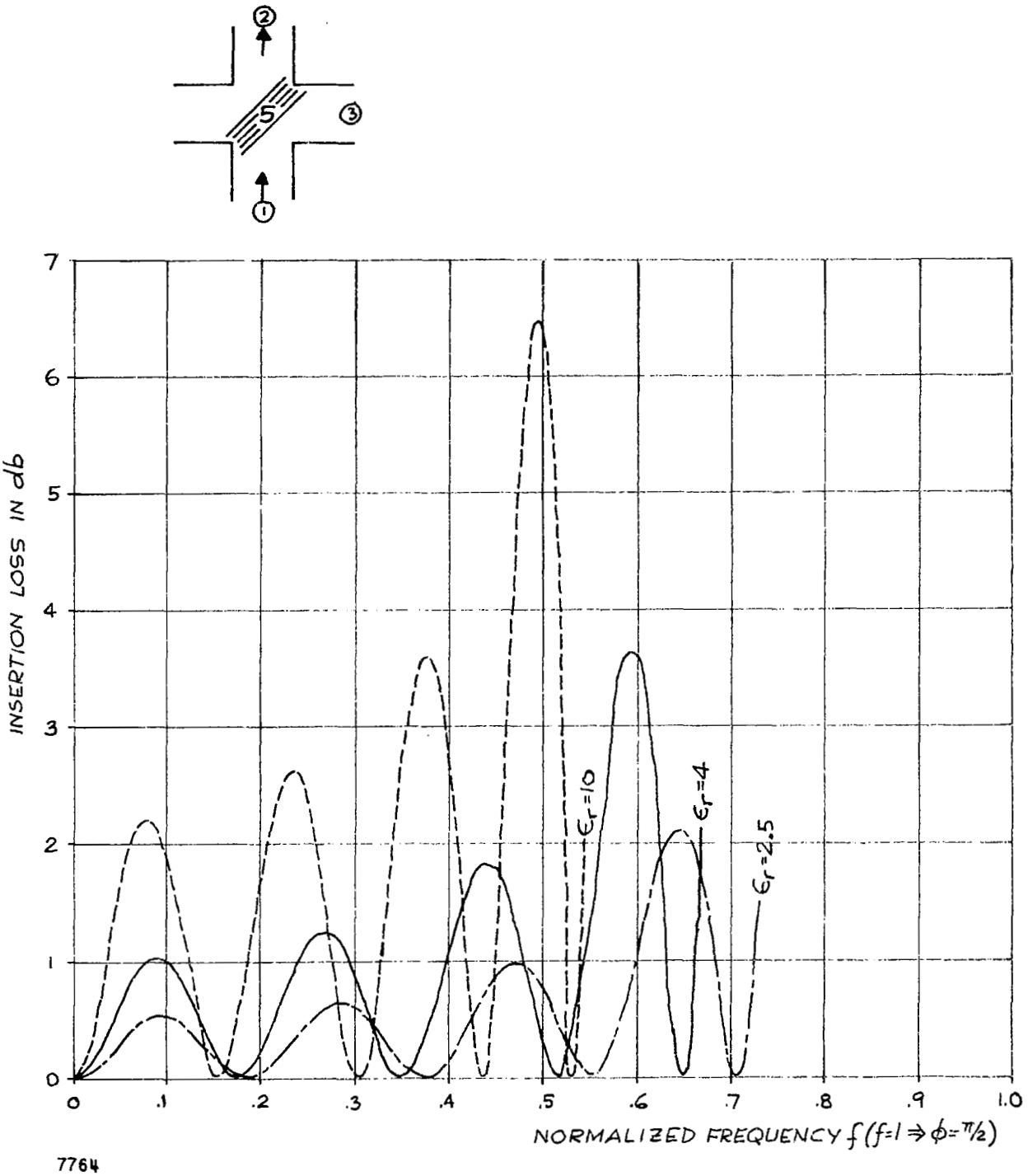

FIGURE 10A. PASSBAND AND REJECTION BAND OF n = 5 FILTER

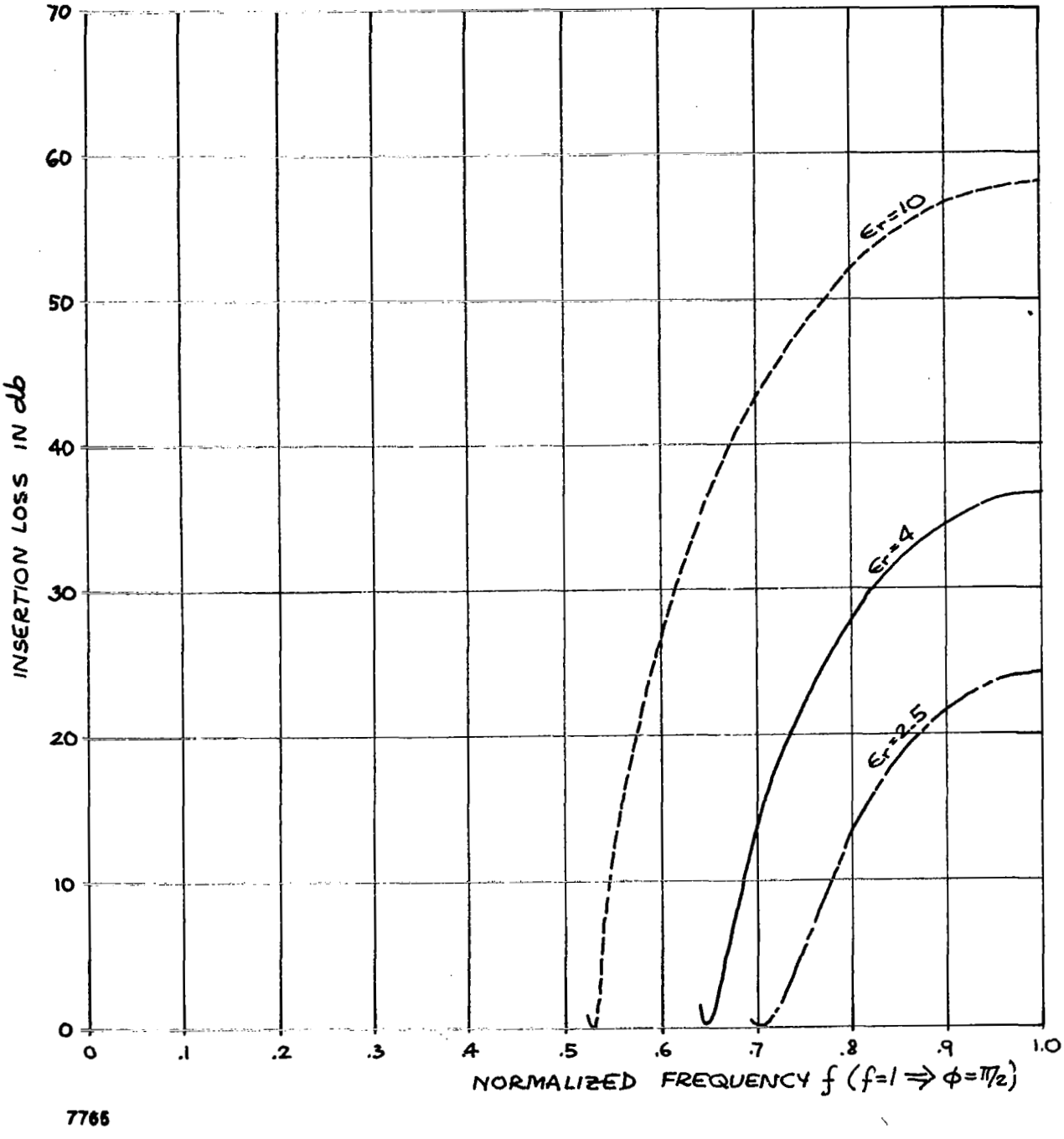

FIGURE 10B. PASSBAND AND REJECTION BAND OF n = 5 FILTER

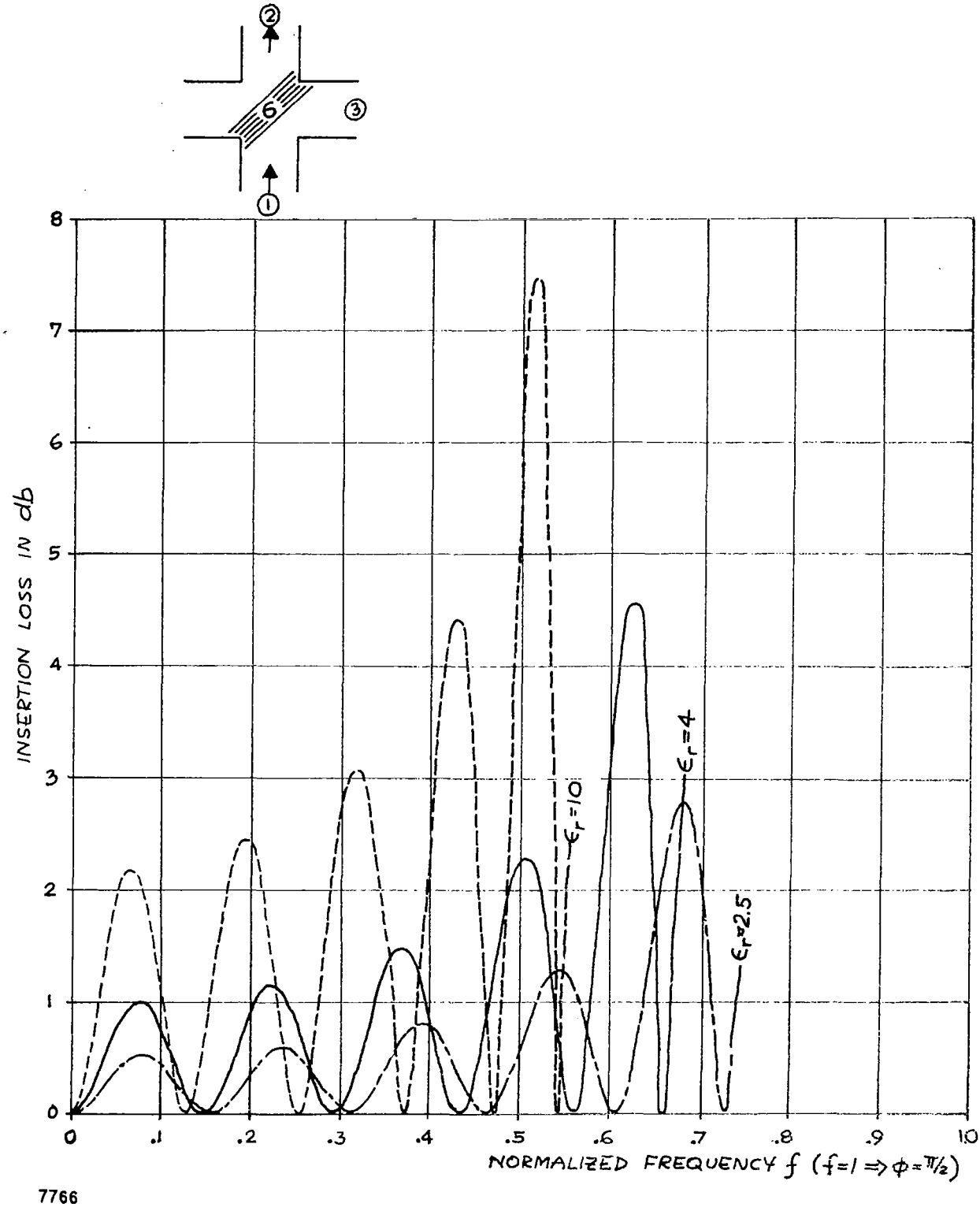

FIGURE 11A. PASSBAND AND REJECTION BAND OF n = 6 FILTER

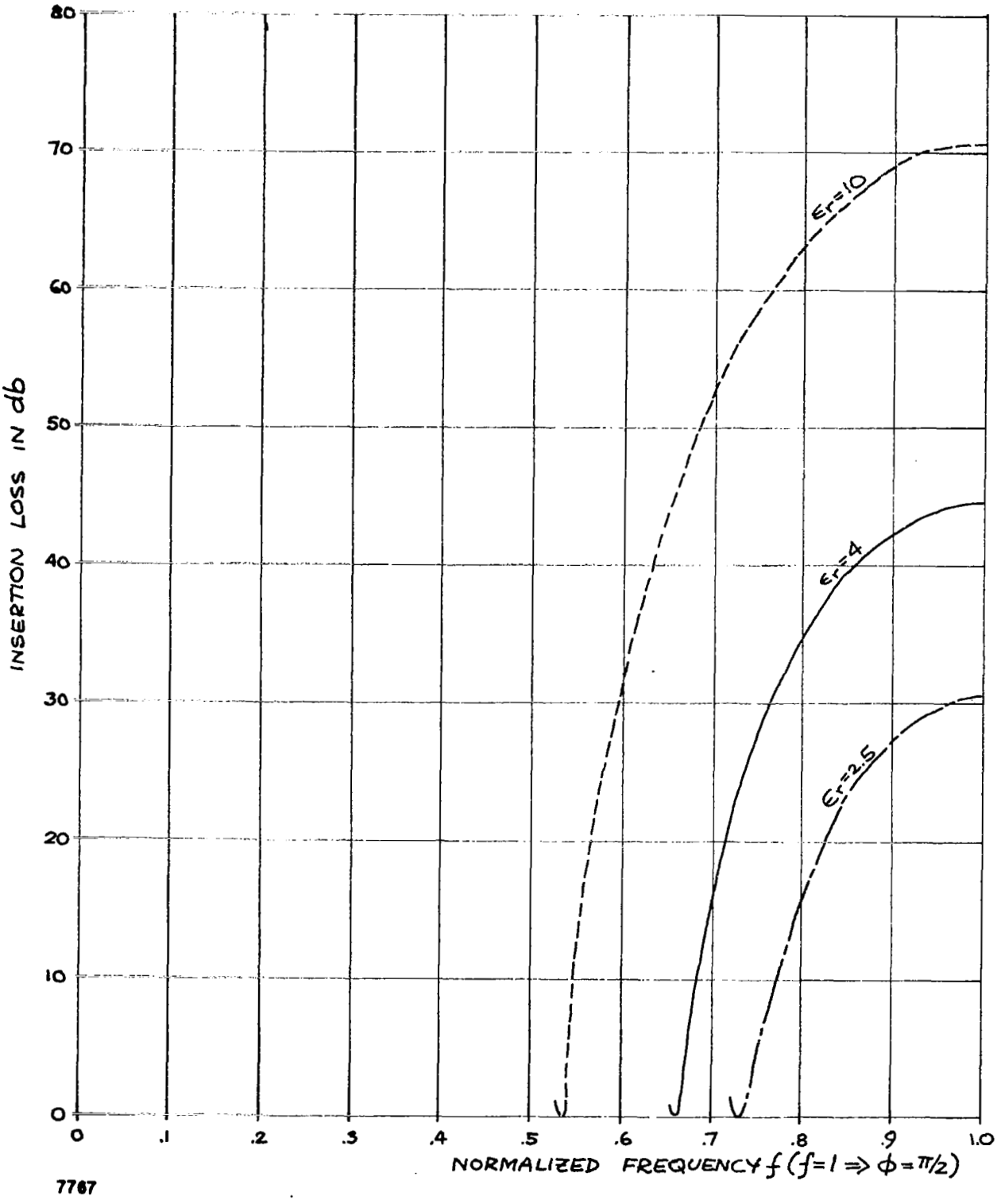

FIGURE 11B. PASSBAND AND REJECTION BAND OF n = 6 FILTER

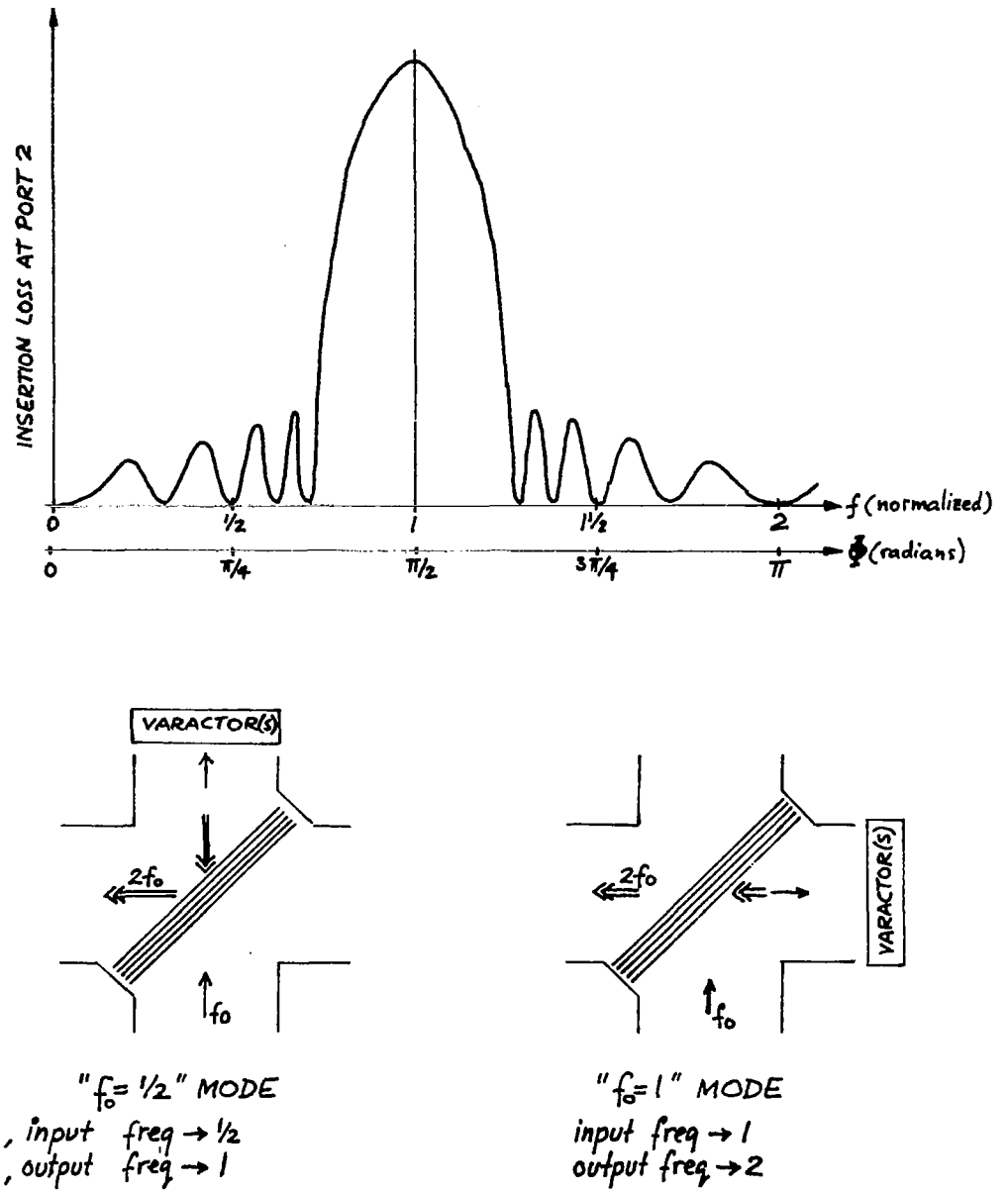

7768

FIGURE 12. TWO MODES OF DOUBLER OPERATION

operated in the $f_o = 1/2$ mode, the electrical distances ϕ (ϕ_e and ϕ_o) equal $\frac{\pi}{2}$ radians at the output frequency. In the other mode of operation, "$\phi = \frac{\pi}{2}$" condition exists for the input frequency, which requires doubling the dielectric slab thicknesses and air space separations between the slabs. This can be advantageous at very high frequencies, for a high degree of oversize in the filter waveguide (oversize ratio more than the presently popular 1 to 10), or when high dielectric-constant materials and few iterations are used. Otherwise, smaller dimensions are usually desirable. In particular, for those instances where many iterations in the filter are required, ambiguity of the reference plane, as shown in Figure 15, is of necessity introduced; this effect is increasingly proportional to the dielectric slab/air space dimensions and may eventually seriously impair the filter performance.

Considering single frequency doubling operations and a 1 to 10 oversize ratio, it is recommended that, at input frequencies below 50 GHz, $f_o = 1/2$ mode of operation be used (varactor located at port 2); at higher input frequencies $f_o = 1$ mode of operation can provide some dimensional advantages.

If wideband doubling is desired, the $f_o = 1$ mode of operation (coupled with the use of a minimum number of iterations and high dielectric constant materials) offers advantage, but for this application, a different design of directional filter should be employed which distributes and reduces ripple in both pass and rejection bands (see page 46--Low Ripple Filter).

Design procedure.--Once the mode of operation is selected, and the tolerable input/output frequency separation levels (that is, the maximum rejection specification) are established, dielectric slab materials can be selected and the number of iterations determined. Figure 13 shows a display of maximum rejection versus dielectric constant for a family of curves representing 1 to 6 iteration cases.

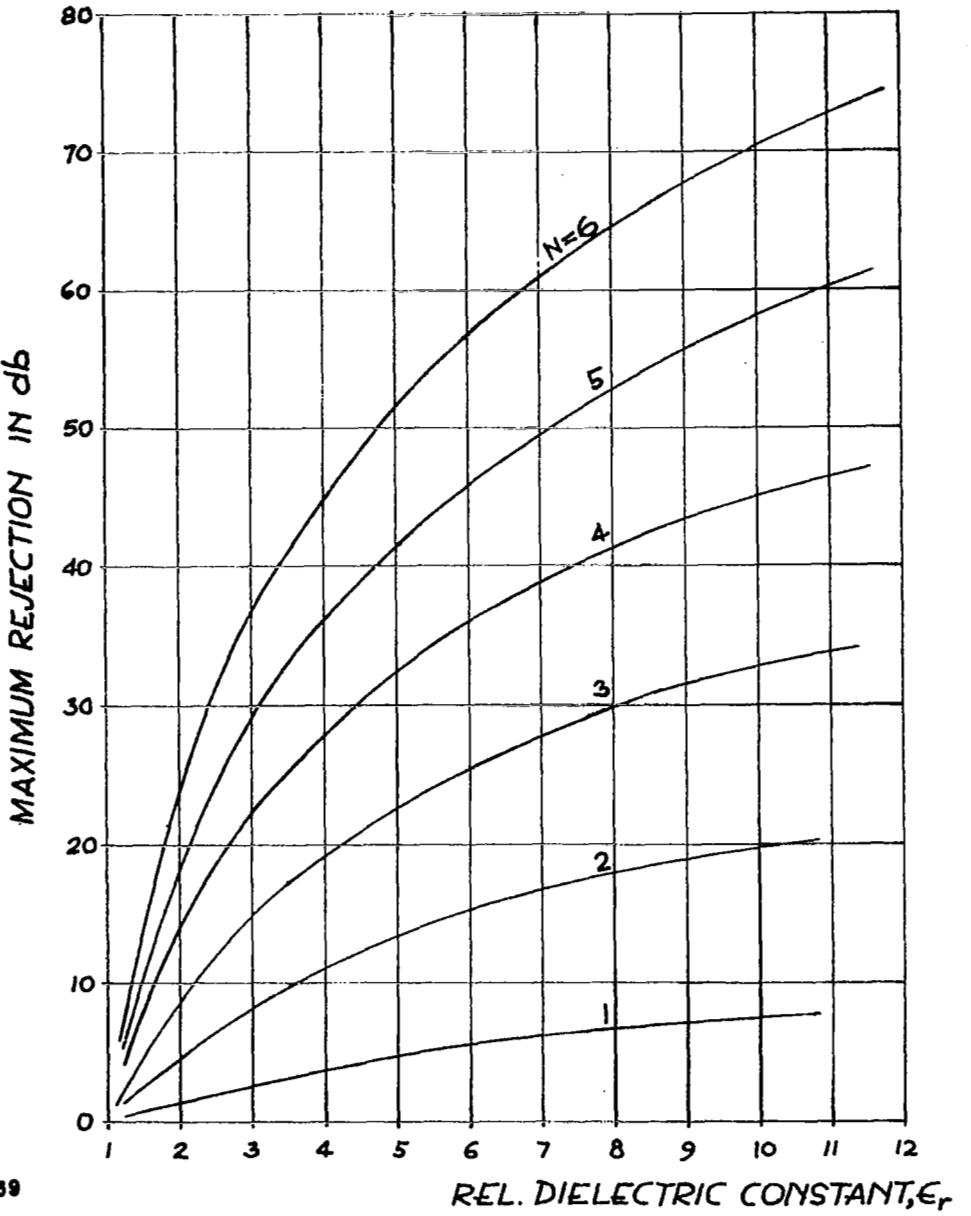

FIGURE 13. MAXIMUM REJECTION VS RELATIVE DIELECTRIC CONSTANT IN n-ITERATION DIRECTIONAL FILTERS

These curves can be applied to the $f_o = 1$ mode case without additional precautions, since at f = 2 there will be a bandpass null regardless of n or ϵ_r values. For the $f_o = 1/2$ mode of operation, an additional set of conditions is given in Figure 14. It shows how far away from f = 0.5 the nearest passband null (at port 2) occurs for a given n and ϵ_r. When $f_o \neq 0.5$ exactly, $2f_o$ will be shifted from the peak rejection amplitude at f = 1 and hence it will occur at a slightly lower value.

Based on the above considerations, a summary of the design procedures of a dielectric/air iterative directional filter for use with a single frequency doubler in a 10-times oversize waveguide system is given below:

Step 1: Select the mode of operation. Recommended selection: $f_o = 1/2$ mode for input frequencies f_o below 50 GHz, $f_o = 1$ mode for $f_o > 50$ GHz.

Step 2: Establish the desired optimum rejection requirement of the filter; 25 db rejection is recommended as sufficient value for most cases.

Step 3:

a. When operating in $f_o = 1/2$ mode, consult Figure 14 for possible need of "safety factor" in rejection requirement and slight frequency shifts ($f_o = 0.5 \pm\Delta$, then $2f_o$ or $f_2 = 1 \pm 2\Delta$) or additional weighing of n versus ϵ_r selection advantages. Then select n and ϵ_r from Figure 13 data.

b. When operating in $f_o = 1$ mode, go directly to Figure 13 to select n and ϵ_r.

Step 4: Calculate the filter dimensions: thickness of the air spaces and the dielectric slabs, d_o and d_ϵ, respectively, using the equations given below:

a. For $f_o = 1/2$ mode:

$$d_o = \frac{f\lambda}{2\sqrt{2}} \text{ (inches)} \tag{11}$$

$$d_\epsilon = \frac{f\lambda}{4\sqrt{\epsilon_r}\cos\left(\sin^{-1}\frac{1}{\sqrt{2\epsilon_r}}\right)} \text{(inches)} \tag{12}$$

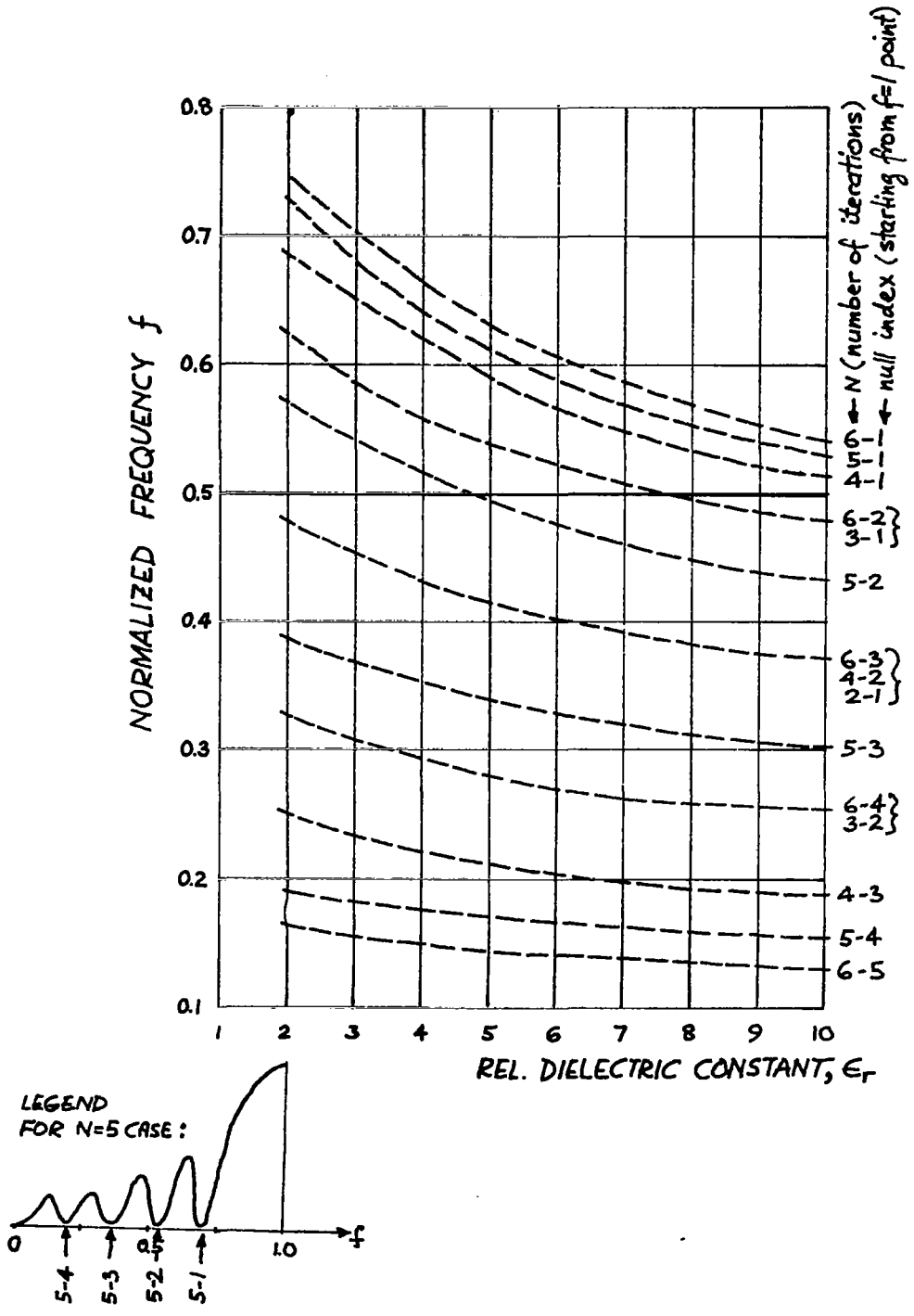

7770

FIGURE 14. PASSBAND NULL LOCATION VS RELATIVE DIELECTRIC CONSTANT (USE FOR f = 1/2 MODE)

where

ϵ_r = relative dielectric constant of the dielectric material

f = abscissa value corresponding to the input frequency selection

λ = free space wavelength at the input frequency in inches

NOTE

f and λ both can be selected at second harmonic frequency--the equation will not change since $f\left[f_{in}\right] = 1/2f\left[f_2\right]$ and $\lambda\left[f_{in}\right] = 2\lambda\left[f_{out}\right]$, hence $\left[f\lambda\right]_{f_{in}} = \left[f\lambda\right]_{f_2}$.

b. For $f_o = 1$ mode:

$$d_o = \frac{\lambda}{2\sqrt{2}} \text{ (inches)} \tag{13}$$

$$d_\epsilon = \frac{\lambda}{4\sqrt{\epsilon_r}\cos\left(\sin^{-1}\frac{1}{\sqrt{2\epsilon_r}}\right)} \text{ (inches)} \tag{14}$$

since f = 1; λ here corresponds to the input frequency free space wavelength.

Step 5: Total thickness, D_T, of the filter element within the oversized waveguide junction area will be given by

$$D_T = nd_\epsilon + (n - 1)\, d_o \text{ (inches)} \tag{15}$$

An example using these steps is given below:

> Desired mode of operation: "f_o = 1/2" 2 f_o (midband)
> rejection desired: minimum of 25 db
>
> Dielectric materials available: quartz, $\epsilon_r = 4$ or
> alumina, $\epsilon_r = 9.6$

It can be seen from Figure 13 that four slabs of quartz or three slabs of alumina would suffice to meet the rejection requirements. A look at Figure 14 shows that for the four quartz-slab filter the passband null closest to $f_o = 0.5$ occurs at $f_o = 0.43$, while for the three alumina-slab filter it is at $f_o = 0.48$. Since each has a sufficient safety factor in terms of rejection at its peak value (28 and 32 db, respectively), slight shifts required of output frequencies from f = 1 to f = 0.86 and f = 0.96 will (from Figures 9 and 8, respectively) show the midband rejection at the second harmonic as 25 and 31 db (approximated from $\epsilon_r = 10$ curve), respectively. Hence, both configurations are acceptable, with alumina slabs showing advantages in terms of slab thickness and the smaller number of slabs--both factors helpful in reducing the slab fringe ambiguities, which are illustrated in Figure 15 and are basically self-explanatory; accumulated thickness produces phase-front irregularities in both complementary output ports. Different configurations depicted in Figure 15 will reduce the effects at one output port while aggravating the conditions at the others.

Modified Equal Iteration Filter

General remarks.--Examination of the insertion loss curves for iterative directional filters ($\phi_\epsilon = \phi_o$) indicates a fair degree of passband ripple activity. These ripples are not theoretically harmful in narrowband (spot frequency) multiplier circuits. However, excessive ripple activity is harmful in practice even in narrowband multipliers because passband circuit loss becomes an unstable parameter. The filter loss would be overly sensitive to temperatue variations and fabrication tolerances. Wider regions of low passband ripple activity are desirable for wideband multiplier designs.

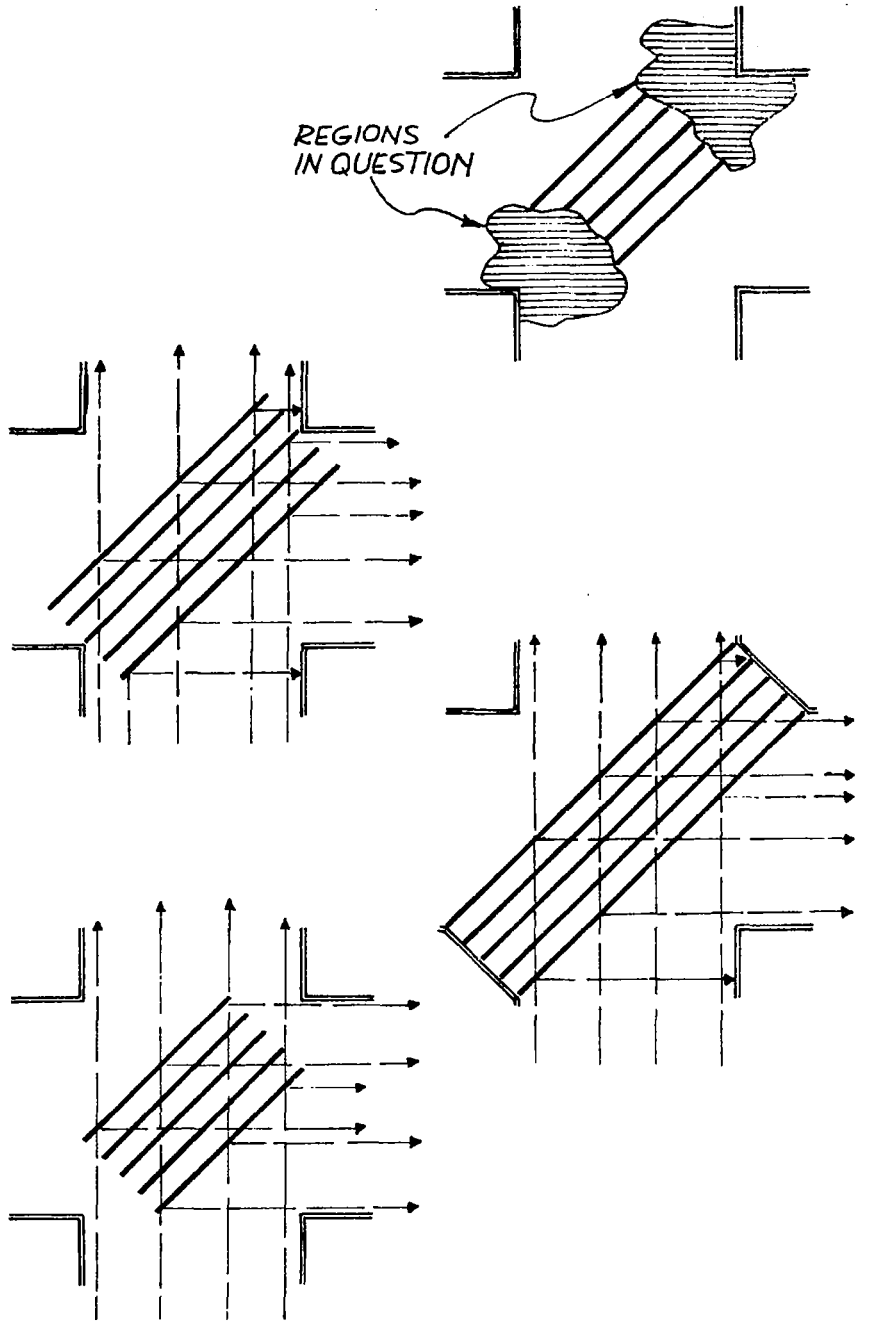

FIGURE 15. ILLUSTRATION OF THE REFERENCE PLANE AMBIGUITY

At quasi-optical frequencies, where quarter wavelengths in dielectrics become extremely small, frequency tuning of a directional filter--if one insists on preserving the $\theta_\epsilon = \phi_o$ condition--may really become very critical. A study of what happens when the electrical lengths in the air and dielectric sections are not equal (that is, if $\phi_o = K\phi_\epsilon$) revealed another family of "irregular filters," which we call modified iterative filters. These filters are not periodic in $n\pi$ unless K is a whole number. A characteristic of this type of filter, which may be harnessed to good use in the multiplier application, is that the passband ripples are irregular and, under certain conditions wide ranges of frequencies within the passband can become void of any such parasitic ripple. Furthermore, the principal rejection portion of such a directional filter suffers little in peak rejection values; the rejection bandwidth and the rejection peak are reduced and shifted, respectively, but neither of these three changes renders this type of filter less fit or objectionable for the use in frequency multipliers. Figures 16A-D and 17A-D present several curves to illustrate the behavior of this filter, when four and five iterations of air and quartz ($\epsilon_r = 4.0$) are used in its construction. Unfortunately, we have not found the optimum K conditions for which the peak rejection and the no-ripple-passband regions are harmonically related. Yet this type of filter provides more flexibility in choice of dielectic material thickness--may allow one to switch from specially ground to less expensive and easily and quickly obtainable standard thicknesses; or select thicker dielectric slabs for increased mechanical strength where necessary--or allows one to readjust or tune the filter to other operating frequencies without changing the dielectric slab thicknesses at, most likely, a small change in electrical performance characteristics.

Design theory. --The filter loss equation, from which the curves of Figures 16A-D and 17A-D have been realized, is of the same form as given

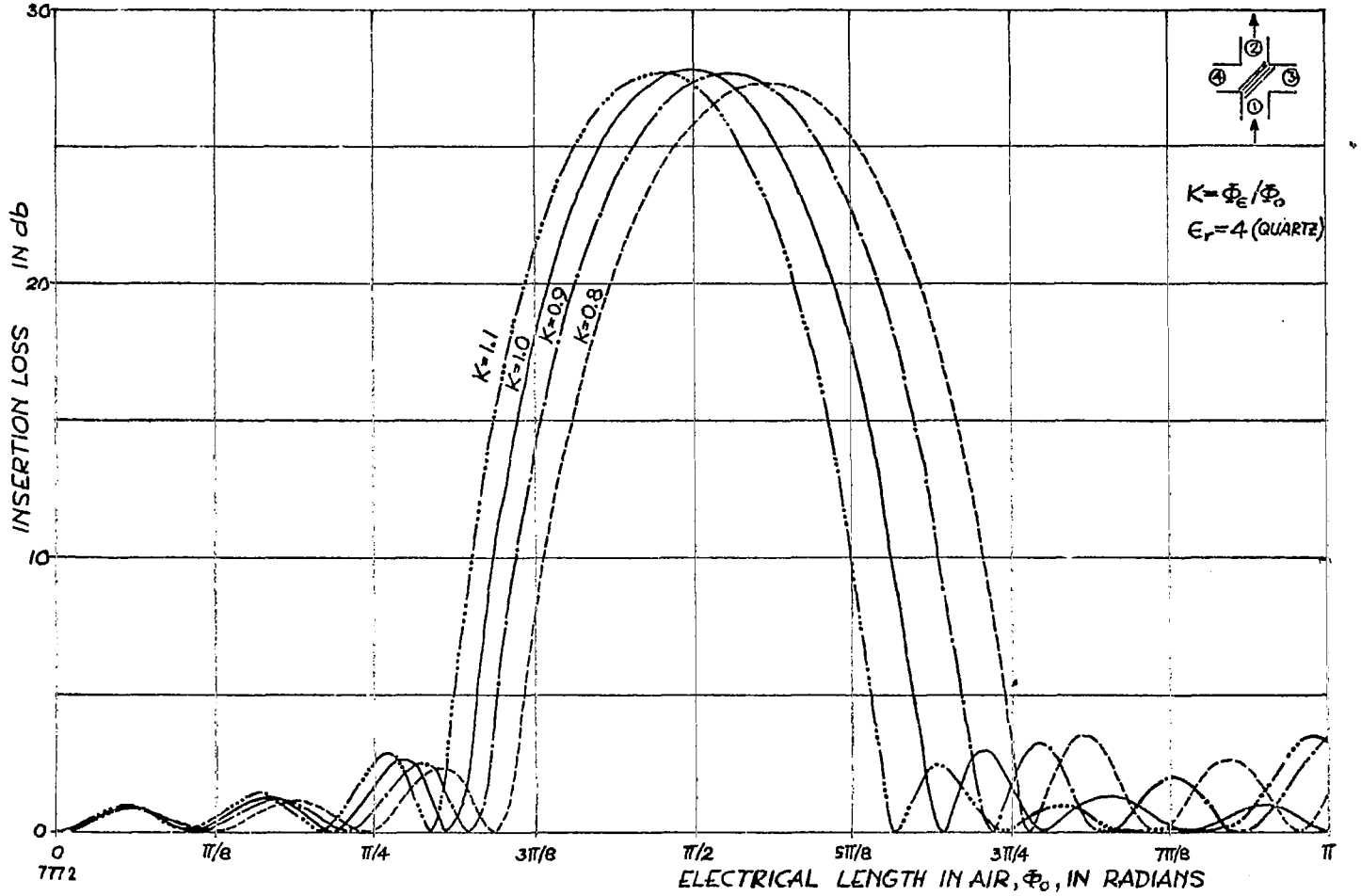

FIGURE 16A. MODIFIED FOUR QUARTZ/AIR EQUAL ITERATION DIRECTIONAL FILTER CHARACTERISTICS

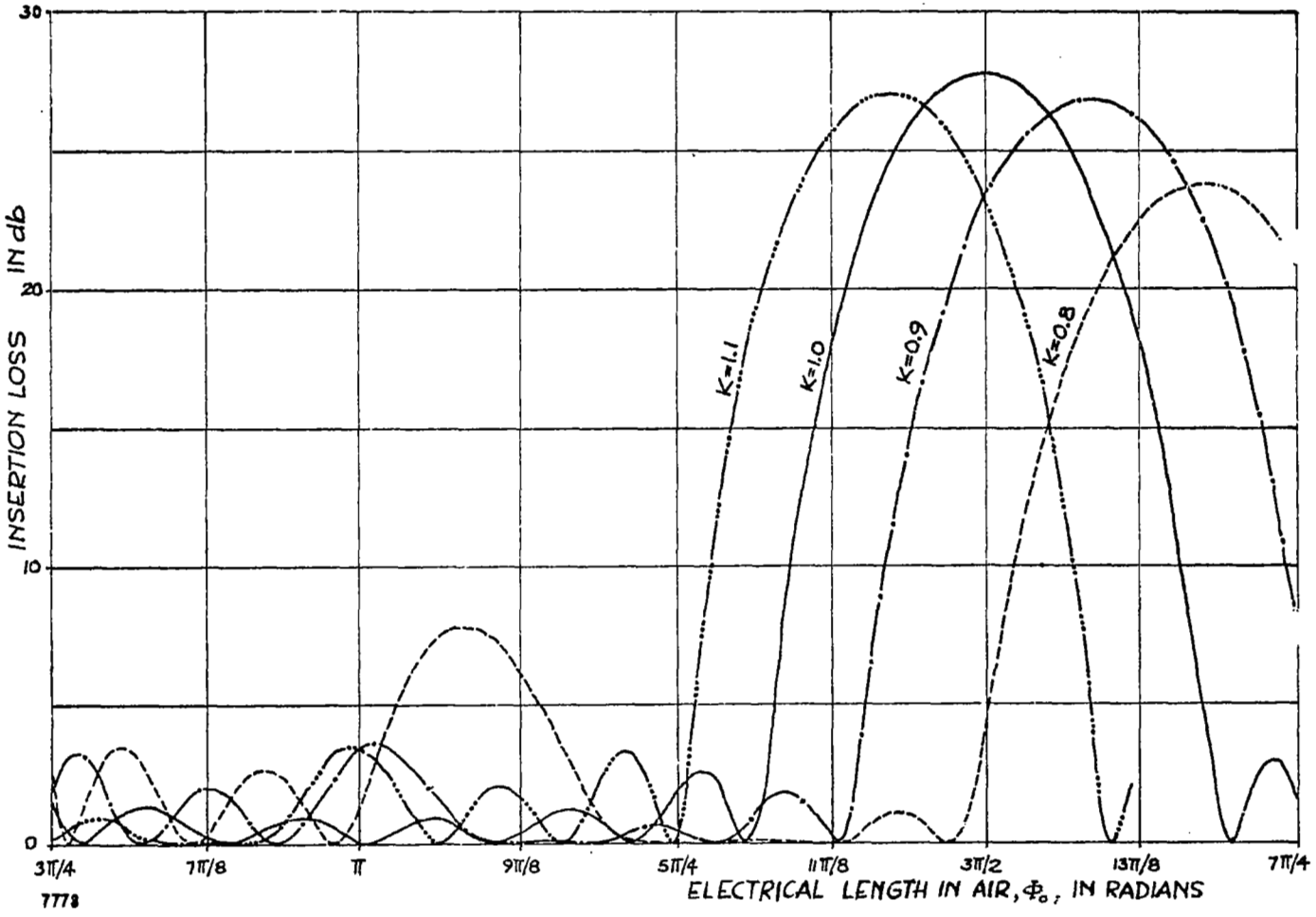

FIGURE 16B. MODIFIED FOUR QUARTZ/AIR EQUAL ITERATION DIRECTIONAL FILTER CHARACTERISTICS

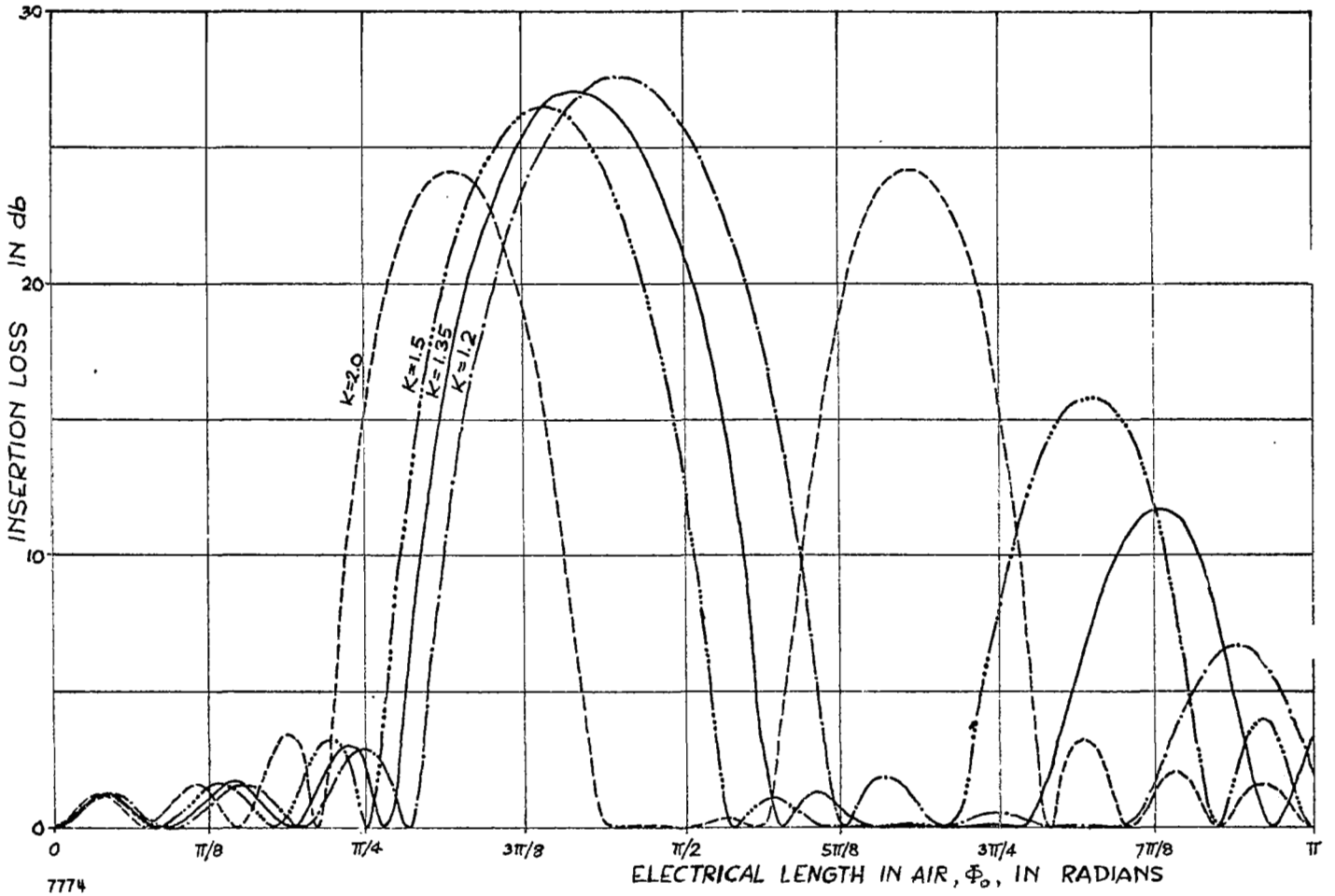

FIGURE 16C. MODIFIED FOUR QUARTA/AIR EQUAL ITERATION DIRECTIONAL FILTER CHARACTERISTICS

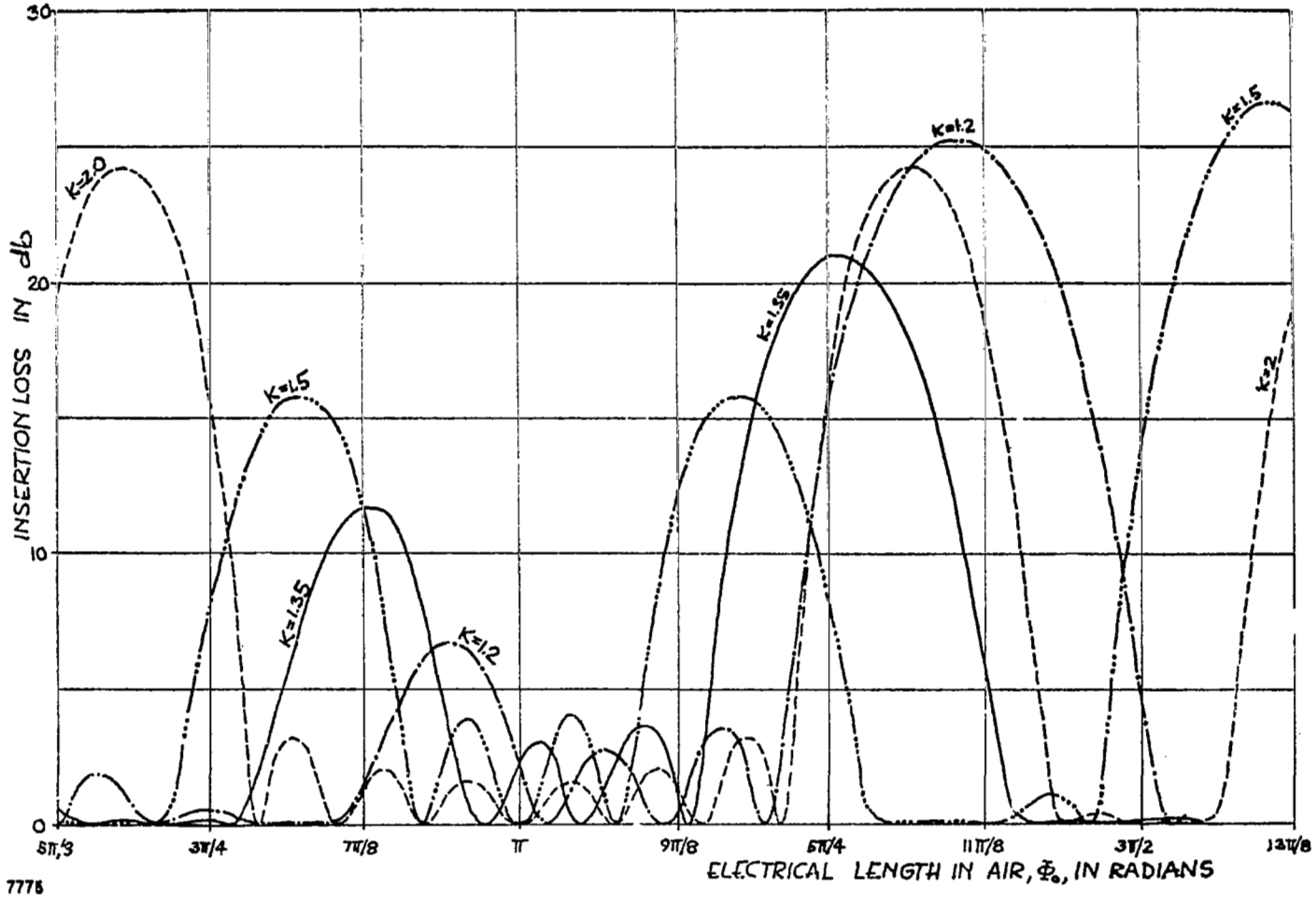

FIGURE 16D. MODIFIED FOUR QUARTZ/AIR EQUAL ITERATION DIRECTIONAL FILTER CHARACTERISTICS

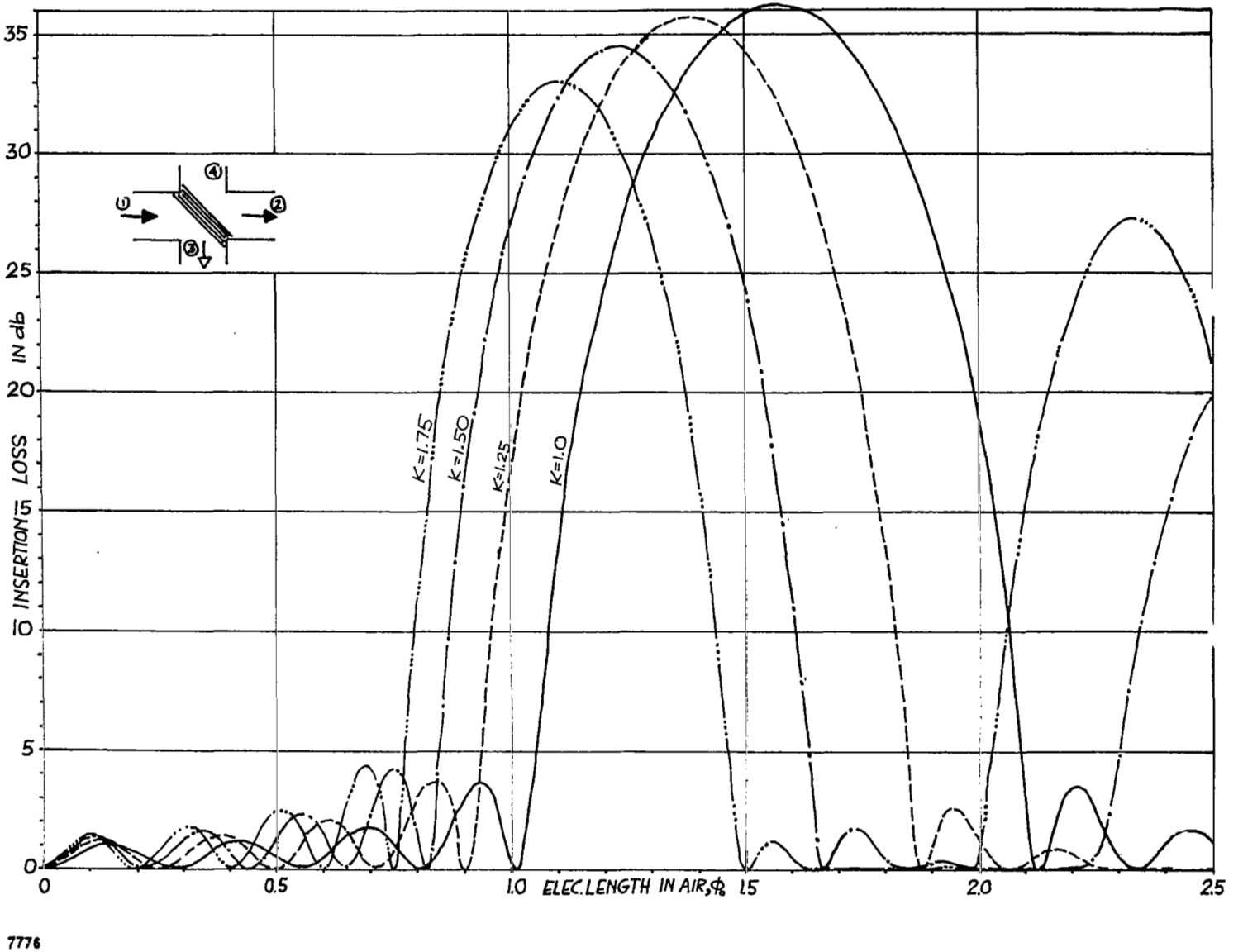

FIGURE 17A. MODIFIED FIVE QUARTZ/AIR EQUAL ITERATION DIRECTIONAL FILTER CHARACTERISTICS

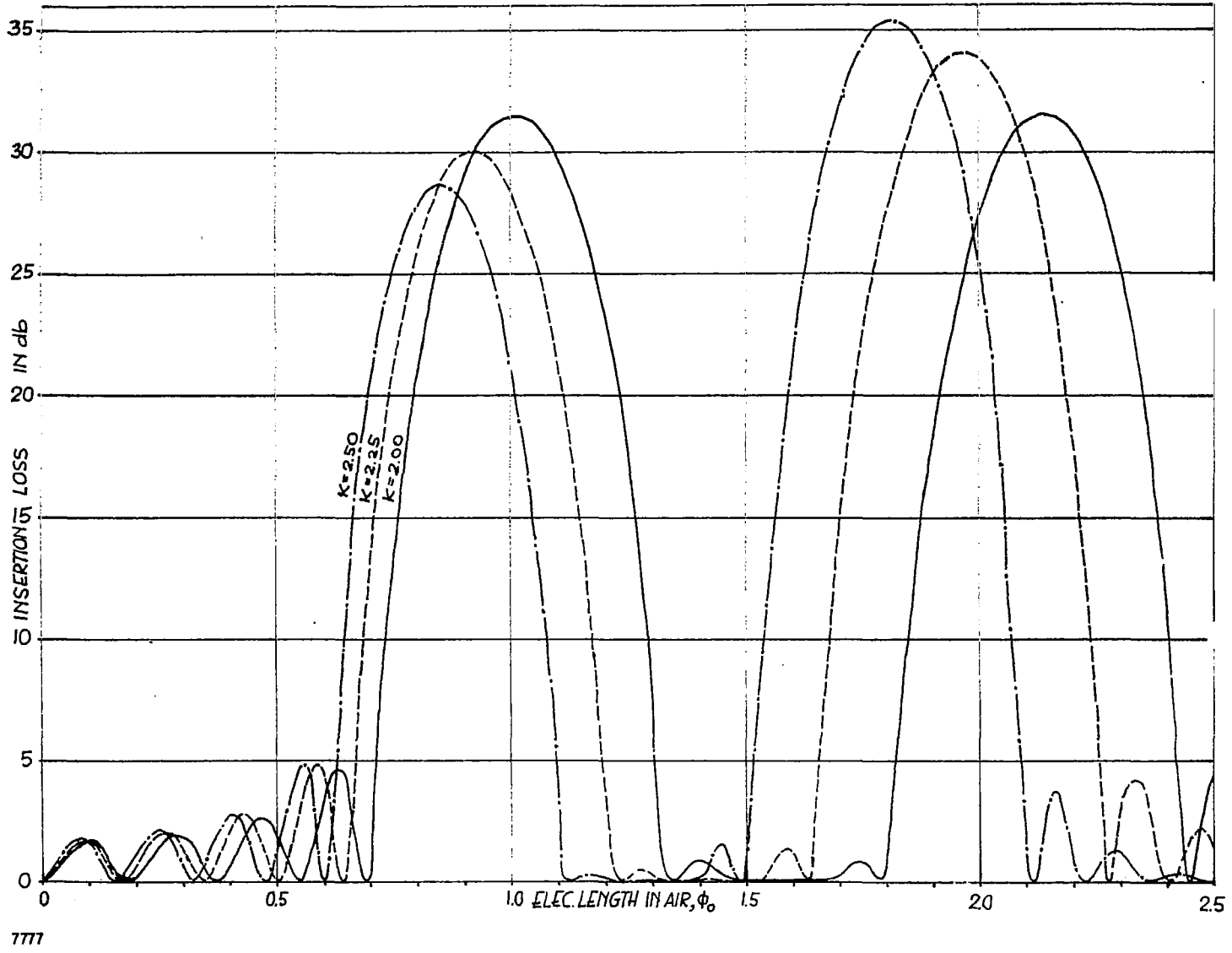

FIGURE 17B. MODIFIED FIVE QUARTZ/AIR EQUAL ITERATION DIRECTIONAL FILTER CHARACTERISTICS

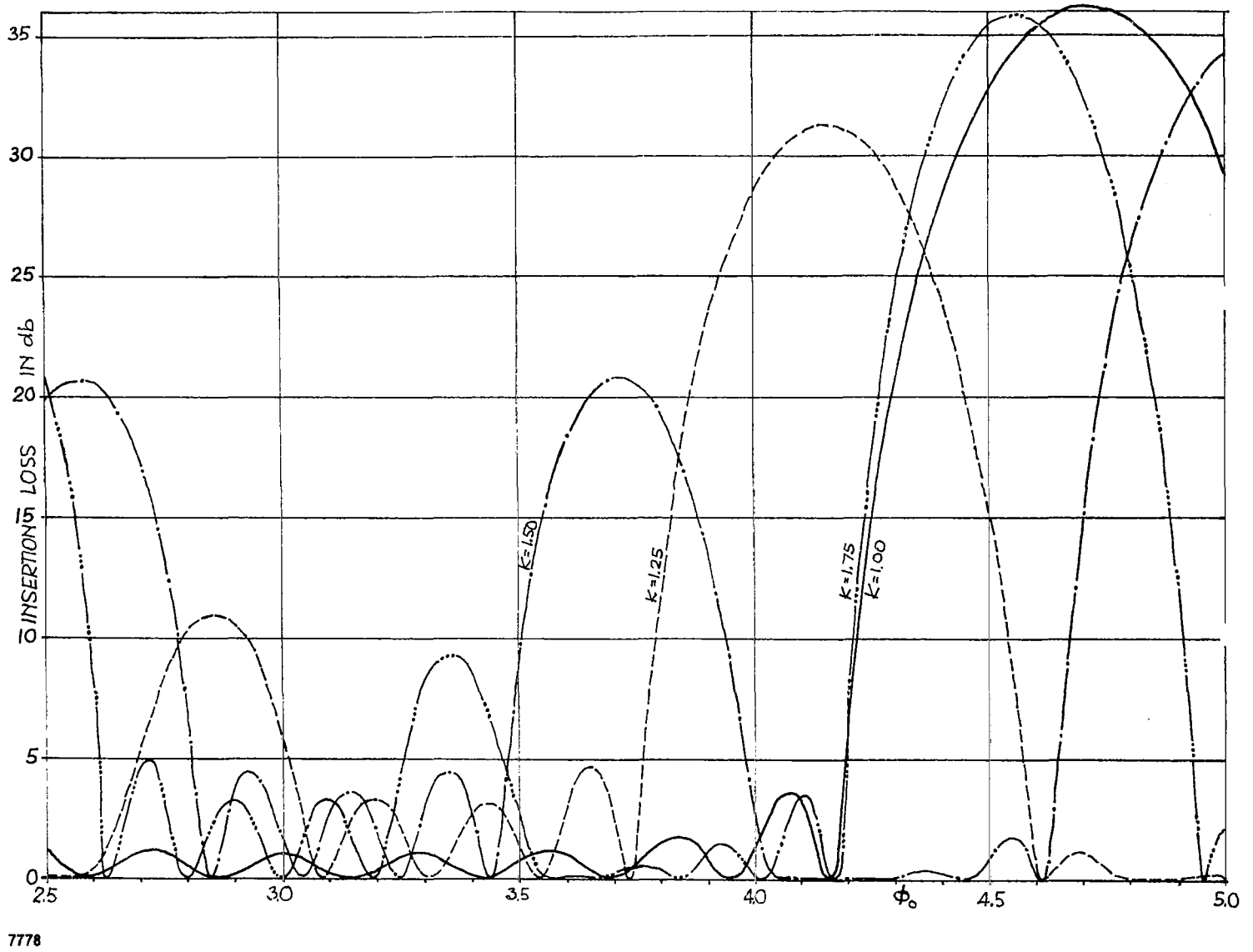

FIGURE 17C. MODIFIED FIVE QUARTZ/AIR EQUAL ITERATION DIRECTIONAL FILTER CHARACTERISTICS

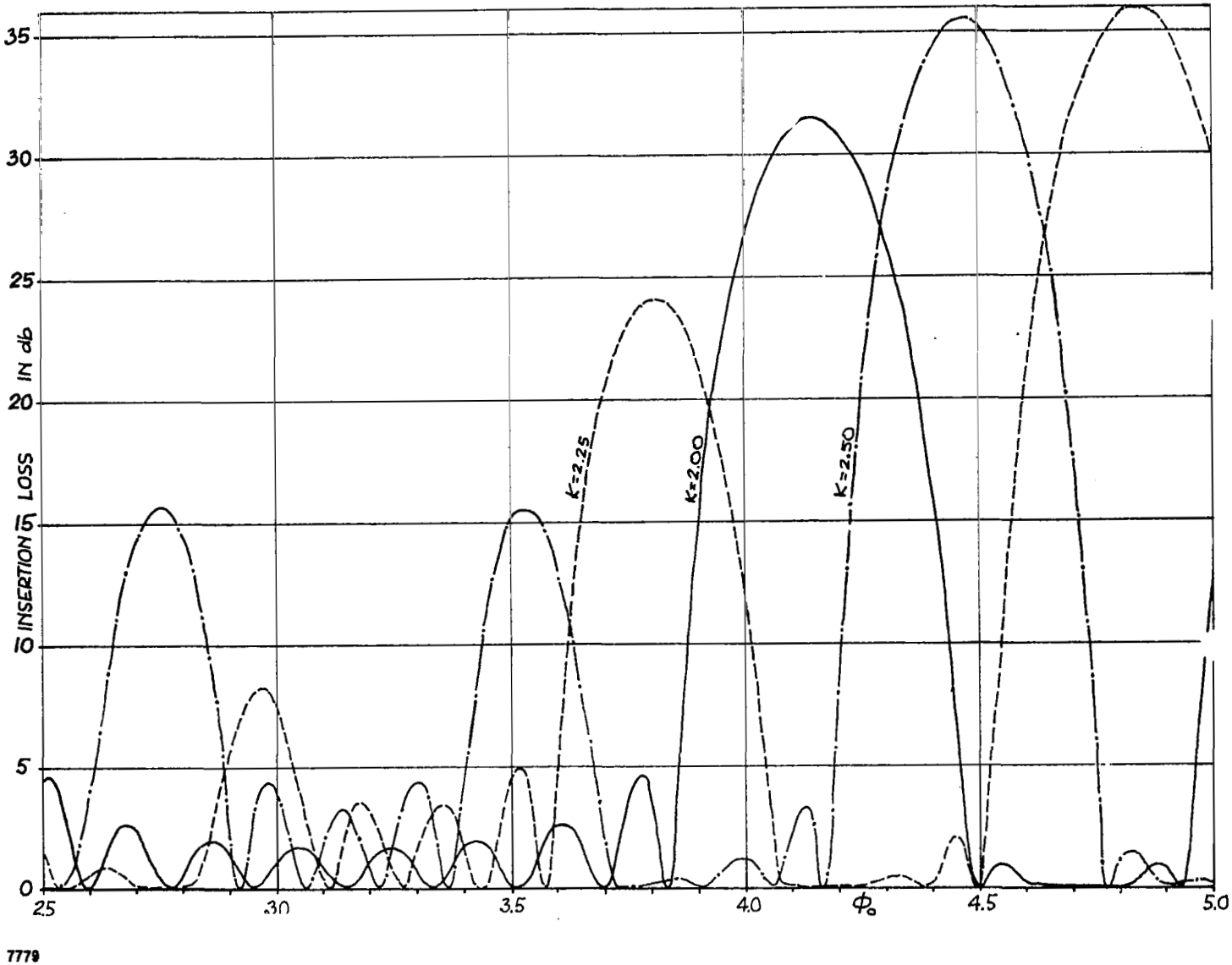

FIGURE 17D. MODIFIED FIVE QUARTZ/AIR EQUAL ITERATION DIRECTIONAL FILTER CHARACTERISTICS

in equation (1) and in Appendix B as equation B - 10, except for a change in expressions of Y and X to negate the assumption $\phi_o = \phi_\epsilon = \phi$ used in the equal iteration filter. Therefore, when $\phi_o \neq \phi_\epsilon$,

$$X = 2 \sin \phi_o \cos \phi_\epsilon + \left(Z + \frac{1}{Z}\right) \sin \phi_\epsilon \cos \phi_o \tag{16}$$

$$Y = 2 \cos \phi_\epsilon \cos \phi_o - \left(Z + \frac{1}{Z}\right) \sin \phi_\epsilon \sin \phi_o \tag{17}$$

$$\text{and } \phi_\epsilon = K\phi_o \tag{18}$$

which then must be substituted into the expressions for Tchebycheff polynomials of the second kind, P_n (equation B-7) and, eventually, insertion loss expression in equations 1 or B-10.

Whereas equal iteration directional filter design ($\phi_o = \phi_\epsilon$ case) involved only n and ϵ_r parameters--choosing $\theta_i = 45^o$ as the most acceptable mechanically-- the modified version of it generates an entire family of curves as functions of K for each ϵ_r within a given n. Figures 16A-D and 17A-D present two families of curves (n = 4 and n = 5 at $\epsilon_r = 4.0$), to illustrate the trends of K variations and, since $\epsilon_r = 4.0$ corresponds to quartz dielectric, all these curves are useful for practical design purposes.

Since the ripple activity in the modified version of the equal iteration filter is not reduced significantly in the region below the first rejection peak, $f_o = 1/2$ mode of operation (where L_{12} is low for f_{in}, high for $2f_{in}$) should ordinarily not be considered. Hence, a preliminary design criterion for the modified equal iteration filter is that L_{12} is high for the input frequency, low for the second harmonic.

A suggested design procedure is as follows:

Step 1: Consider available (or desired) dielectric material to be used in the filter. Establish its relative dielectric constant, ϵ_r (keeping in mind that a lower ϵ_r material will require a greater number of iterations, n, to achieve the required results), and its loss characteristics at the highest operating frequency (greater n will aggravate the filter losses).

Step 2: Select a provisional n value--for the chosen ϵ_r-- and check the L_{12} versus ϕ_o curves for that n to see whether the first, or primary rejection peak somewhat exceeds the specified minimum value (usually, 25 db constitute sufficient minimum) for all K parameters under consideration. This "safety margin" is required because the filter will operate on the rejection band slope at its input frequency, f_{in}.

Step 3: Select a L_{12} versus ϕ_o curve corresponding to a particular K value and seek out a flat low-loss response region between the primary and the secondary rejection regions. Note the ϕ_o value--let us call it ϕ_o'. Look for the L_{12} value on the same curve at the $\phi_o'/2$ point. If it is less than the required minimum (25 db), shift the ϕ_o' to the right until 25 db is reached at $\phi_o'/2$ or ϕ_o' is no longer in a low-loss region. If the latter occurs first, choose another curve corresponding to a different K value. If all K's do not provide proper operating points, choose a higher n and start again. When the proper operating points are established, note the final ϕ_o' and $\phi_o'/2$ values in radians.

Step 4: Establish the thickness dimensions of the air space and the dielectric slab, d_o and d_ϵ, respectively, using the equations given below:

$$d_o = \left[\frac{\phi_o'}{2}\right] \frac{\lambda}{\sqrt{2\,\pi}} \text{ (inches)} \qquad (19)$$

and

$$d_\epsilon = \left[\frac{\phi_o'}{2}\right] \frac{K\lambda}{2\pi\sqrt{\epsilon_r}\cos\left(\sin^{-1}\frac{1}{\sqrt{2\epsilon_r}}\right)} \text{ (inches)} \tag{20}$$

where

λ = freespace wavelength at the input frequency in inches

$\left[\frac{\phi_o'}{2}\right]$ = the ϕ_o value at the lower operating point in radians

K = the K value for the respective IL_{12} versus ϕ_o curve

ϵ_r = relative dielectric constant of the dielectric material

The above two equations could also use $\left[\phi_o'\right]$ and λ values corresponding to the second harmonic, since $\left[\frac{\phi_o'}{2}\right]\lambda\,(f_{in}) = \left[\phi_o'\right]\lambda\,(2\,f_{in})$.

Step 5: Total thickness, D_T, of the filter element within the oversized waveguide junction area will be given by:

$$D_T = nd_\epsilon + (n-1)\,d_o \text{ (inches)} \tag{21}$$

where

n = number of iterations

d_o and d_ϵ are as obtained in Step 4.

An example follows. Given requirements are: $L_{12} \geq 25$ db at 30 GHz; $L_{12} \leq 1$ db at 60 GHz; dielectric material quartz, $\epsilon_r = 4.0$; number of iterations n not to exceed 5.

Design procedure starts with selection of the proper family of L_{12} versus ϕ_o curves: $\epsilon_r = 4$; n = 5 are given in Figure 17A-D. Choosing K = 1.75 for a first try (it is presented separately in Figure 18 for clarity),

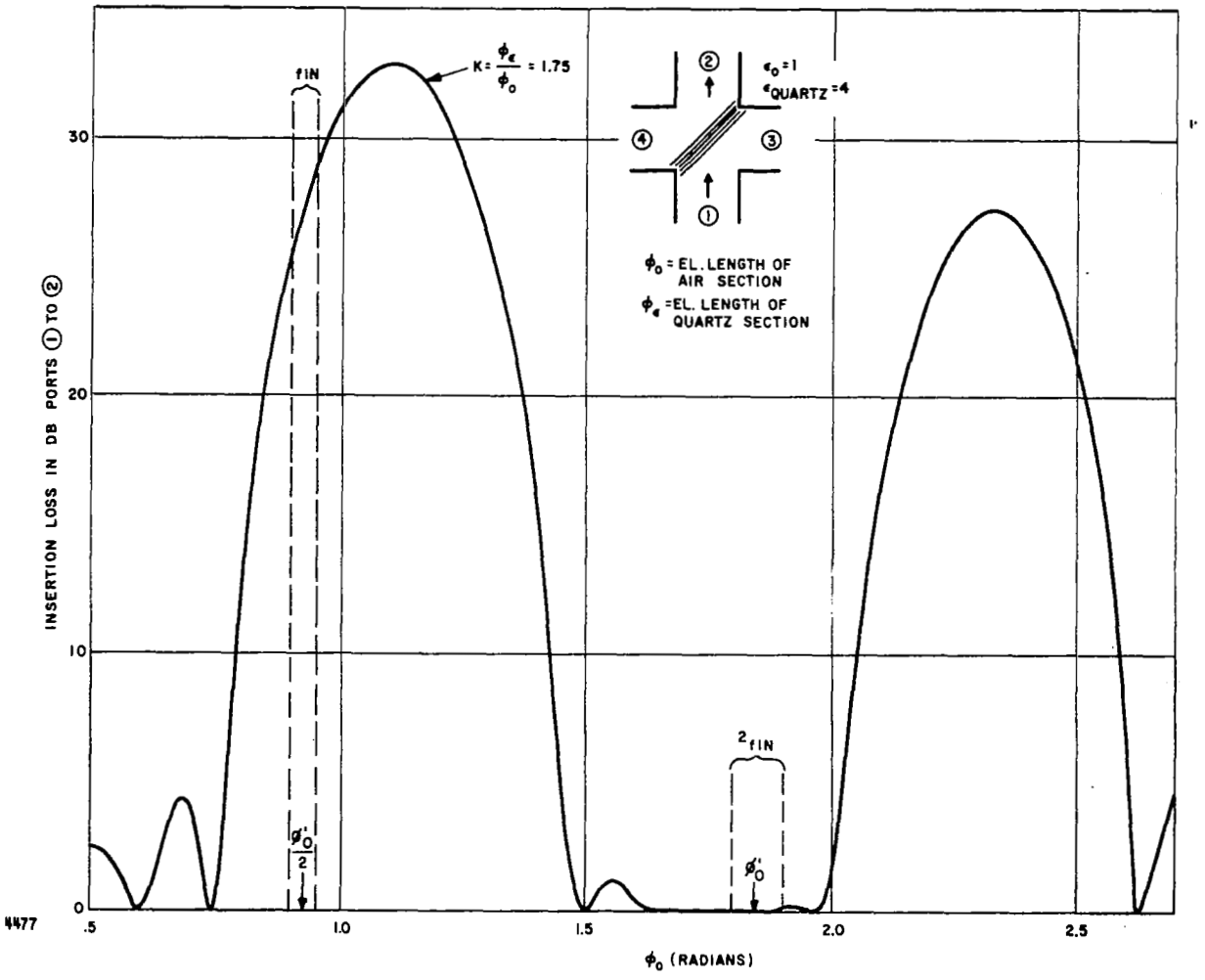

FIGURE 18. CHARACTERISTICS OF MODIFIED FIVE QUARTZ/AIR ITERATION FILTER WHEN K = 1.75

one observes a flat no-loss region at $1.64 < \phi_o < 1.90$ and the principal high-loss region (25 db or better) at $0.90 < \phi_o < 1.32$. The portions of these two regions which satisfy the requirement of harmonic relationship, that is: ϕ_o (at high loss) = $1/2\ \phi_o$ (at low loss), are $1.8 \leq \phi_o \leq 1.9$ and $0.9 < \phi_o < 0.95$ as indicated in Figure 18. Selecting ϕ_o values at the center of each respective region, $\phi_o' = 1.85$ radians, $\frac{\phi_o'}{2} = 0.925$ radians to correspond to 60 and 30 GHz, respectively, one obtains $d_o = 0.082"$ and $d_\epsilon = 0.0542"$ via Step 4 (equations 19 and 20) and the total filter element thickness from equation 21, $D_T = (0.054" \times 5) + (0.082" \times 4) \doteq 0.598"$ which would be reasonable thickness in a WR284 waveguide (inside dimensions $2.840" \times 1.340"$). Since the energy at 60 GHz would have to traverse the cumulative thickness of quartz corresponding to $5\phi_\epsilon = (1.75)\ (1.85)\ (5) = 16.2$ radians or $2.58\ \lambda$, moderate dielectric losses within the material of between 0.5 and 1.0 db are to be expected. The remarks made for equal iteration ($\phi_o = \phi_\epsilon$) filter, concerning fringe ambiguities due to excessive filter element thickness as shown in Figure 15, are applicable in this filter also.

Low-Ripple (Stepped Impedance) Filter

Design considerations.--Here we consider the design of quasi-optical filters formed by cascaded dielectric slabs in terms of its relationship to modern network theory. The reason for doing this is the promise of lower passband ripple than is achievable with the iterative approaches. Specifically, these structures are related via the impedance concept for plain wave propagation to stepped impedance low-pass filters, the synthesis of which has been treated in rigorous detail by Levy (reference 10). He gives tables for a wide variety of Tchebycheff designs.

In general, there is a tradeoff between pass bandwidth, maximum passband VSWR, number of impedance steps and maximum rejection. Also, a filter with high maximum rejection will require greater impedance swing at

adjacent steps; this will in turn require a wider range of dielectric constants (a narrow range is more desirable--all other things being equal). An example of one possible design is given below; it also serves to indicate the steps to be taken in the design of these filters.

Assume that the desired maximum rejection is 20 db and the maximum passband VSWR is 1.2. From reference 10 we note that N (the number of impedance steps) is 8. Reference 10 gives the normalized (to the generator) impedance of each step; they are listed in the second column of Table I. These values are then renormalized to the highest impedance value (impedance step 5)--this is necessary because the maximum dielectric slab impedance occurs when $\epsilon_r = 1$. The relative dielectric constant of each step for the case of normal incidence is then calculated from:

$$\epsilon_{ri} = \left(\frac{1}{z_i}\right)^2 \tag{22}$$

where z_i is the normalized impedance of the ith step (given in the third column). Values of ϵ_{ri} are given in the fourth column. The last column gives the dielectric constant for 45 degrees incidence (the directional filter case); it was calculated from the relationship $\epsilon_{45^o} = \frac{\epsilon \text{norm} + 1}{2}$.

The above filter will yield the results promised by Levy only if the generator loading is equal to 1/1.78 or 0.562. The normalized load impedance should be 0.562 × (maximum VSWR), or 0.562 × 1.2 = 0.674.

These conditions cannot be satisfied at all frequency ranges but broadband $\lambda/4$ transformers that provide these impedances in the passband of our filter will suffice; mismatched generator and load effects are less critical in the rejection band.

TABLE I

LOW-RIPPLE FILTER IMPEDANCE AND DIELECTRIC CONSTANT STEPS

Step No.	Normalized Impedance	Impedances Normalized to Step 5	Relative Dielectric Constant for a Normal Incidence Filter	Relative Dielectric Constant for a 45^{o} Incidence Filter
1	1.33	0.745	1.8	1.4
2	0.78	0.438	5.2	3.1
3	1.70	0.95	1.1	1.05
4	0.675	0.378	7.0	4.0
5	1.78	1.0	1.0	1.0
6	0.705	0.394	6.4	3.7
7	1.54	0.865	1.34	1.17
8	0.902	0.506	3.9	2.45

A two-section $\lambda/4$ transformer on each end will suffice. From Young (reference 11), the generator side (a VSWR of 1.78 exists if not matched) over a 3 to 1 band will be within a maximum VSWR of 1.21 and this requires $\lambda/4$ sections have $Z_1 = 0.678$ and $Z_2 = 0.828$. These impedances are normalized to that of free space

The load side will match a 1.49 VSWR to 1.22 over a 4 to 1 band and requires $Z_1 = 0.777$ and $Z_2 = 0.864$. The $\lambda/4$ transformer impedance data is then converted to dielectric constants as shown below.

	Generator Side			Load Side		
	Z value	ϵ_{norm}	ϵ_{45^o}	Z value	ϵ_{norm}	ϵ_{45^o}
Z_1	0.678	2.12	1.56	0.777	1.65	1.33
Z_2	0.828	1.46	1.23	0.864	1.33	1.16

Figure 19 shows the structure, the dielectric constants, and the thicknesses of the dielectric slabs.

The thickness (ℓ_ϵ) values were calculated from

$$\phi = \frac{2\pi}{\lambda}\sqrt{\epsilon_r}\,\ell_\epsilon \cos\theta_\epsilon = \frac{2\pi\ell_\epsilon}{\lambda}\sqrt{\epsilon_r - \frac{1}{2}} \tag{23}$$

For the eight filter sections $\phi = \pi/2$ at the maximum rejection wavelength λ_R. We shall place the design center of the $\lambda/4$ transformers at $\phi = \pi$ when $\lambda = \lambda_R$. Thus, we have

$$\ell_\epsilon = \frac{\ell_R}{4\sqrt{\epsilon_r - \frac{1}{2}}} \tag{24}$$

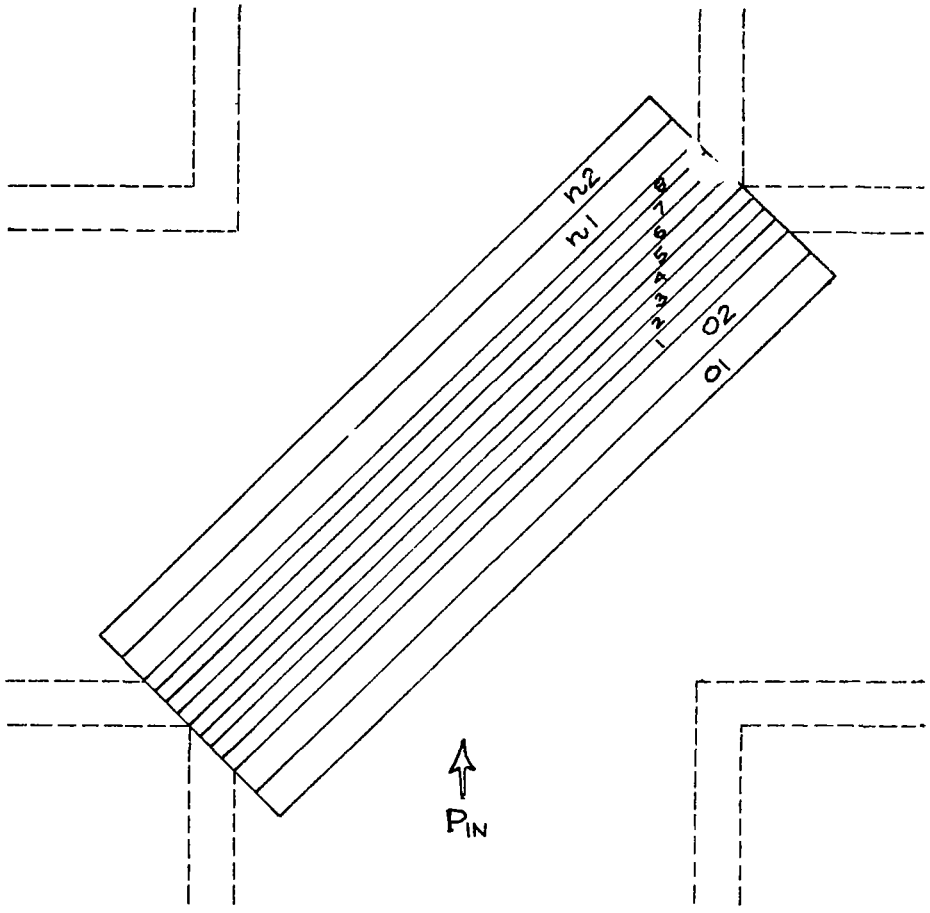

SLAB INDEX	01	02	1	2	3	4	5	6	7	8	n1	n2
SLAB THICKNESS ℓ IN CM	.582	.486	.263	.155	.338	.134	.353	.140	.306	.179	.309	.275
SLAB RELATIVE DIELECTRIC CONST ϵ_r	1.23	1.56	1.40	3.10	1.05	4.00	1.00	3.70	1.17	2.45	1.16	1.33

7780

FIGURE 19. LOW RIPPLE FILTER DESIGN PARAMETERS

for the filter sections and

$$\ell_{\epsilon} = \frac{\lambda}{2\sqrt{\epsilon_r - \frac{1}{2}}} \tag{25}$$

for the transformer sections.

These data together with the design of two section transformers using Young's tables complete this theoretical design.

The next step is one of realizing in practice that dielectric constants required. Since most of these values do not exist in low-loss natural dielectrics, it requires the use of artificial dielectrics. This topic is considered next.

Artificial dielectrics.--The realization of the low passband-ripple directional filter described in the previous report requires the availability of materials whose dielectric constants range between ϵ_o and $4\epsilon_o$.

Many of the values required are not available in their natural state. While certain foam (Eccofoam) and ceramic (Ray K) dielectrics are available in a wide range of values, the former is limited to low (2 or less) relative dielectric constant values and the latter's loss properties at millimeter wavelengths are poor. Two approaches are described herein: (1) a three-dimensional array of spherical conductors or dielectrics, and (2) a two-dimensional array of holes in a dielectric slab. These offer the possibility of obtaining a wide variety of dielectric constants with low dielectric loss tangents. Both types are shown in Figure 20. The second approach is preferred but more design information is required.

Array of metallic or dielectric spheres.--The effective relative dielectric constant and permeabilities of metallic and dielectric spheres that

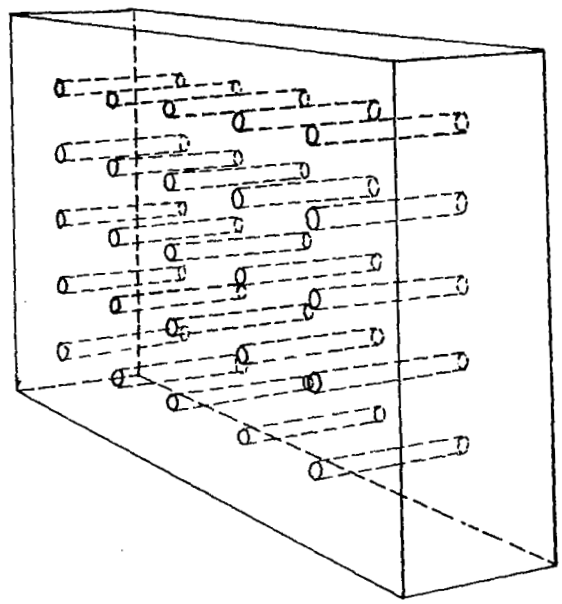

a) DIELECTRIC SLAB WITH AIR HOLES

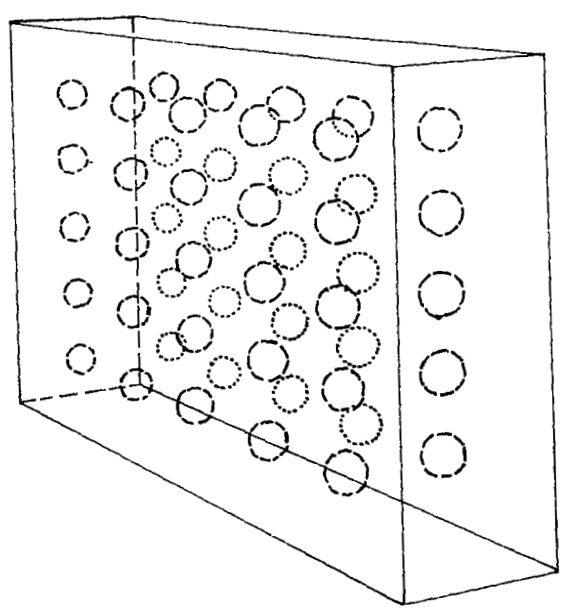

7781 b) THREE DIMENSIONAL ARRAY OF METALLIC OR DIELECTRIC SPHERES

FIGURE 20. SOME ARTIFICIAL DIELECTRICS

are embedded (in a regular three dimensional pattern) in a supporting dielectric medium, have been derived in reference 12. The results are

$$\epsilon_{eff} = \epsilon_1 \frac{|1 + 2fC|}{|1 - fC|} \tag{26}$$

and

$$\begin{aligned} \mu_{eff} &= \mu_1 \text{ for dielectric spheres} \\ \mu_{eff} &= \mu_1 \frac{|1 - f|}{|1 + f_{12}|} \text{ for metallic spheres} \end{aligned} \tag{27}$$

where

f = ratio of sphere volume to total volume, or filling factor

ϵ_1 = relative dielectric constant of the surrounding medium

$C = \frac{\epsilon_s - \epsilon_1}{\epsilon_s + 2\epsilon}$ for dielectric spheres, = 1 for metal spheres

ϵ_s = relative dielectric constant of the spheres

In our application it is easier to use the dielectric sphere case because we prefer to avoid variation in permeability. Figure 21 shows curves of $\epsilon_{eff}/\epsilon_1$ as a function of f with ϵ_s/ϵ_1 as a parameter. These curves are useful in determining the sphere filling factor required to achieve a given dielectric constant. They also apply to the metallic sphere case ($\epsilon_s \longrightarrow \infty$). For example, if $\epsilon_{eff} = 2.3$ is desired for a case where all spheres use air ($\epsilon_s = 1$) as the dielectric and the base dielectric is Rexolite ($\epsilon_1 = 2.55$) one has $\epsilon_{eff}/\epsilon_1 = 0.902$ and $\epsilon_s/\epsilon_1 = 0.555$; a value of $f = 0.19$ is required. The specific sphere diameters should be chosen such that there is a center-to-center spacing, s, much less than a free space wavelength. Thus, at λ = 1 cm (30 GHz) spacings of 0.1 cm would be desirable. The filling factor is related to sphere spacing s and the sphere radius a by

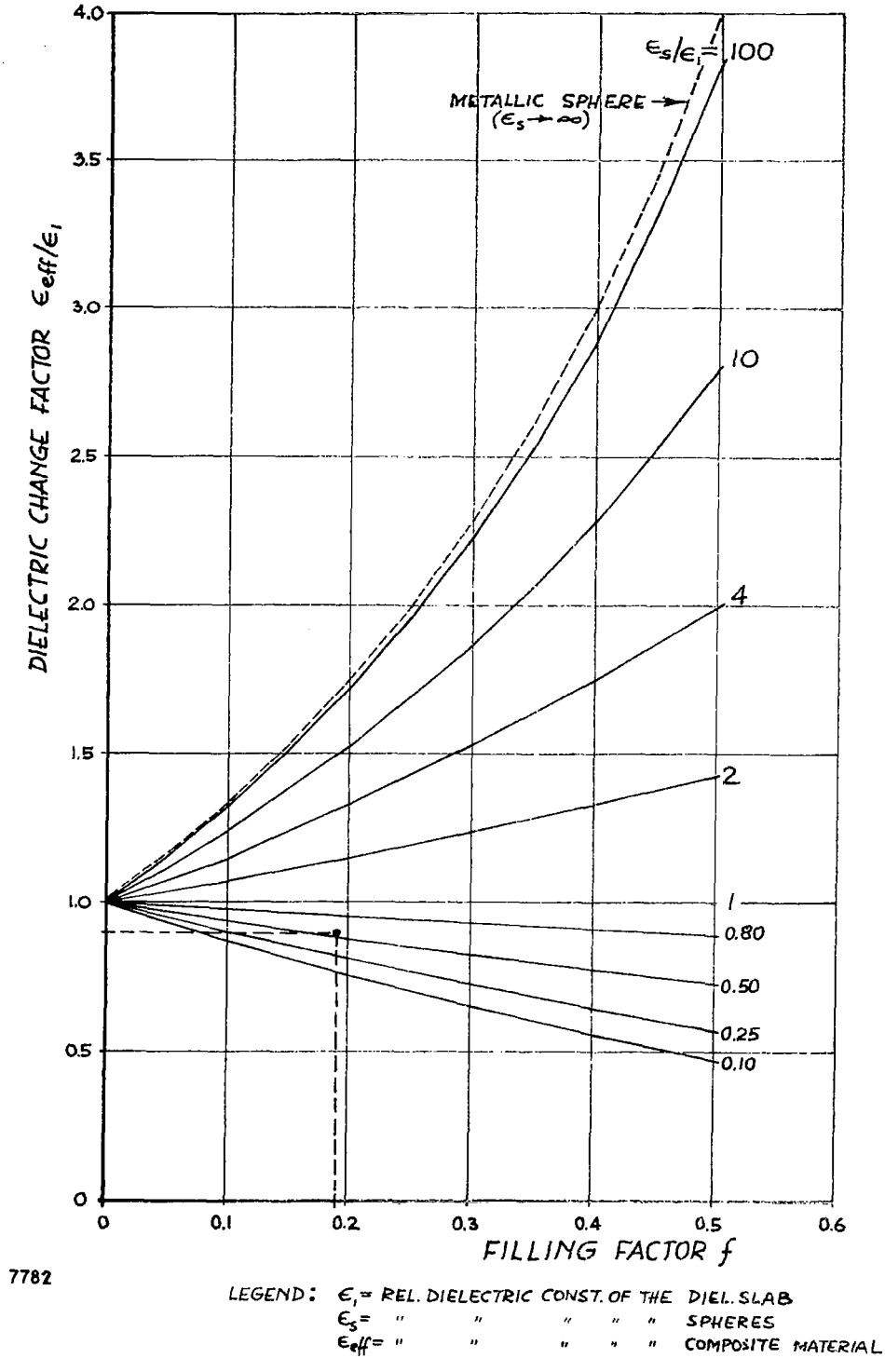

FIGURE 21. DIELECTRIC CHANGE FACTOR VS FILLING FACTOR

$$f = \frac{4\pi a^3}{3s^3} \tag{28}$$

Substituting the above values of f and s gives a = 0.036 cm. In like fashion other dielectric constant values can be achieved.

Array of holes in a dielectric medium. --The presence of an array of holes (dielectric constant ϵ_o) in a medium of relative dielectric constant ϵ_3/ϵ_o results in an effective relative dielectric constant that is less than ϵ_3/ϵ_o but greater than unity. No exact formulas exist but approximate formulas have been used in the design of quarter-wave transformers for surface matching. Reference 13 gives a formula for the ratio of hole area to total surface area (R_{hole}) required to match dielectrics ϵ_3 and ϵ_1, to each other. It is

$$R_{hole} = \frac{(\epsilon_3 + \epsilon_1)\left\{\epsilon_3 - p^2 - \left[(\epsilon_1 - p^2)\ (\epsilon_3 - p^2)\right]^{1/2}\right\}}{2\epsilon_3\,(\epsilon_3 - \epsilon_1)} \tag{29}$$

where $p = (\epsilon_1^{1/2} \sin\theta_1)$, and θ_1 is the angle of incidence. In our case $\epsilon_1 = 1$ (air holes) and $\theta_1 = 45^o$, hence

$$R_{hole} = \frac{(1 + \epsilon_3)\left\{\epsilon_3 - 1/2 - \left[(\epsilon_3 - \frac{1}{2})\ \frac{1}{2}\right]^{1/2}\right\}}{2\epsilon_3\,(\epsilon_3 - 1)} \tag{30}$$

The matching section is equivalent to a relative dielectric constant

$$\epsilon_2 = 1/2 + (\epsilon_3 - 1/2)^{1/2} \tag{31}$$

Thus, for example, air holes drilled in quartz $(\epsilon_r = 4)$ according to the above, would produce an artificial dielectric with $\epsilon_2 = 2.37$. For other values one can experimentally determine the variation of ϵ_2 with hole area. We also expect to develop a theoretical expression for hole area applicable to any desired ϵ_2 value. In any event, the use of artificial dielectrics, whether the design data are theoretically or experimentally determined, offers a practical method of obtaining the dielectric constant values required for fabricating low passband-ripple directional filters.

TUNERS

Adjustable impedance transformers or tuners are required in order that multiplier circuits present the desired generator and load impedances to the varactor. Considered herein are three basic types of quasi-optical waveguide tuners.

Type 1: The tuner consists of two equal fixed value susceptance gratings whose separation and distance from the load to be matched are variable; this tuner is illustrated in Figure 22.

Type 2: This tuner consists of two variable susceptance gratings that are located at fixed positions; Figure 23 shows one possible design. The variable susceptance is achieved by using slot-type apertures in each grating. Rotation of the grating produces a continuous range of susceptance values between the minimum value (slot axis perpendicular to the polarization direction) and the maximum (slot axis parallel to the polarization direction).

Type 3: A variable susceptance grating whose distance from the load is movable constitutes this tuner; it is the quasi-optical equivalent of a slide screw tuner. Figure 24 shows one possible embodiment. The variable susceptance is achieved by moving one plate relative to the other; the effective aperture areas are varied by prescribed misalignment of identical apertures within each metallic plate, thereby changing the susceptance value at that transverse plane. In addition, this variable susceptance plane can be moved along the longitudinal axis of the waveguide.

To assess the electrical properties of each type, the analysis of the conditions required for matching arbitrary loads and the resultant tuner dissipation losses are presented. In these analyses, the assumption is made that the oversized waveguide dissipation contribution is negligible compared to that of the susceptance gratings.

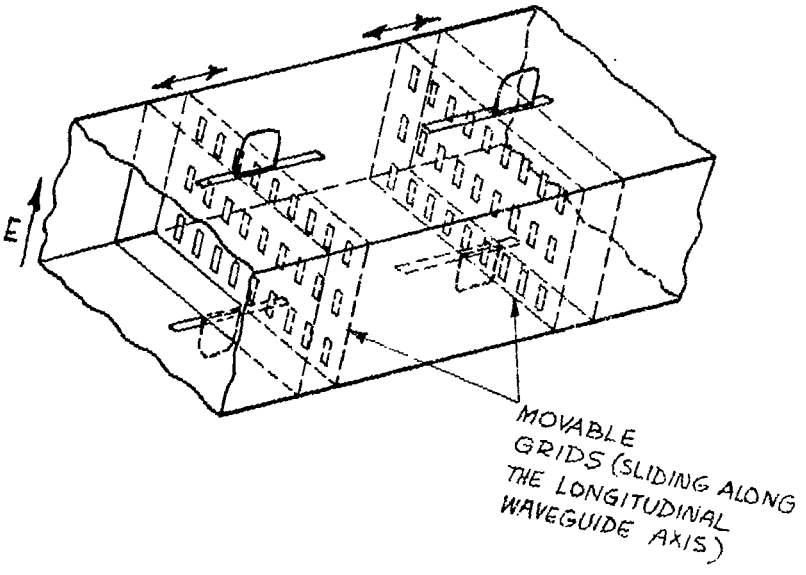

FIGURE 22. TYPE 1 TUNER

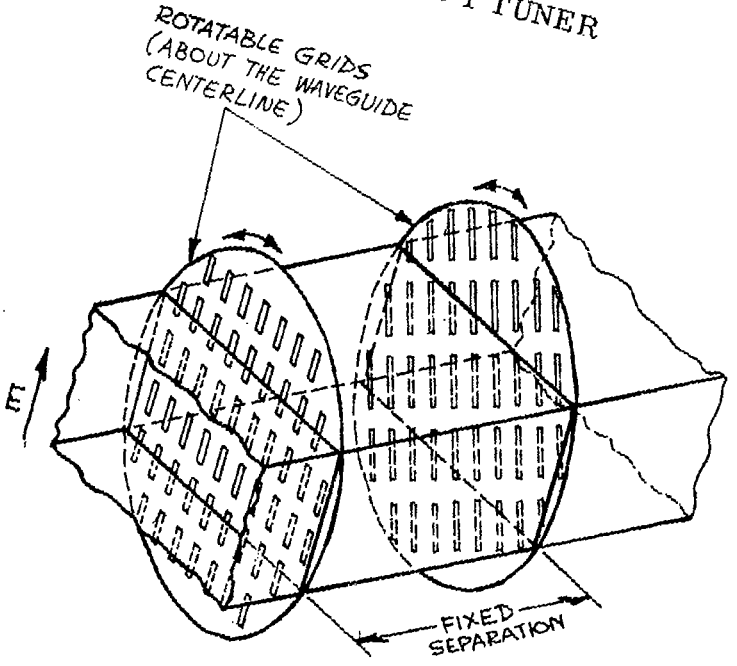

FIGURE 23. TYPE 2 TUNER

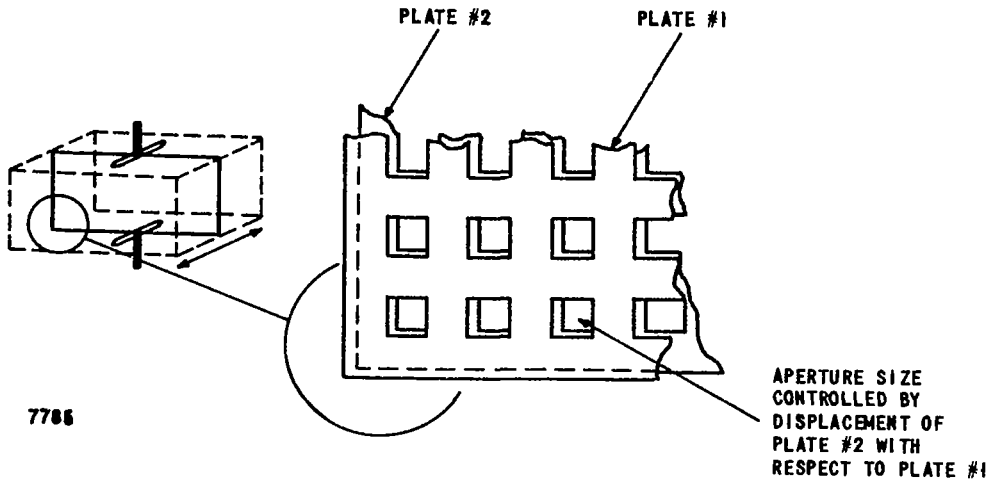

FIGURE 24. POSSIBLE TYPE 3 TUNER CONFIGURATION

Type 1 Tuner

Matching conditions.--By moving the position of plane aa relative to bb (variation of θ_L) in Figure 25, it is possible to present a load reflection coefficient of magnitude $|\Gamma_L|$ and of arbitrary phase ϕ. We have matched the load when $\Gamma_{aa} = |\Gamma_L| e^{-j\phi}$; Γ_{aa} is defined as the reflection coefficient looking to the left of aa. Since ϕ is arbitrary, the only new condition to be set is $|\Gamma_{aa}| = |\Gamma_L|$.

The value of Γ_{aa} is obtained from transmission line theory:

$$\Gamma_{aa} = \frac{j(b^2 \sin\theta - 2b\cos\theta)}{(2\cos\theta - 2b\sin\theta) - j(2\sin\theta - b^2\sin\theta + 2b\cos\theta)} \qquad (32)$$

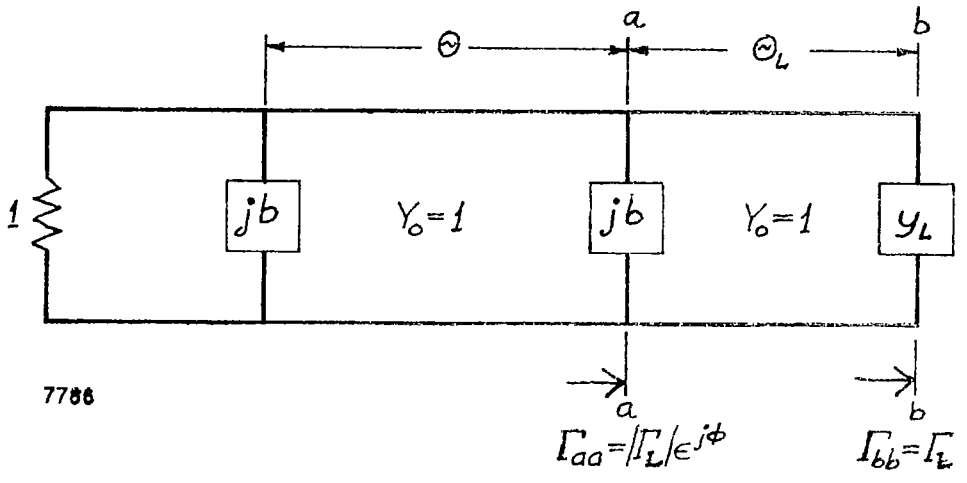

FIGURE 25. EQUIVALENT CIRCUIT OF A TYPE 1 TUNER

Letting $|\Gamma_L|^2 = a$, the matching condition is $|\Gamma_{aa}|^2 = a$ or

$$a = \frac{1}{1 + \frac{4}{b^4 + (4b^2 - b^4)\cos^2\theta - 2b^3 \sin 2\theta}} \tag{33}$$

where

b = normalized tuner susceptances

θ = separation between the two susceptances

A plot of a vs θ with two equal normalized susceptance values b as a parameter is shown in Figure 26; values of b of 0.50 cannot match any values of a greater than 0.21. Large b values give a greater range of matching effectiveness but the separation becomes critical when small values of a must

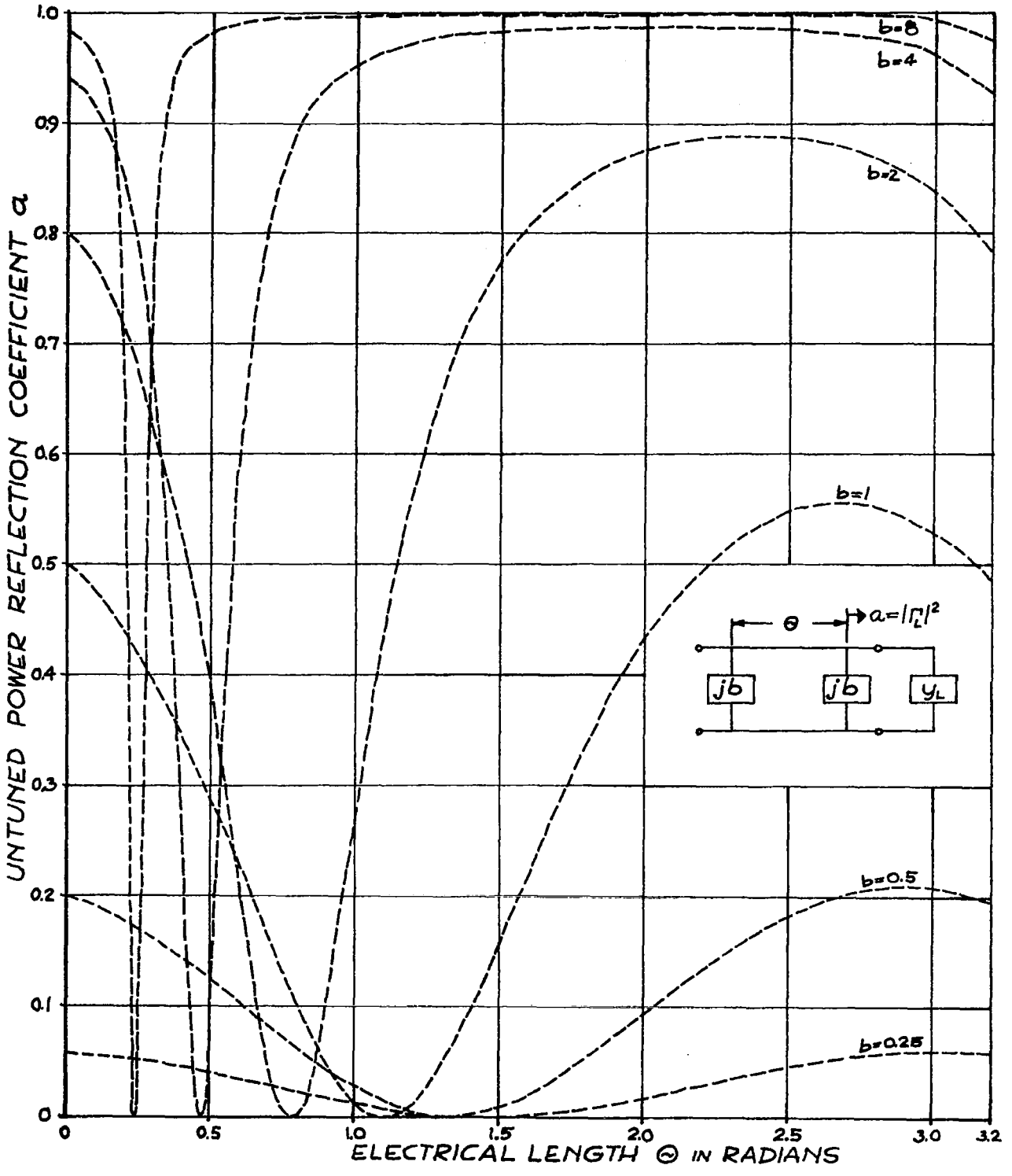

7787

FIGURE 26. TYPE 1 TUNER CHARACTERISTICS

be matched, as evidenced by the sharp notch in the high b curves. A choice of b = 2 appears to be a good compromise; it can tune out loads with a values from 0 to 0.88 (1 to 32 VSWR) and its low VSWR notch is not overly critical.

Dissipation loss. --The first step in the analysis of dissipation loss for the type 1 tuner is to obtain a suitable model; this model is related to the type of grating employed. We shall assume that the two equal susceptances will be formed from strip gratings of dimensions a, t, and γ as shown in Figure 27. This grating is characterized by a normalized reactance x = 1/b with losses represented by a series resistance, r; it is also convenient to represent the loss as a shunt resistance $g \approx x^2/r = xQ$ for $x/r << 1$. A formula for Q has been derived in Appendix C.

The second step is to calculate the tuner's insertion loss under different susceptance positions that match a variety of loads. Referring to Figure 28, we desire to calculate the insertion loss as a function of g with g_L or a as a parameter.

A table is given, Figure 28, that shows θ and ψ (the positions of the susceptances) for several g_L or a values. Using these θ and ψ values, the insertion loss is calculated with the aid of ABCD matrices.

The insertion loss is:

$$L = \frac{|A + B + C + D|^2}{4\, g_L} \tag{34}$$

where

$$g_L = \frac{1 + \sqrt{a}}{1 - \sqrt{a}} \tag{35}$$

and the ABCD terms are obtained from multiplication of the five matrices as shown:

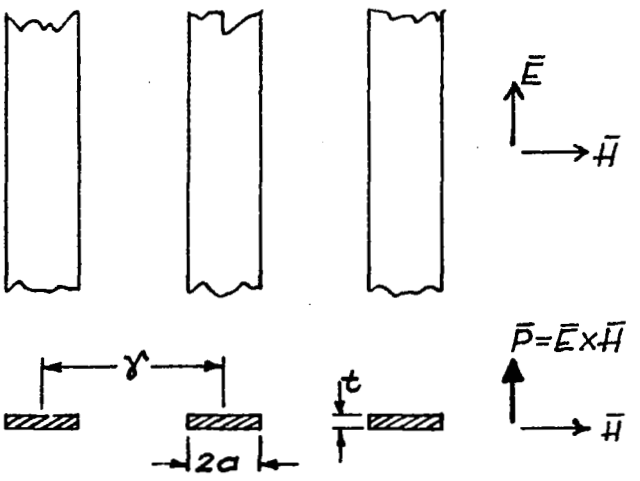

a) STRIP GRATING (TWO VIEWS)

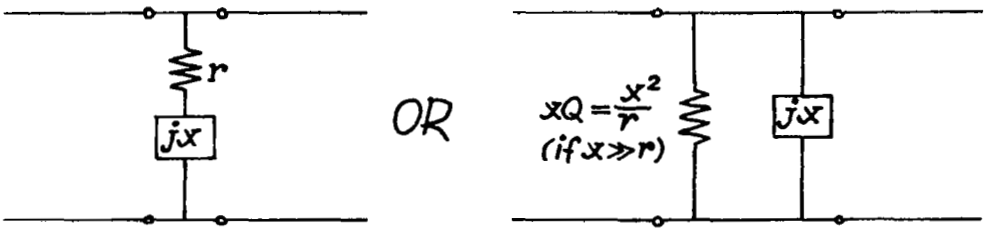

7788

b) NORMALIZED EQUIVALENT CIRCUITS

FIGURE 27. GRATING REPRESENTATION

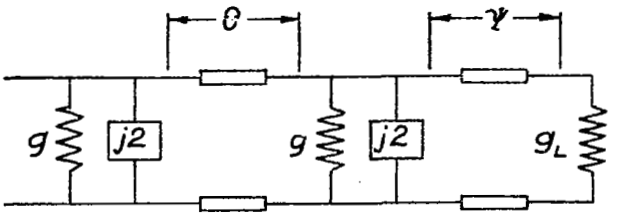

CURVE	Θ	Ψ	a	g_L
1	0	13.28°	0.80	18.05
2	45.8°	60.00°	0	1.00
3	57.3°	50.90°	0.27	3.15
4	68.7°	41.07°	0.51	6.00
5	80.2°	35.14°	0.72	12.35
6	91.6°	31.22°	0.80	18.05

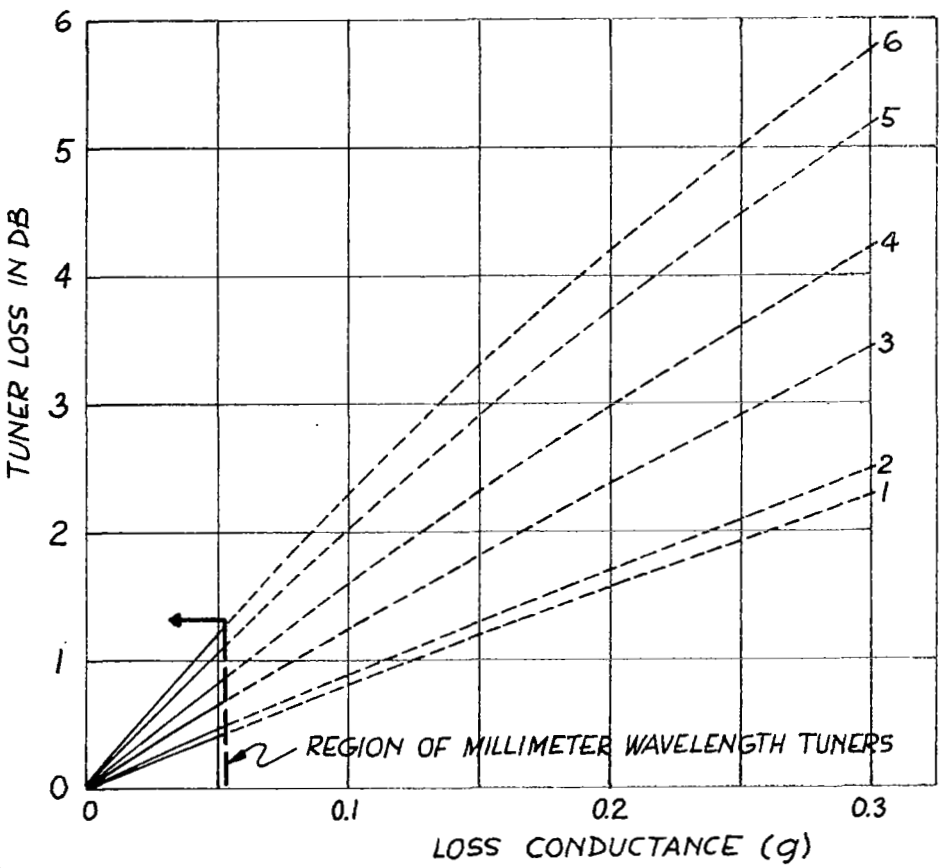

FIGURE 28. DISSIPATION OF A MOVABLE SUSCEPTANCE (TYPE 1) TUNER VS INCIDENTAL SHUNT CONDUCTANCE WITH g_L AS A PARAMETER

$$\begin{pmatrix} A & B \\ C & D \end{pmatrix} = \begin{pmatrix} 1 & 0 \\ (g + j2) & 1 \end{pmatrix} \begin{pmatrix} \cos\theta & j\sin\theta \\ j\sin\theta & \cos\theta \end{pmatrix} \begin{pmatrix} 1 & 0 \\ (g + j2) & 1 \end{pmatrix} \begin{pmatrix} \cos\psi & j\sin\psi \\ j\sin\psi & \cos\psi \end{pmatrix} \begin{pmatrix} 1 & 0 \\ (g - 1) & 1 \end{pmatrix} \tag{36}$$

The insertion loss vs g_L for various g values (and their corresponding θ and ψ values) was obtained with the aid of a digital computer and is shown in Figure 28.

The values of g for a metallic strip grating can be determined from Q formulas given in Appendix C. Examination of Figure 28 shows that $g = 0.1$ results in a tuner dissipation loss of 2.3 db or less; the g for the copper grating operating at 30 GHz (described in the Appendix C) is 1.33×10^{-3}. Its loss can be accurately determined by interpolation. Thus, an upper bound for the tuner loss is

$$L = \frac{2.33 \times 1.33 \times 10^{-3}}{0.1} = 0.031 \text{ db} \tag{37}$$

These results indicate that dissipation loss should be negligible in the example chosen. The loss increases only as the square root of frequency, hence these conclusions are probably accurate up to 300 GHz, where the estimated tuner loss is 0.1 db.

Type 2 Tuner

Matching conditions.--The ability of this device to match a wide range of impedances is a function of the separation between the variable susceptances. An equivalent circuit of this tuner is given in Figure 29 and the analysis for the case of $3/8\lambda$ separation is given in Appendix D. Other separations ($\lambda/4$ and $\lambda/2$) have also been considered but they are more limited. Thus, only the best case is presented. The analysis shows that any conductance equal to or

less than 2 and any value of susceptance can be matched. For any reasonably high Q varactor, the conductance should be considerably less than 2. It thus appears that this type of matching is theoretically adequate. Practical limits on the range of susceptance will further restrict the matching range.

Dissipation loss.--With the aid of Appendix D one obtains for the lossless $3/8\lambda$ separation case:

$$b_1 = -1 \pm \sqrt{(2/g) - 1} \tag{38}$$

$$b_2 = (b - 1) \pm g \sqrt{(2/g) - 1} \tag{39}$$

where $g + jb$ represents the admittance to be matched and b_1, b_2 are the two tuner susceptances. For simplicity, assuming $b = 0$ and considering only the $b_1 = -1 + \sqrt{(2/g) - 1}$ case, which consequently results in $b_2 = -1 + g \sqrt{(2/g) - 1}$ representing the "matching" condition, let us introduce tuner losses. The equivalent circuit is shown in Figure 30. The tuner grating losses are designated as $\alpha |b_1|$ and $\alpha |b_2|$, where α is closely related to a reciprocal of grating Q factor, that is $g_i \approx |b_i|/Q_{ui}$. This relation, we believe, could be reasonably assumed to be true within a small multiplying factor (of 2 or 3) from the point of grating current considerations for high and low susceptance limits. The equivalent circuit in Figure 30 is accompanied by the element ABCD matrices and the insertion loss equation. The results are plotted in Figure 31 in terms of tuner insertion loss (both gratings included) vs r, the normalized load resistance ($r = 1/g$). The range of $10 < r < 100$ should include the practical application values for low-loss varactor loads. Referring to Appendix C, where Q's of strip gratings are analyzed, the practical Q values are estimated at about 1500, hence the expected tuner losses should be at or below 0.2 db in a given practical varactor multiplier application.

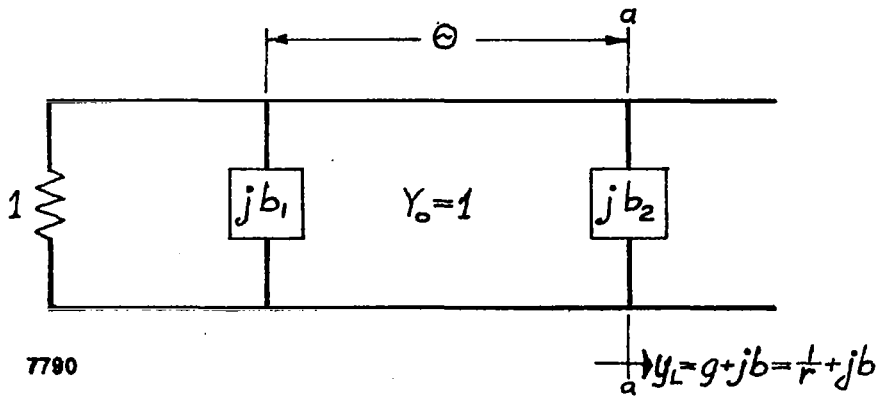

FIGURE 29. EQUIVALENT CIRCUIT OF A LOSSLESS TYPE 2 TUNER

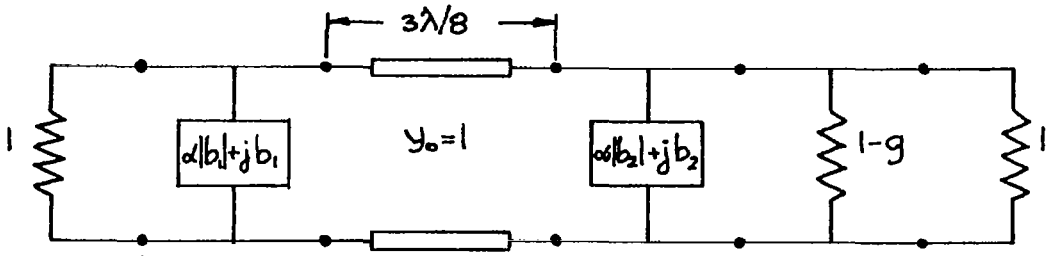

$$\begin{bmatrix} 1 & 0 \\ (\alpha|b_1|+jb_1) & 1 \end{bmatrix}\begin{bmatrix} -1/\sqrt{2} & j/\sqrt{2} \\ j/\sqrt{2} & -1/\sqrt{2} \end{bmatrix}\begin{bmatrix} 1 & 0 \\ (\alpha|b_2|+jb_2) & 1 \end{bmatrix}\begin{bmatrix} 1 & 0 \\ (g-1) & 1 \end{bmatrix}=\begin{bmatrix} A & B \\ C & D \end{bmatrix}$$

where: $b_1=-1+\sqrt{(2/g)-1}$

$$b_2=-1-g\sqrt{(2/g)-1}$$

$$\alpha\approx 1/Q_u$$

$$I_L=\frac{|A+B+C+D|^2}{4g}$$

7791

FIGURE 30. LOSSY TYPE 2 TUNER REPRESENTATION

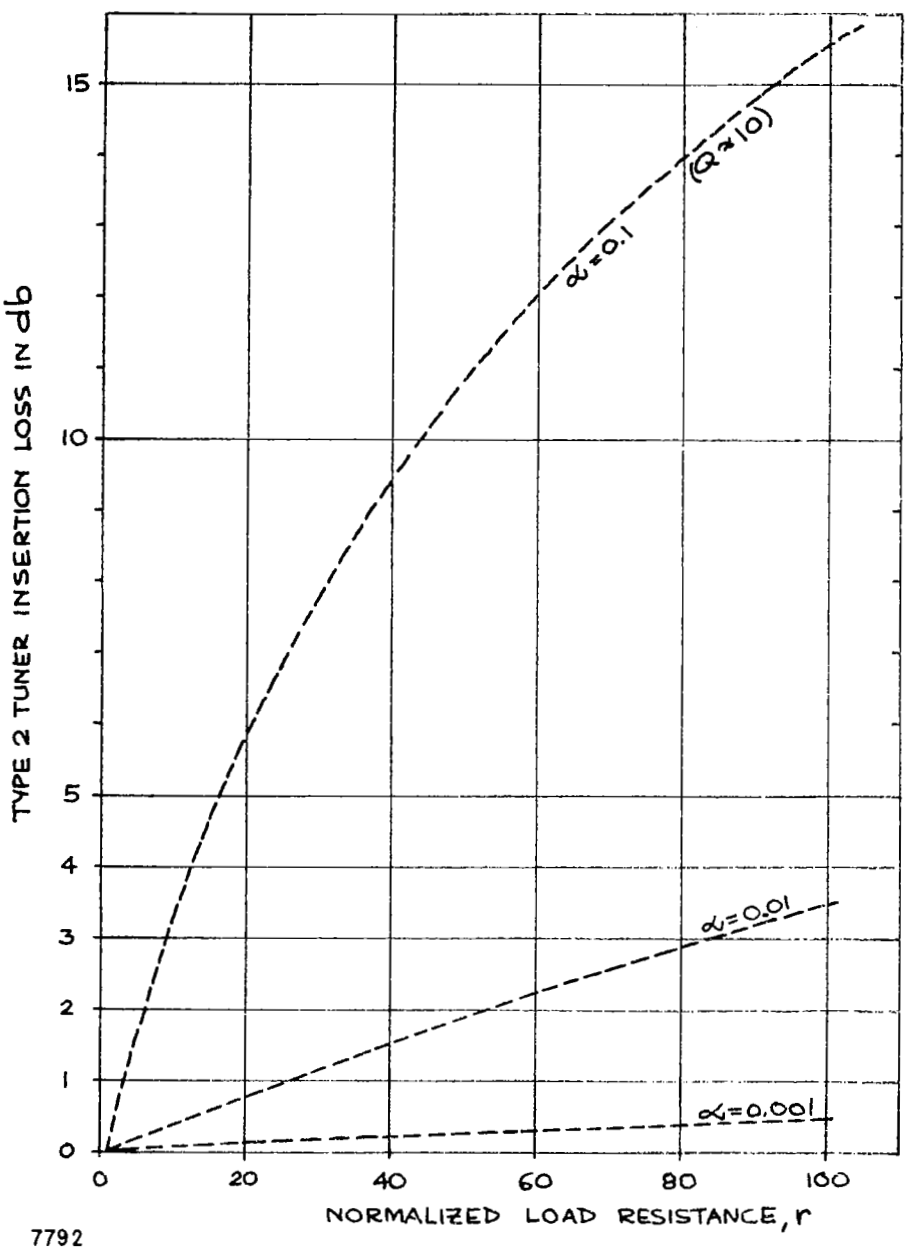

FIGURE 31. TYPE 2 TUNER LOSSES

Type 3 Tuner

Matching conditions.--The schematic for analysis purposes is an exact equivalent of a slide-screw tuner within a regular waveguide as shown in Figure 32. The complex load admittance y_L, to simplify the analysis, is viewed from a plane at some distance toward the generator where it can be represented as a conductance g_L. In other words, representing this operation on the Smith Chart, we have added a segment of transmission line in front of the load y_L necessary to rotate it along the constant VSWR line into the constant resistance (or conductance) axis. Furthermore, to facilitate the use of the ABCD matrix in the analysis, the load conductance is represented as shown in Figure 32B. From the ABCD matrix:

$$\begin{pmatrix} A & B \\ C & D \end{pmatrix} = \begin{pmatrix} 1 & 0 \\ jb & 1 \end{pmatrix} \begin{pmatrix} \cos\theta & j\sin\theta \\ j\sin\theta & \cos\theta \end{pmatrix} \begin{pmatrix} 1 & 0 \\ (g_L - 1) & 1 \end{pmatrix} \tag{40}$$

the input admittance at a plane immediately in front of the tuner susceptance sheet, looking toward the load is:

$$y_{in} = \frac{g_L + j\,[b\cos^2\theta + b g_L^2 \sin^2\theta + (1 - g_L^2)\sin\theta\cos\theta]}{\cos^2\theta + g_L^2 \sin^2\theta} \tag{41}$$

The matching conditions then are obtained equating $g_{in} = 1$ and $b_{in} = 0$ and reducing the resultant expressions of the position and susceptance parameters in terms of the load conductance as given below:

$$\ell = \frac{\lambda_g}{4\pi} \cos^{-1}\left(\frac{g_L - 1}{g_L + 1}\right) \tag{42}$$

$$b = \frac{g_L - 1}{\sqrt{g_L}} \tag{43}$$

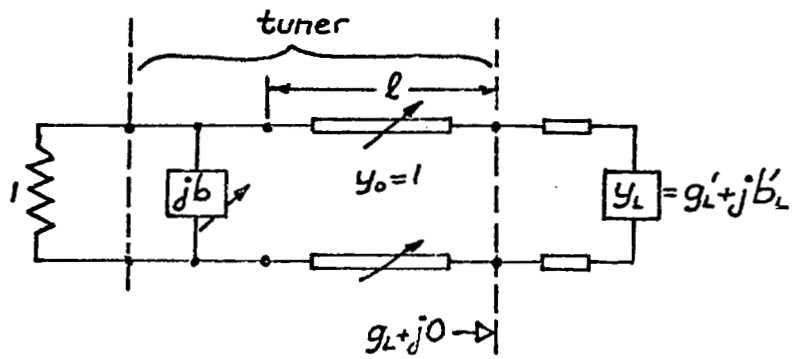

a) EQUIVALENT CIRCUIT OF LOSSLESS TYPE 3 TUNER

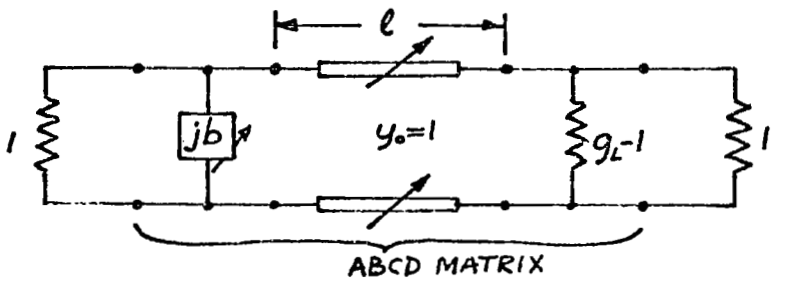

b) SAME CIRCUIT IN A FORM SUITABLE FOR ABCD MATRIX ANALYSIS

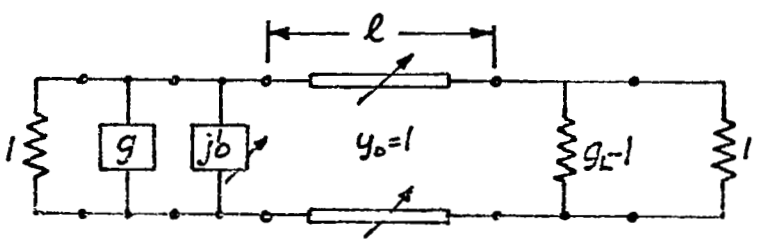

7793

c) EQUIVALENT CIRCUIT OF A LOSSY TYPE 3 TUNER

FIGURE 32. TYPE 3 TUNER

where 1 is equal to the distance between the susceptance plane and the reference plane where the complex load appears as a pure conductance.

The above expressions are valid for all values of g_L, greater or smaller than unity ($g_L = 1$ being a trivial case). The susceptance spread required to tune out the load mismatches can be seen in Figure 33 where $|b|$ vs VSWR is shown (+b is required when VSWR value corresponds to g_L, -b when VSWR corresponds to $r_L = 1/g_L$). Distance ℓ (defined previously) varies between $0.1\lambda_g$ and $0.01\lambda_g$ when $200 < g_L < 2$; for $200 < r_L < 2$ parameter ℓ varies between $0.15\lambda_g$ and $0.24\lambda_g$. Considering the maximum additional (slightly less than $0.25\lambda_g$) length that may be required to transform the complex admittance into a pure real (conductance) value, the desirable travel distance of the variable susceptance plate would approach a half wavelength, if the maximum possible tuning range is desired.

Dissipation.--The losses are introduced for the susceptance plate only in the form of a shunt conductance, which--as in the previous two types of tuners--can be assumed to be directly proportional to the magnitude of the susceptance and inversely to the unloaded Q of the susceptance plate, that is, $g \approx |b|/Q_u$. The new schematic, shown in Figure 32C, will have the element jb changed to g + jb. The insertion loss is obtainable from

$$L = 10 \log \frac{|A + B + C + D|^2}{4g_L} \tag{44}$$

with the previously determined matching conditions applied. This results in

$$L = 10 \log \left(1 + \frac{g}{2}\right)^2 \tag{45}$$

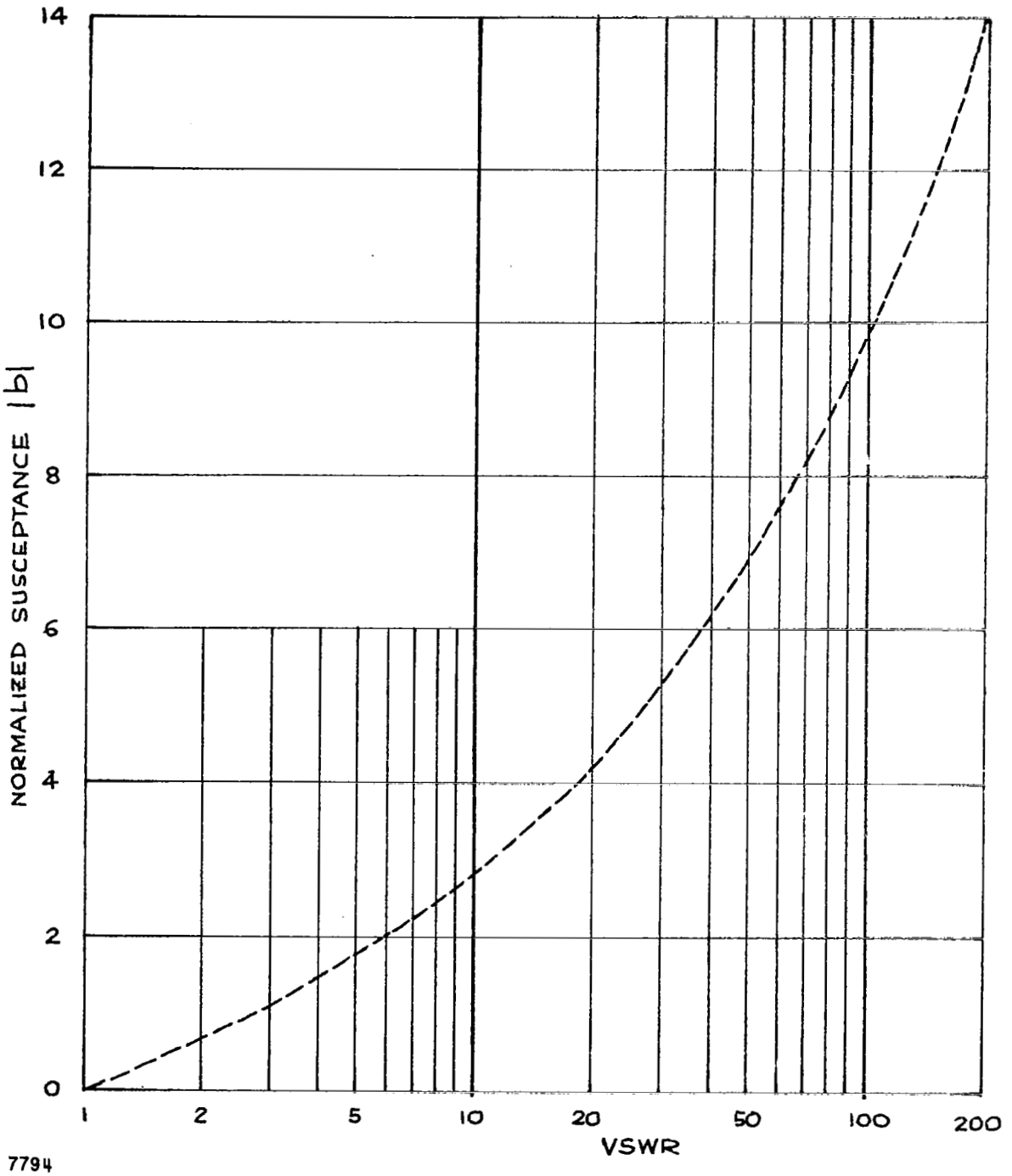

FIGURE 33. NORMALIZED SUSCEPTANCE OF TYPE 3 TUNER VS VSWR

but since

$$g \approx |b|/Q_u = \left| \frac{g_L - 1}{Q_u \sqrt{g_L}} \right| \tag{46}$$

the final expression becomes:

$$L = 20 \log \left(1 + \left| \frac{g_L - 1}{2Q_u \sqrt{g_L}} \right| \right) \tag{47}$$

The insertion loss versus VSWR (before tuning), is shown in Figure 34 for Q_u = 10, 100, and 1000. Due to the absolute value term in the insertion loss expression, VSWR in this case corresponds directly to g_L or r_L magnitude. Here again, for susceptance Q's in excess of 1000, the tuner loss is small; it is under 0.1 db.

Comparison of Tuner Types

The analyses of the three types of tuners indicate that type 2 has a limited range of impedances that it can tune and is therefore least desirable. Types 1 and 3 are not so limited. All tuner types have low dissipation loss (less than 0.2 db). The preferred tuner is type 3 because it is the one most likely to produce a broader band match; this is because tuning can be placed closer to the varactor mount than is possible with the type 1 tuner. The subsequent discussion of practical tuner realizations will stress the type 3 tuner.

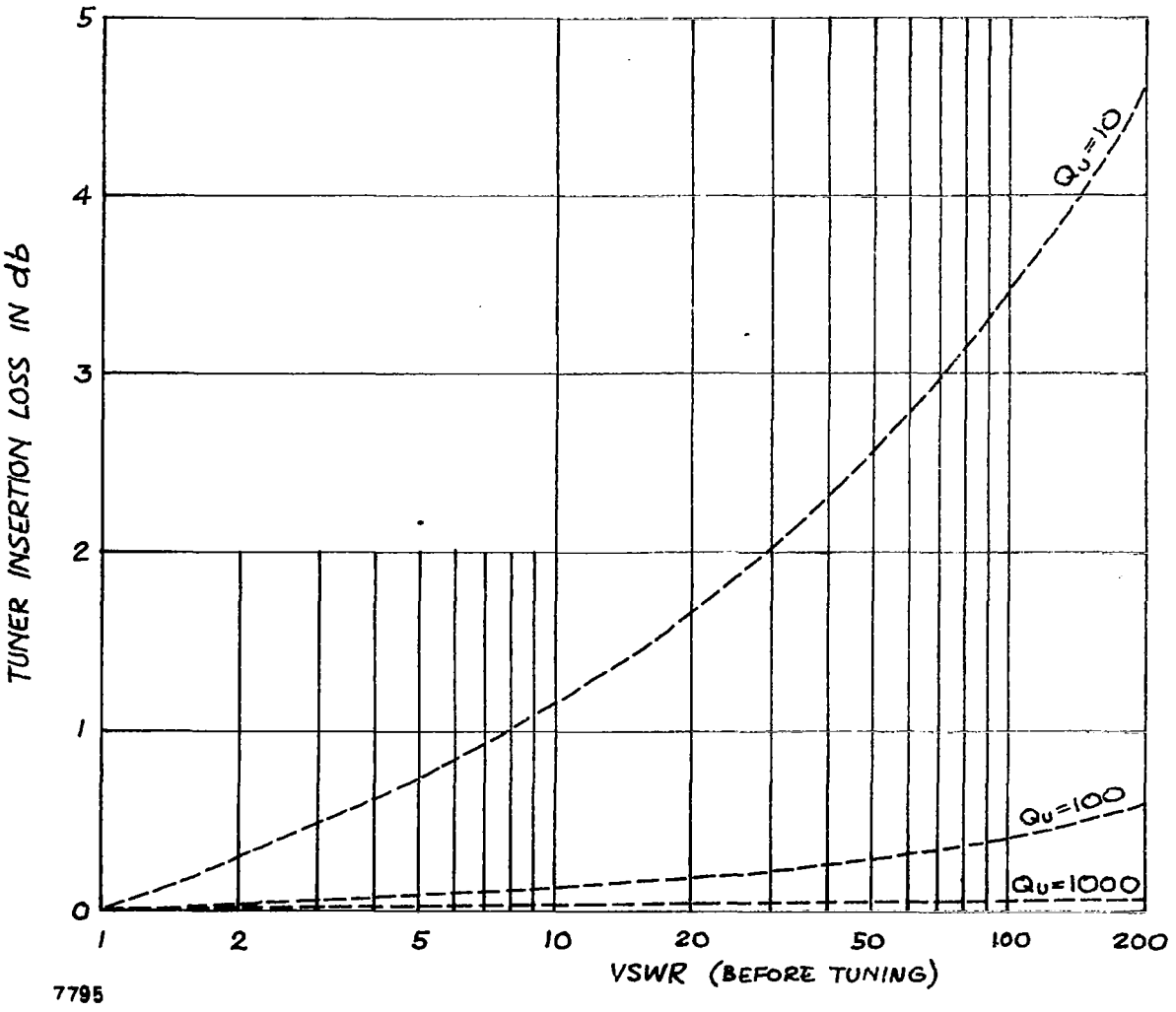

FIGURE 34. TYPE 3 TUNER INSERTION LOSS VS VSWR WITH TUNER PLATE Q_u AS A PARAMETER

Mechanical Design Considerations (Type 3 Tuner)

The mechanical design of the type 3 tuner is essentially that of realizing a susceptance that is variable in value and position along an oversized waveguide. One possible design is shown in a cross section side view in Figure 35.

The variable susceptance consists of two thin dielectric (probably quartz) slabs. One surface side of each dielectric slab contains a deposited metal grid-work containing a pattern of evenly spaced square (or rectangular) holes within a metallic sheet, as shown in Figure 36, or horizontal and vertical metallic lines. Both slabs have identical grid patterns and, when assembled the metallic sides will face each other, but will not contact each other or the waveguide walls at any point on the metal surface.

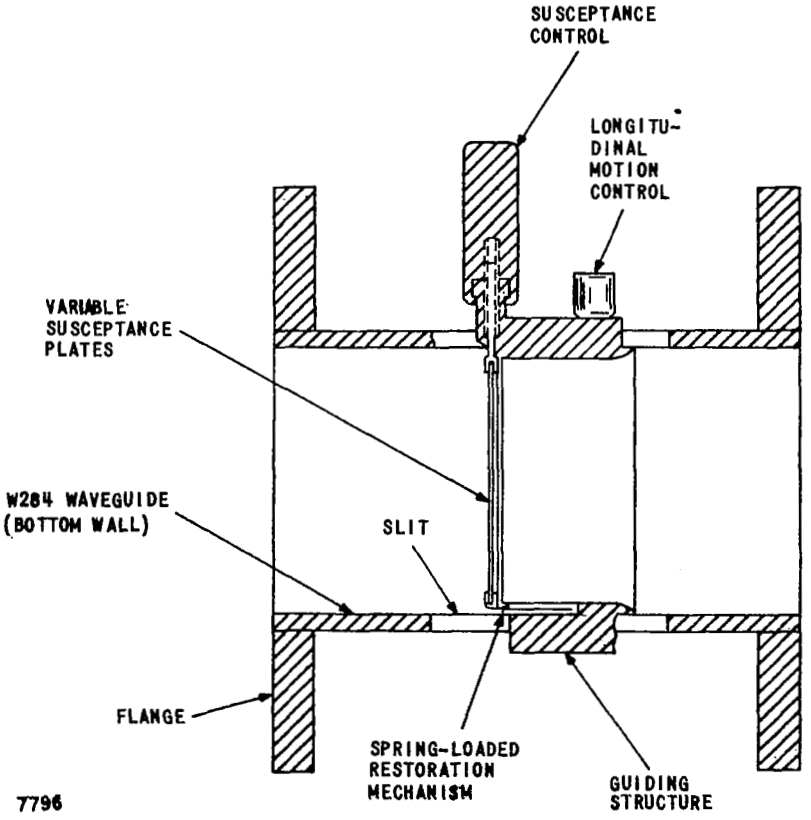

FIGURE 35. SIDE VIEW OF TYPE 3 TUNER

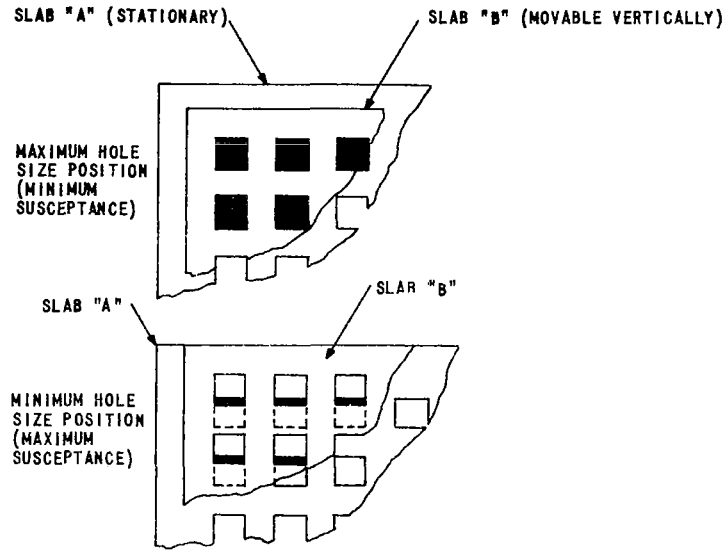

FIGURE 36. SUSCEPTANCE VARIATION PRINCIPLE

One of the two dielectric slabs, marked A on Figure 36, would be stationary, and the other would move in the vertical direction. This results in changing geometrical configurations of the rectangular grid holes from square to rectangular slits, as illustrated in Figure 36, thereby changing the susceptance value of the combined susceptance plate.

The mechanical means of susceptance variation within the plate and the longitudinal motion of the combined plate and its guiding structure within the waveguide are illustrated in Figure 37. The slits on the top and the bottom waveguide walls are located at electrically inert surface areas (where the

electromagnetic currents are parallel to the slit), and the gear mechanism is to keep the susceptance plate perpendicular to the longitudinal waveguide axis at all times to reduce the possibility of generation of higher order modes within the waveguide.

Additional Tuner Design Problems

The practical design of tuners with moving and variable susceptances produces some effects which are considered herein.

Moving susceptance effects.--Tuner designs requiring moving susceptances (including types 1 and 3) can be designed with sliding contacts or without any contacts. The sliding contact approach implies the use of spring fingers which ultimately create intermittent difficulties. Thus, we prefer the noncontacting approach provided its effect can be tolerated. The effect of no contacts on the susceptance of a tuner plate is considered below.

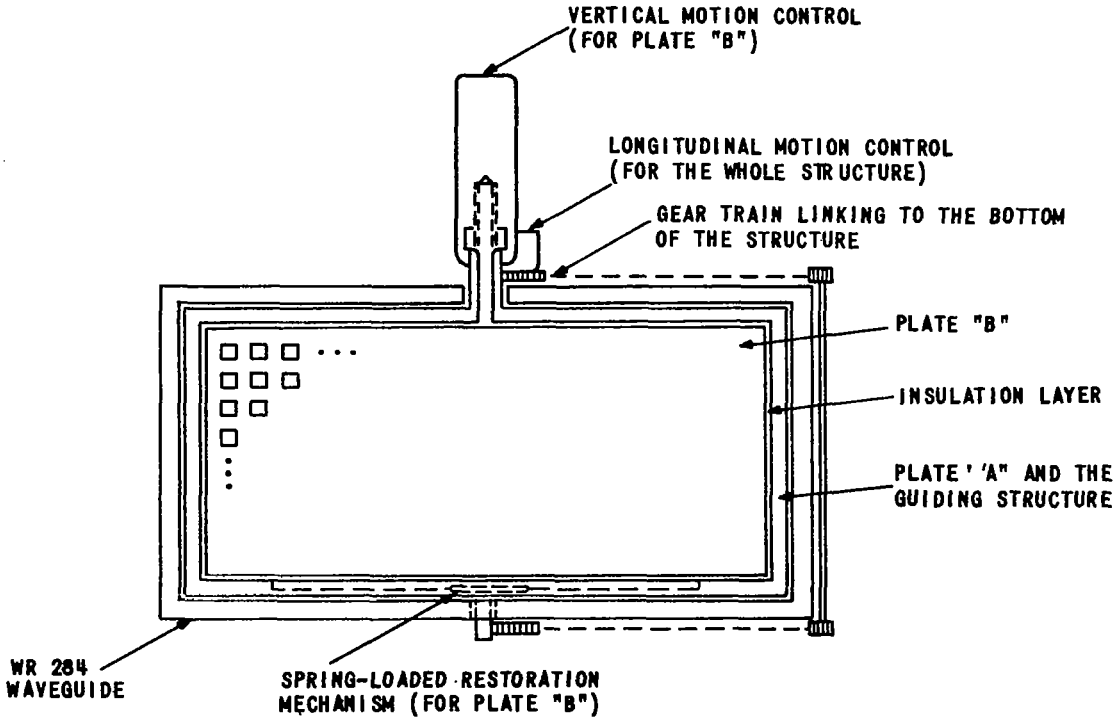

7798

FIGURE 37. FACE VIEW OF TYPE 3 TUNER

Let us assume that a tuner susceptance is removed from the four waveguide walls by an air gap of width d as shown in Figure 38. The air gap will add four reactances in series with the desired reactance X_p. The sum of the horizontal gap reactances (X_h) is given in Marcuvitz (reference 14). By using the relations for a capacitive obstacle with d << b one obtains

$$X_h \approx - \frac{\lambda_g}{2b \ln\left(\frac{2b}{\pi d}\right)} \tag{48}$$

Similarly for X_v one uses the relation for inductive obstacles with d << a. This yields

$$X_v \approx \frac{2a}{\lambda_g}\left(\frac{\pi d}{2a}\right)^4 \tag{49}$$

For the oversize waveguide size of current interest a = 2.84" and b = 1.42 "; the gap d may be as large as 0.003". For these values one obtains at 30 GHz (λ_g = 0.39"), $X_h = 1.1 \times 10^{-10}$ and $X_v = 1.33 \times 10^{-2}$. The sum of these two values is essentially X_v.

The X_v value is a factor only in so far as it adds to the desired reactance. When tuning out low VSWR's the desired reactance will generally be at least 100 times greater than X_v and is therefore negligible. For large VSWR's X_p may have to be as low as 0.1, in which case X_v has a 13 percent effect. While not negligible, it does not limit the ability of the device to tune out large VSWR's.

In summary, a noncontacting susceptance will behave satisfactorily and is, therefore, the preferred approach.

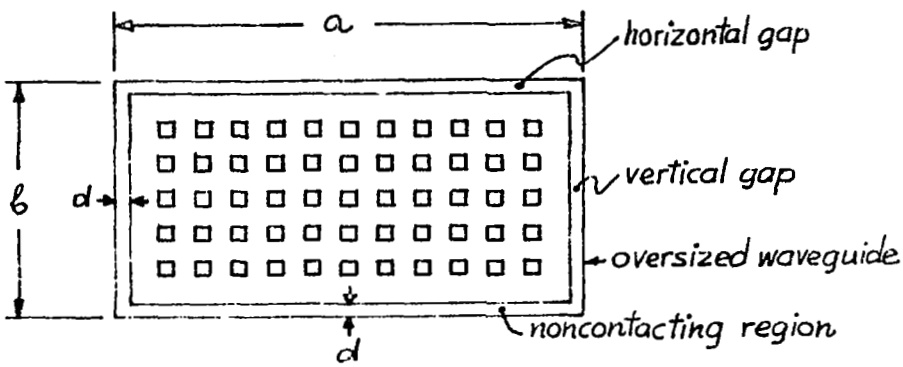

a) Tuner Plate

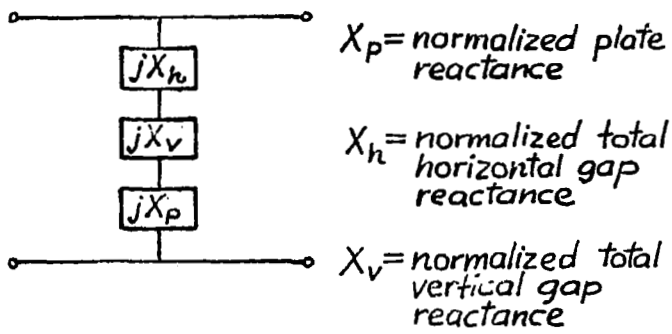

b) Equivalent Circuit

7799

FIGURE 38. NONCONTACTING TUNER PLATE REPRESENTATION

Effect of a dielectric substrate on tuner performance. --It may be necessary to form the susceptance on a dielectric substrate. A susceptance formed by etching a metal surface that was vacuum deposited on a dielectric (such as quartz) substrate (Figure 39) will be a function of the dielectric constant and its thickness. This can be represented by its composite ABCD matrix.

$$\begin{bmatrix} 1 & 0 \\ jb & 1 \end{bmatrix} \begin{bmatrix} \cos \phi_\epsilon & j Z_\epsilon \sin \phi_\epsilon \\ j \frac{\sin \phi_\epsilon}{Z_\epsilon} & \cos \phi_\epsilon \end{bmatrix} \tag{50}$$

where

$$\phi_\epsilon = \frac{2\pi t \sqrt{\epsilon_r}}{\lambda_g}$$

t = Dielectric thickness

$Z_\epsilon = 1/\sqrt{\epsilon_r}$, the normalized impedance

The net ABCD values are

$$A = \cos \phi_\epsilon, \quad B = j Z_\epsilon \sin \phi_\epsilon$$

$$C = j \left[b \cos \phi_\epsilon + \frac{1}{Z_\epsilon} \sin \phi_\epsilon \right] \tag{51}$$

$$D = \cos \phi_\epsilon - bZ_\epsilon \sin \phi_\epsilon$$

In one design, the thickness can be chosen such that $\phi_\epsilon = \pi$ and 2π at the fundamental and second harmonic respectively. For this case:

$$A = 1, \quad B = 0, \quad C = jB, \quad \text{and} \quad D = 1$$

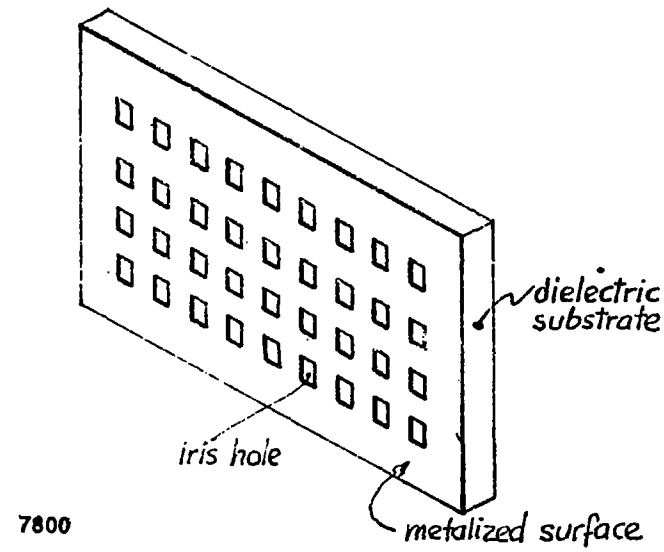

FIGURE 39. SUSCEPTANCE FORMED ON A SUBSTRATE

This would be equivalent to a pure shunt susceptance at the frequencies of interest and the tuner would therefore be unaffected by the presence of the dielectric.

In another case one may have an electrically thin ($\phi_\epsilon << 1$) dielectric. The ABCD values become:

$$A \approx 1,\ B = j\,\phi_\epsilon,\ C = j\,(b + \phi_\epsilon / Z_\epsilon) \qquad (52)$$

$$D = 1 - b\,Z_\epsilon \phi_\epsilon$$

The voltage transfer coefficient is:

$$T = \frac{2}{A + B + C + D} = \frac{2}{2 - b Z_\epsilon \phi_\epsilon + j [b + \phi_\epsilon (Z_\epsilon + 1/Z_\epsilon)]} \tag{53}$$

Examination of T shows that for:

$$b = - \phi_\epsilon (Z_\epsilon + 1/Z_\epsilon) \tag{54}$$

$$T = \frac{2}{2 + \phi_\epsilon^2 Z_\epsilon (Z_\epsilon + 1/Z_\epsilon)} \approx 1 \tag{55}$$

and for $b \longrightarrow \infty$, $T \longrightarrow 0$.

Values of T between 0 and 1 are obtained for intermediate values of b. Since the network is lossless, the magnitude of the reflection coefficient is

$$|\Gamma| = \sqrt{1 - |T|^2} \tag{56}$$

Thus $|\Gamma|$ can be set to any value between 0 and 1 by varying b and the effect of the substrate is therefore not serious.

Concluding Remarks

The theoretical investigation of tuners indicates that the type 3 tuner is the most desirable. A preliminary mechanical design appears to be feasible. It is believed that the next step is the construction and evaluation of the type 3 tuner. This work will be undertaken on a future NASA ERC contract.

VARACTOR MOUNTING TECHNIQUES AND REPRESENTATION

General Remarks

A varactor or a group of varactors constitute the most important part of a varactor frequency multiplier; selection of a suitable varactor and imbedding (mounting) it properly within the circuit determines the multiplier efficiency and mode of operation. Presently, the varactor mounting techniques and their equivalent circuit representations are little-explored areas in the quasi-optical frequency multiplier component design field.

Several years ago, when only the encapsulated varactors in a pill or so-called double-ended package were commercially available, the problems they caused at high frequencies (starting at K-band) were stemming from parasitic package inductances or stray capacitance and the comparatively low self-resonance frequencies. With the recent introduction of the beam-lead varactors (and varistors as well) into the market the parasitic susceptance effects become less prominent. The efficiencies of such varactors at multimeter wavelength are improved by quite a margin. The problem still present in the multiplier circuit design concerns efficient varactor mounting techniques--proper impedance matching, lossless connections, and reduced parasitic susceptance elements in the mount.

Most of the results of varactor multiplier design theory developed for multiplier circuits in the conventional single-mode transmission line, like input/output impedance tuning, power handling, and efficiency predictions, are most likely applicable to quasi-optical varactor multiplier circuits without major modifications. Yet now the varactor imbedding circuits must be developed to reflect the oversize waveguide propagation techniques--proper interception of the energy propagating in the oversize waveguide, minimum possibility of excitation of higher order modes, crosspolarization of fields in the waveguide, etc.

After a careful consideration of various factors, advantages, practical realizability and limitations, the acceptable basic varactor mounting configurations have been reduced to three:

1. Focused varactor mount (single varactors)
2. Large varactor array mount
3. Partially focused small varactor array mount

These three basic mounts are shown in Figure 40 and discussed below.

Varactor Mounting Techniques

Focused varactor mounts. --This varactor mount consists of a single varactor situated within or without the oversized waveguide area and a focusing device (lens or reflector), as shown in Figure 41.

The energy focusing devices, such as dielectric lenses or conducting metal reflectors, have an inherent imperfection, or so-called circle of confusion, at their focal point at finite incident wavelengths. The diameter d of this circle of confusion (or "focal point diameter") can be expressed in terms of the focal length of the device F, incident wavelength λ, and aperture dimension D (diameter of a circular antenna aperture or side length of a square antenna aperture) in this manner.

$$d = \frac{F \lambda k}{D} \tag{57}$$

The constant k usually assumes values $0.89 \leq k \leq 1.5$ depending on the illuminated aperture edge contour shape and the incident power distribution.

Actually, the circle of confusion is part of a fringe pattern of the power reflected by the antenna at its focal plane, shown in Figure 42. The circle of confusion diameter is defined as the distance between half-power points (3 db below peak reflected power) of the main lobe. From the equation, it

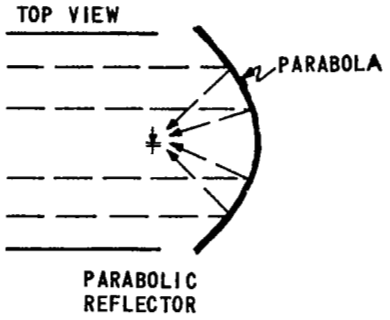

A. SINGLE DIODE FOCUSSING

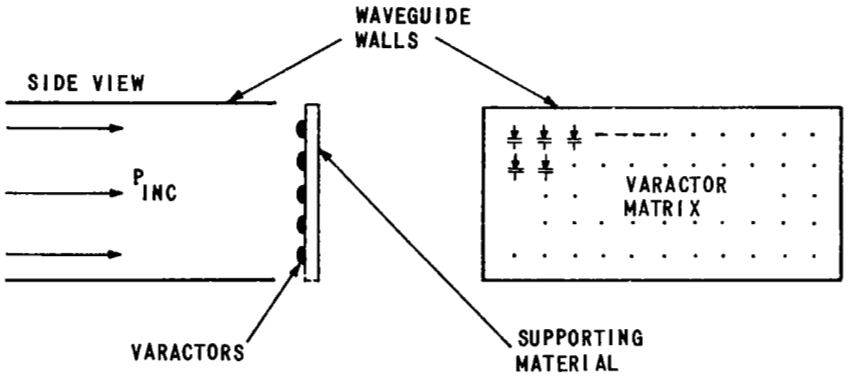

B. VARACTOR ARRAY

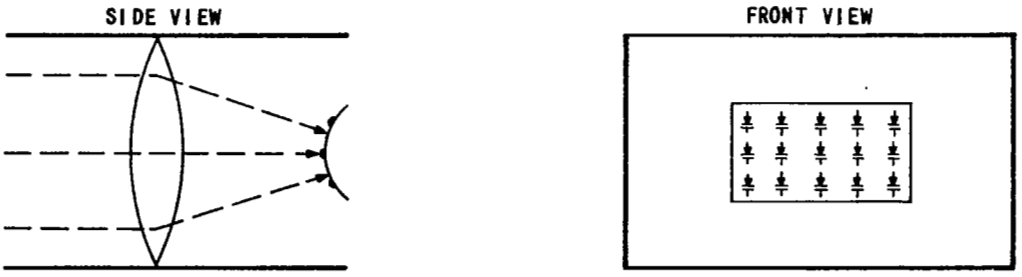

7801

C. PARTIAL FOCUSING

FIGURE 40. VARACTOR MOUNTING TECHNIQUES

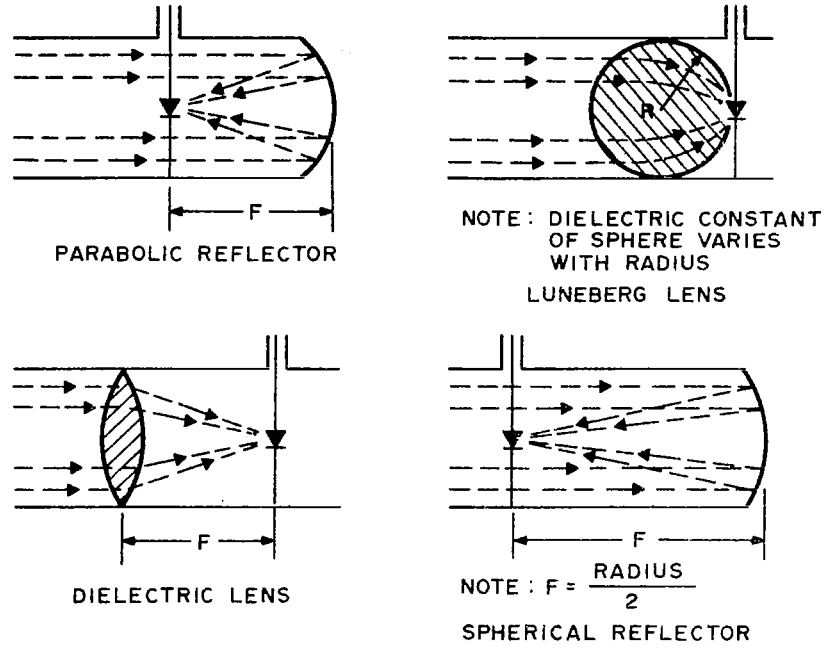

A. VARACTOR FOCUSING DEVICES (SIDE VIEW)

F = FOCAL LENGTH
d = FOCAL POINT DIAMETER
● = DIODE

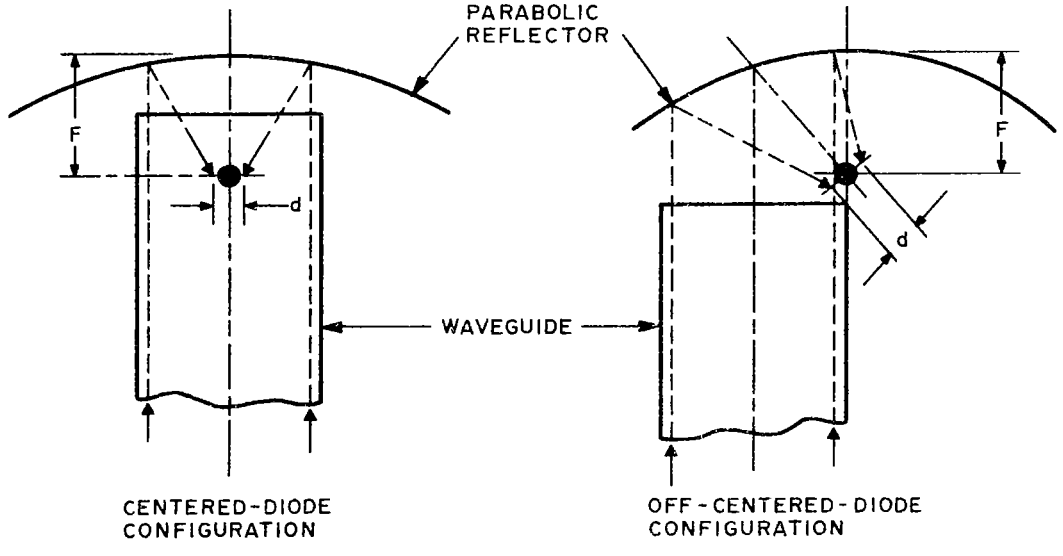

4489

B. VARACTOR MOUNTING CONFIGURATION (TOP VIEW)

FIGURE 41. FOCUSED VARACTOR MOUNTS

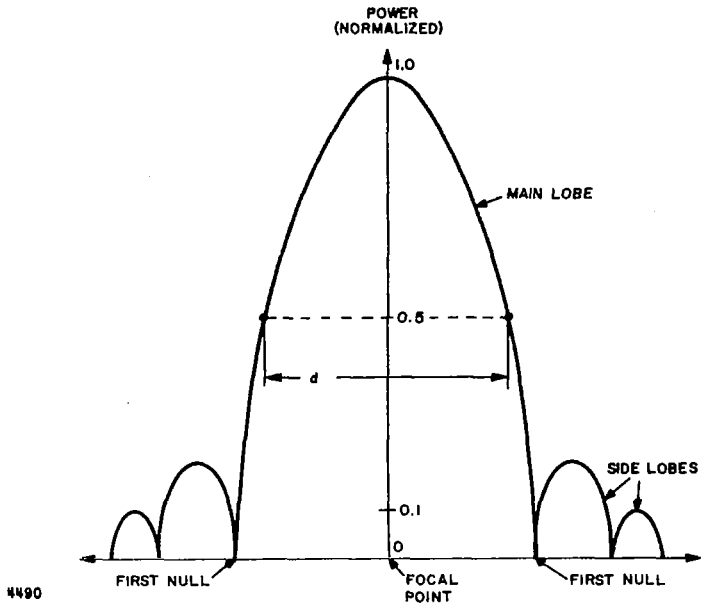

FIGURE 42. FRINGE PATTERN AT FOCAL PLANE

is evident that the circle of confusion would be negligible (that is, ideal point-focus solution of geometric optics applies), if the illuminated aperture is very large, as in a case of antenna dishes, or the wavelength is very small (for example, visible light spectrum). In our case neither is true. The energy density in an oversize waveguide is not evenly distributed as in a plane wave case over the cross-sectional area of the waveguide, but rather resembles TE_{10} mode distribution (that is, peak density at the center, receding sinusoidally toward the sidewalls). At 33 GHz, $\lambda = 0.358$ inch in WR 284 waveguide, which is 10 times oversize D = 2.1 inches (average of 2.840 inches and 1.420 inches). Using F = 2-inch parabolic reflector, the circle of confusion has a diameter d = 0.35 inch. Some input energy would therefore be lost due to phasing differences at the varactor located at the focal point, but the efficiency of a varactor multiplier should not suffer excessively at this point.

Another problem which remains is to launch a wave at the harmonic frequency via the focusing device back into the waveguide. This needs experimentation, since by applying theory alone (which could not possibly contain a rigid solution), prediction could be excessively far from practical truth.

Varactor array. --Another way of mounting a number of varactors in an oversized waveguide is to connect them in a prearranged pattern within a single cross-sectional plane as shown in Figure 40B. The optimum number of varactors to be used in such an array is very hard to determine presently due to lack of experimental evidence. If the point of view used in design and representation of passive oversized waveguide obstacles (like susceptance grids), where the obstacle is required to present a most uniform possible pattern over the entire cross-sectional area, were accepted in the active array case it would imply that "spheres of influence" exist for each individual diode. In other words, two diodes would absorb more energy than one, until the interference or overlap of the "spheres of influence" brings in the law of diminishing returns. Many diodes would be required to intercept a plane wave in a given open space; yet a single diode (or several in series at one point) is the most efficient way to absorb energy in one-moded waveguide (that is TE_{10} mode). Where, in between the two extremes, a 10 times oversized waveguide is best located can be determined by judicious experimental techniques.

Partially focused mount. --This type of mount, shown in Figure 40C, is a combination of the focused and array mounts. Possible advantages over the focused mount will be reduction of this "circle of confusion" effect and over the varactor array will be that fewer matched varactors are required. However, there are enough varactors to generate an acceptable wave pattern at the harmonic frequency within the oversized waveguide. The partial focusing technique is closely related to that used in the Goubau beam waveguide (reference 15) and to that used in laser resonators (reference 16).

Equivalent Circuit Representation

A varactor mount in an oversized waveguide frequency multiplier has to be considered from two vantage points: at the fundamental (input) frequency the mount has to be capable of absorbing the optimum amount of input energy, and at the harmonic (output) frequency the mount has to generate a proper field pattern to duplicate or at least resemble the "oversize-TE_{10}" or quasi-plane mode configuration.

Keeping this criterion in mind--and realizing that at least some experimental support is needed to derive a proper equivalent circuit--the thoughts given below should serve as theoretical introduction to equivalent circuit representation solution.

Taking each circuit individually, let us begin with the focused mount. It resembles--at the input frequency--a taper from an oversized to a regular waveguide mount. If some kind of directivity can be achieved for the generated energy at harmonic frequency, same type of equivalency would be valid at the output frequency. Any further predictions on higher mode excitation, suppression, or conversion at the harmonic frequencies would be purely guesswork.

One way of viewing the frequency multiplication process by a varactor array in an oversized waveguide is to assume that the action of the varactor array resembles digital sampler characteristics. It receives, converts, and regenerates a portion of the total pattern without altering the field distribution or energy density configuration within the waveguide. Figure 43 depicts this process. The incident and identical harmonic electric field distribution and the varactor pattern is represented as a vertically polarized electric dipole antenna array. Assumptions necessary for this rather simplified representation are quite restrictive. All the varactors in the array should be identical, which includes the input/output impedances and efficiency parameters at different input power levels. This is necessary to maintain the electric field

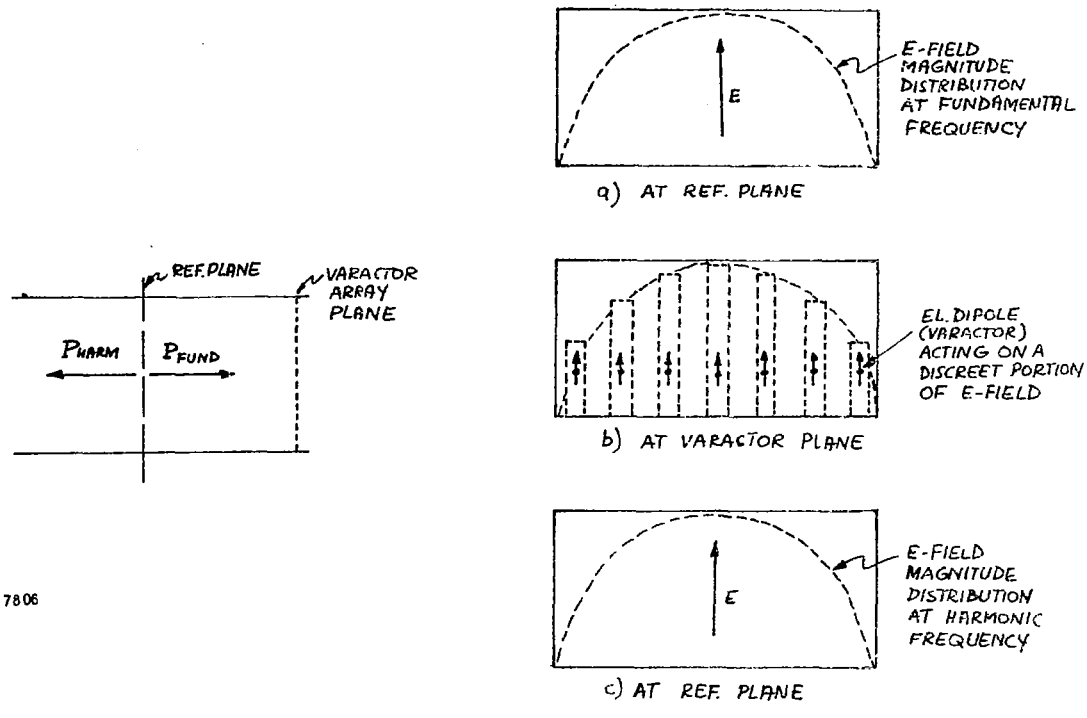

FIGURE 43. FREQUENCY MULTIPLICATION PROCESS BY AN ARRAY (DIGITAL SAMPLER MODEL)

distribution (relative magnitudes within the overall pattern) and the wavefront (relative phase) unaltered. Further restrictions on the varactor spacing (vertically and horizontally) may be required.

If this point of view were a true picture of the multiplication process, the varactor array would be the most appropriate of all the varactor mouting methods. The wiring for introduction of d.c. bias (or self-bias induced by series-connected parallel resistance and capacitance to ground) is not shown in the varactor array drawings. These may be introduced by vacuum-deposited thin-film techniques on the supporting plane on which the varactors would be mounted.

The partially focused type of varactor mount has an equivalent prototype that is a linear taper to some lower degree of oversizedness waveguide (for example, from 10 times to 4 times oversized) terminated by a reduced varactor array plate. This prototype is probably accurate enough in the theoretical analysis of this type of mount.

MEASUREMENTS

The experimental evaluation of quasi-optical oversized waveguide components requires special measurement techniques and equipment. Several measurement techniques and equipment related to frequency multiplier circuits have been studied. They are presented herein; preferred measurement approaches are indicated. The material covered includes

- Transitions
- Mode conversion
- VSWR measurements
- Frequency measurements
- Power measurements
- Loss or efficiency measurements

Transitions (Tapers)

Transitions are required from standard-sized to oversized (typically 10 times oversize) waveguide. This must be performed gradually if the single mode present in the standard guide is to be preserved. An overly abrupt transition generates higher modes that can cause large measurement errors.

It has been found that a linear taper (Figure 44A) from standard rectangular to 10 times oversized rectangular waveguide will maintain 99 percent of its power in the dominant TE_{10} mode if it is at least 50 wavelength in axial length. A curved taper (Figure 44B) with a cosine shape can achieve this degree of mode purity in 10 wavelengths. Furthermore, a curved taper that is as long as the linear taper can have a mode purity that is 10 to 20 db better. The only disadvantage of a curved taper is its fabrication expense. Most of AIL's work to date in oversized guide has been with

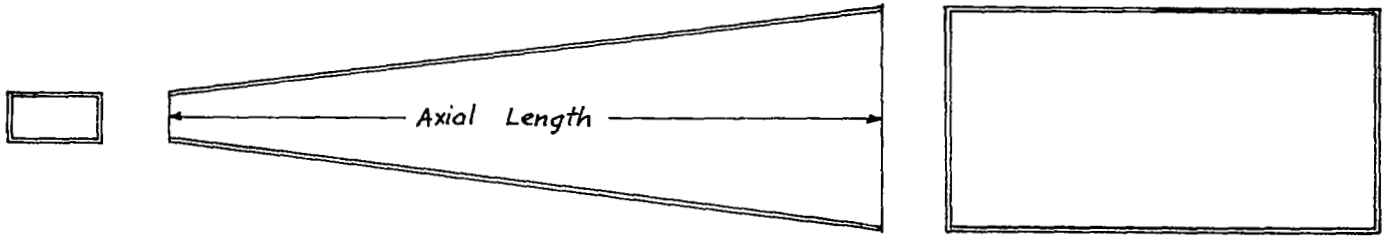

A. LINEAR TAPER

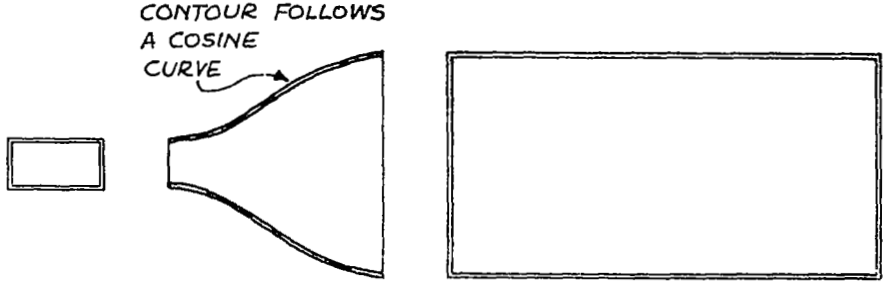

B. CURVED TAPER

FIGURE 44. TAPERED TRANSITIONS FROM STANDARD TO OVERSIZED WAVEGUIDE

linear tapers. A typical linear taper for 30 GHz work is about 3 feet long. We believe that a linear taper is adequate and is therefore recommended for future work.

Mode Conversion

The effect of higher modes can be troublesome in impedance or insertion loss measurements because it can cause internal resonances that can modify the desired properties of the component. This occurs when a component is being measured between a pair of tapers (as shown in Figure 45A). Any higher mode that is due to one or the other taper is trapped within the structure because the external standard-sized waveguide is below cutoff for all but the lowest mode. This trapped mode can, under certain conditions that are a function of frequency, component, and taper geometry, form a high Q resonance as indicated in Figure 45B. At resonance, it has a maximum effect on the properties of the network. It could easily cause errors of 1 db even in a good taper if care is not taken to suppress this effect.

We have found (reference 6) that the inclusion of a tee junction as shown in Figure 46 eliminates most of the mode trapping. This approach has been able to reduce mode trapping errors to 0.2 db when used to measure the insertion loss of a component placed between a pair of 3-foot linear tapers. Additional mode filtering in the form of horizontal resistive sheets (reference 17) may also help. In any event present methods for minimizing the trapped mode resonance effects are adequate. Measurement errors due to this effect should be less than 0.2 db.

VSWR Measurements

As in regular circuit development a means of measuring the input impedance of a component is desirable. Knowledge of its impedance will be helpful in designing matching networks. While slotted line measurements can be made in oversized guide, it requires a particularly loosely coupled

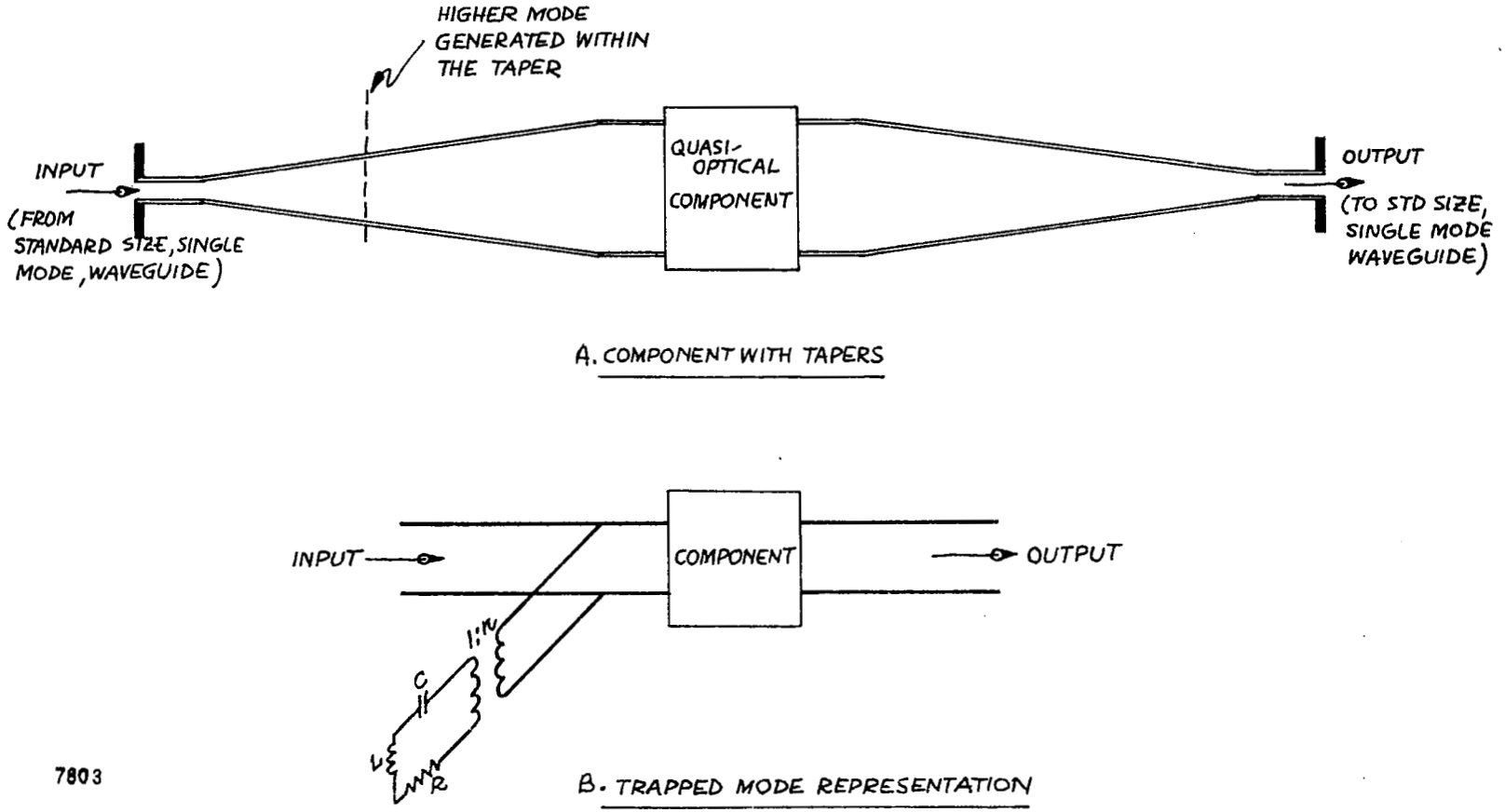

FIGURE 45. HIGHER MODE EFFECT ON INSERTION LOSS MEASUREMENT

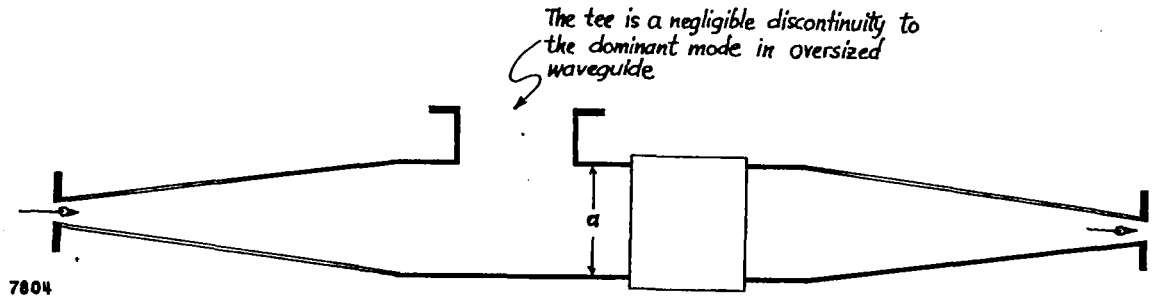

FIGURE 46. USE OF TEE JUNCTION AS A TRAPPED MODE FILTER

probe to avoid the launching of higher modes. Furthermore, at millimeter and submillimeter wavelengths it is difficult to locate the minimum and maximum positions.

Measurement of the reflection coefficient is more practical and is the recommended approach. Figure 47 shows an arrangement of two directional couplers that can monitor the incident and reflected power. With the aid of Figure 47, the magnitude of the reflection coefficient is:

$$|\Gamma| = \sqrt{\frac{P_2}{P_1}} \; \frac{k_1}{k_2 \sqrt{(1 - k_1^2)(1 - k_2^2)}} \tag{58}$$

where

P_1 and P_2 = power levels measured at the indicated ports of couplers 1 and 2

k_1 and k_2 = voltage coupling ratios for the directional couplers

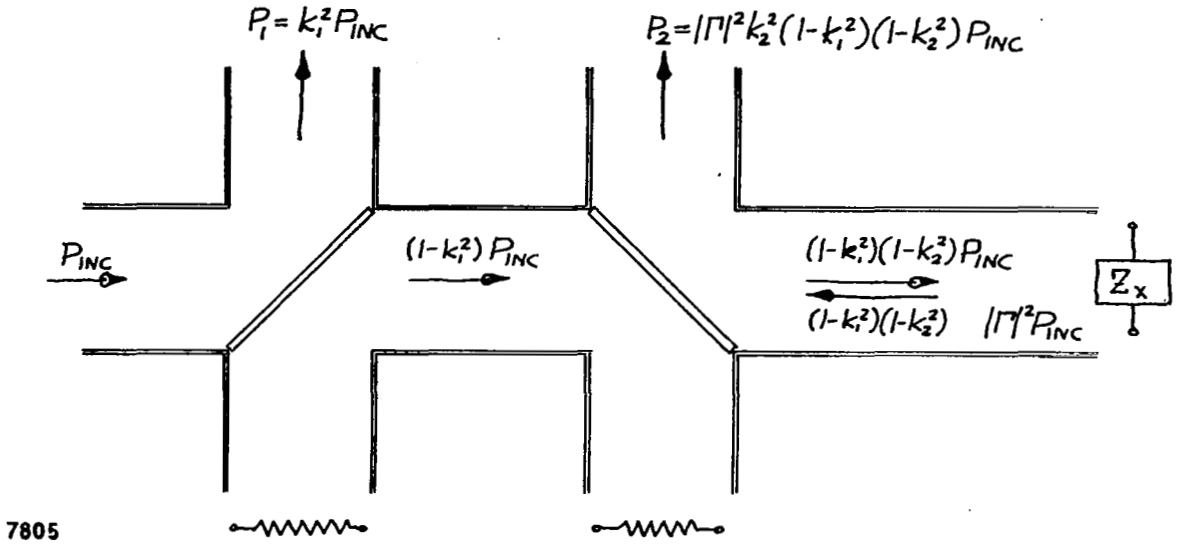

FIGURE 47. PREFERRED METHOD OF REFLECTION COEFFICIENT OR VSWR MEASUREMENT

For the case of two identical directional couplers, $k_1 = k_2 = k$ we have:

$$|\Gamma| = \sqrt{\frac{P_2}{P_1}} \; \frac{1}{1 - k^2} \tag{59}$$

The VSWR is determined from $|\Gamma|$ and is

$$r = \frac{1 + \sqrt{\frac{P_2}{P_1}} \left(\frac{k_1}{k_2 \sqrt{(1 - k_1^2)} \sqrt{(1 - k_2^2)}} \right)}{1 - \sqrt{\frac{P_2}{P_1}} \left(\frac{k_1}{k_2 \sqrt{(1 - k_1^2)} \sqrt{(1 - k_2^2)}} \right)} \tag{60}$$

Each directional coupler contains a dielectric slab placed diagonally across the center of a four-waveguide junction. The coupling ratio is a function of the slab thickness, dielectric constant, and frequency. It is equivalent to an n = 1 dielectric slab directional filter. The coupling values can thus be readily obtained from the directional filter curves given in Figure 6 of this report.

Frequency Measurements

Frequency measurements are important in multiplier circuit work to ascertain the level of undesired harmonics and to determine the existence of parametric oscillations.

The preferred method of measuring frequency in a quasi-optical circuit is a Michaelson interferometer technique as shown in Figure 48. A double-prism coupler is used to split the available power equally into two ports that are terminated in short circuits. One short is fixed and the other is movable. A detector, connected to port 4 through a taper, notes the amplitude of the power at port 4 as a function of the position of the moving short. This variation is similar to the standing wave pattern indicated in Figure 48. The separation between successive minima is $\lambda/2$ or $n\,\lambda/2$ between the n minima.

The sharpest minima are achieved when the coupler is set for 3 db, but it can operate reasonably well with couplings between 1 and 10 db. Thus, one can use a simpler fixed coupler, such as a single dielectric slab directional filter. Its coupling will vary as a function of frequency, but it can be kept within the 1 to 10 db range for the frequencies of interest (30 to 90 GHz).

Power Measurements

It is desirable to measure absolute power when evaluating the frequency multiplier efficiency because the multiplier efficiency is a function of the fundamental frequency power (or drive) level. The absolute power level generated at the desired harmonic is of obvious interest.

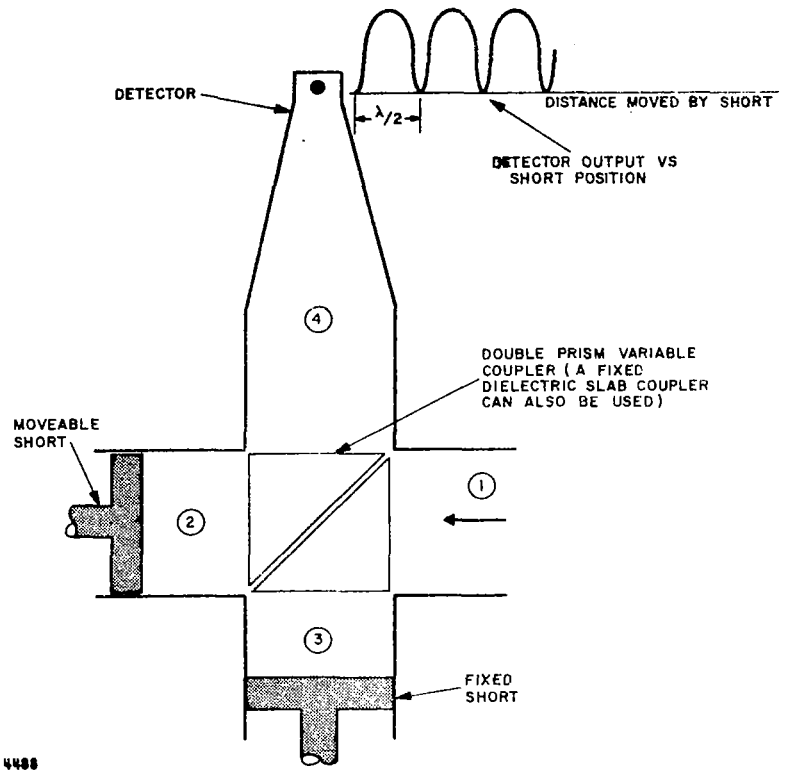

FIGURE 48. INTERFEROMETER FOR FREQUENCY MEASUREMENTS

The power meters designed for a single mode operation in a standard-size waveguide cannot be used in an oversized multimoded waveguide for several reasons: the power sensing element is mismatched and inefficient outside its waveguide housing unit frequency domain (hence, an S-band bolometer/thermistor mounted in an WR284 waveguide cannot be applied to measure power at 30 GHz in a 10-times oversized waveguide), and, if a power meter is used for its designated frequency domain, inevitably a taper will be required from the oversized to standard waveguide, which is equivalent of reconverting from the quasi-optical to the microwave technique.

For quasi-optical power measurements a distributed power sensing element is desired which intercepts the power over the entire cross-section of the waveguide, and which is uniformly efficient over a very wide range of frequencies. Such an element had been developed at AIL in a 4H mm waveguide (reference 18), and it has already been proposed to scale up this device to K_a-band waveguide for use in conjunction with the oversized S-band waveguide system. This would constitute an intermediate (microwave-quasi-optical) power measuring technique, since a taper is still required, but at both waveguide sizes the multimode condition exists. The measurement procedure does not deviate from the standard microwave technique.

Loss or Efficiency Measurements

Figure 49 shows three different setups that are useful in measuring component losses. A discussion of the features of each approach follows.

The first block diagram represents a standard insertion loss measurement. The change in output power expressed in db is noted when the component is removed. This is also a measurement of multiplier circuit efficiency provided the detector or power meter sensitivity is known at the harmonic as well as the fundamental frequency. This setup is also useful in measuring the power output by employing an absolute power meter as the detector. This type of measurement is straightforward and is applicable when loss accuracy of ± 0.3 db is adequate.

In some of our circuits it is of interest to measure losses with greater accuracy. One example is the measurement of the dissipative loss component of the two susceptance tuner. This loss may well be as little as 0.1 db. Low losses can be measured with reasonable accuracy by means of impedance circuit diagrams obtained for different positions of a moving short. Since only VSWR is convenient to ascertain in oversized waveguide, one cannot obtain this circle. It is possible however to obtain the minimum and maximum VSWR which can be used to approximately estimate the dissipative loss of a component.

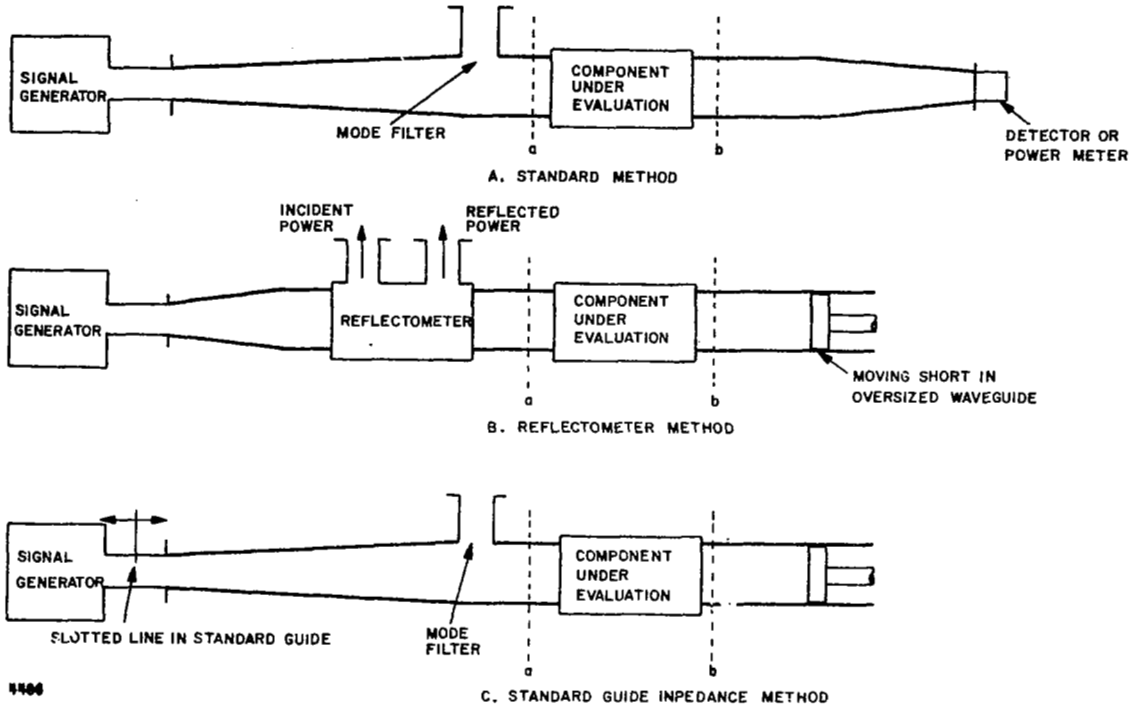

FIGURE 49. SOME LOSS MEASUREMENT METHODS

Figure 49C shows a setup for obtaining data for plotting the impedance circle from measurements taken with a standard guide slotted line. This measurement suffers from the uncertainty of the loss of the taper and mode filter.

It is however, possible to measure the loss of the taper and mode filter separately by obtaining their impedance circle with the component removed. In each case the intrinsic or dissipative loss is determined; the difference between the two intrinsic losses is the dissipative loss of the component.

These measurement techniques are recommended for use with actual multiplier circuits and should be tried on future programs in this area.

CONCLUSIONS

This study of quasi-optical circuits has indicated that millimeter varactor multipliers can be realized using these techniques. Directional filters can be designed using the theory and procedures described herein; agreement with experiment is within 1 to 2 db. The study of tuner circuits (to be used for varactor mount matching) has indicated that the type 3 (variable susceptance-variable position) tuner is preferred because it can match closest to the source and is capable of matching a wide range of impedances. All tuner circuits should have low (<0.25 db) dissipation loss. A number of ideas for predicting the equivalent circuits of varactor mounts (both focused and array) have been described. This must be considered as preliminary information that requires experimental substantiation. Some methods for measuring frequency, VSWR, power, and insertion loss have been described. The findings from this study have led to a number of suggestions for future work.

Future work in this area will now concentrate on the development of millimeter varactor doublers using quasi-optical circuit techniques. This will center about the following five tasks:

1. Development of suitable directional filters.
2. Development of tuners such as the variable - susceptance variable - position tuner; tuning at the fundamental and second harmonic frequencies. These are to be placed as close to the varactor mount as possible.
3. Evaluation of various varactor mounts such as focused, array, and partially focused.
4. Development of suitable measurement techniques for evaluation of varactor multipliers; this includes power, impedance and frequency measurements.

5. Assembly of the filter, tuner, and varactor mount circuits in such a manner that efficient (consistent with available varactor characteristics) operation results.

REFERENCES

1. Copeland, J.: A New Mode of Operation for Bulk Negative Resistance Oscillators. Proc. IEEE, Vol. 54, pp. 1479-1480, Oct. 1966.

2. DeLoach, B. C.: Verbally reported at the 1969 Solid State Circuits Conference, Philadelphia, Pa.

3. Swan, C. B.: High Power CW IMPATT Oscillator Techniques. 1967 NEREM Record, p. 22, IEEE Catalog No. F-85.

4. Liegey, P., et. al.: Development of 50°K Uncooled Parametric Amplifier. Report No. 2, Contract No. DA-28-043-AMC-02523(S), Prepared for the U.S. Army Satellite Communications Agency.

5. Penfield, P, and Rafuse, R. P.: Varactor Applications. The M.I.T. Press, Cambridge, Mass. 1962.

6. Taub, J. J., et. al.: Submillimeter Components Using Oversize Quasi-optical Waveguide: IEEE Transactions on Microwave Theory and Techniques, Vol. 11, Sept. 1963.

7. Taub, J. J. and Hindin, H. J.: Design of Quasioptical Components. Microwaves, Jan. 1964.

8. Taub, J. J. and Hindin, H. J.: Permittivity Measurements at Submillimeter Wavelengths. Rev. Sci. Instr., Sept. 1963.

9. Taub, J. J. and Cohen, J.: Quasioptical Filters for Millimeter and Submillimeter Wavelengths. Proc. IEEE, Vol. 54, pp. 647-656, April 1966.

10. Levy, R.: Tables of Element Values for the Distributed Low-Pass Prototype Filter. IEEE Trans., Vol. MTT-13, pp. 514-536, Sept. 1965.

11. Young, L.: Tables for Cascaded Homogeneous Quarter-Wave Transformers. IRE Trans., Vol. MTT-7, pp. 233-237, April 1959.

12. Corkum, R. W.: Isotropic Artificial Dielectric. Proc. IRE, Vol. 40, pp. 574-587, May 1952.

13. Morita, T. and Cohn, S.: Microwave Lens Matching by Simulated Quarter-Wave Transformer. IRE Trans., Vol. AP-3, pp. 33-39, Jan. 1956.

14. Marcuvitz, N.: Waveguide Handbook. Rad. Lab. Series Vol. 10, McGraw Hill, New York, New York, 1951.

15. Goubau, G. and Schwering, F.: On the Guided Propagation of Electromagnetic Wave Beams. IRE Trans. AP, Vol. 9, No. 3, May 1961.

16. Kogelnick, H. and Li, T.: Laser Beams and Resonators. Proc. IRE, Vol. 54, No. 10, Oct. 1966.

17. Butterweck, H. J.: Mode Filters for Oversized Rectangular Waveguides. IEEE Trans., Vol. MTT-16, pp. 274-281, May 1968.

18. Allen, C., Arams, F., and Bradley, C.: A Practical Detector for the Millimeter-To-Infrared Gap. IEEE Spectrum, p. 4A, Oct. 1968.

B1 Reed, J. and Wheeler, G. J.: A Method of Analysis of Symmetrical Four-Port Networks. IRE Trans. on Microwave Theory and Techniques, Vol. MTT-4, pp. 246-252, Oct. 1956.

B2 Ramo, S. and Whinnery, J.R.: Fields and Waves in Modern Radio, ch. 7, Wiley, New York, 1954.

B3 Storch, L.: The Transmission Matrix of N Alike Cascaded Networks. AIEE Trans. (Communication and Electronics), Vol. 73, pp. 616-618, Jan. 1955.

C1 Ulrich, G., et. al.: Tunable Submillimeter Interferometers of the Fabry-Perot Type. IEEE Trans. on Microwave Theory and Techniques, pp. 363-371, Sept. 1963.

APPENDIX A
CONTRACT WORK STATEMENT

Directional Filters

The theory of quasi-optical directional filters shall be reviewed and applied to directional filters compatible with multiplier requirements. Complete design equations and procedures shall be evolved. This will include curves and tables that will readily relate insertion loss, bandwidth, and rejection to the dielectric constant of materials used, dielectric slab thickness, and the number of dielectric slabs. These design procedures will be applicable as a minimum to doublers and triplers. Application to high order multipliers will also be considered. Experimental verification of these design procedures shall be provided.

Tuners

Quasi-optical tuners shall be theoretically studied. Insertion loss as a function of VSWR to be matched shall be computed. Design details necessary for construction of these devices including mechanical and electrical tolerances shall be presented.

Matching

A theoretical study of varactor matching and mounting techniques shall be commenced. This includes the derivation of equivalent circuits of focused and array mounts. The relative merits of various matching circuits shall be studied.

Measurement Techniques

Methods of obtaining accurate measurements of quasi-optical varactor multiplier circuits shall be analyzed and recommendations given for the

preferred approach. This shall include, as a minimum, impedance, absolute power, and frequency.

APPENDIX B

INSERTION LOSS VERSUS ELECTRICAL LENGTH OF ITERATED DIELECTRIC-SLAB FILTERS

This appendix derives the formulas for the insertion loss versus electrical length of the dielectric slab filter shown in Figure 5. From Reed and Wheeler (reference B1), the ABCD matrix for a transmission line of length d is:

$$\begin{bmatrix} \cos \phi & jZ \sin \phi \\ j\frac{1}{Z} \sin \phi & \cos \phi \end{bmatrix} \tag{B-1}$$

where

Z = characteristic impedance of transmission line,

$\phi = \beta d$ = electrical length of line,

β = propagation constant of transmission line.

From Ramo and Whinnery (reference B2), a slab of dielectric of thickness d is equivalent to a transmission line of length d. The characteristic impedance of the equivalent transmission line can be written in terms of the parameters of the dielectric.

The characteristic impedance of the equivalent transmission line for a linearly polarized wave having its electric field perpendicular to its plane of incidence on a dielectric slab, with the angle of incidence being θ_i is:

$$Z_a = \frac{120\pi \sec \theta_i}{\sqrt{\epsilon_r}} . \tag{B-2}$$

The dielectric slabs are assumed to be infinite in extent.

Using equation B-2, the normalized impedance Z of the other dielectric section to that of the air is:

$$Z = \frac{Z_\epsilon}{Z_0} = \frac{\cos \theta_i}{\sqrt{\epsilon_r} \cos \theta_\epsilon} \tag{B-3}$$

Using equations B-1 and B-3, the ABCD matrix of the typical iteration is:

$$\begin{bmatrix} \cos \phi_\epsilon & jZ \sin \phi_\epsilon \\ j \frac{1}{Z} \sin \phi_\epsilon & \cos \phi_\epsilon \end{bmatrix} \begin{bmatrix} \cos \phi_0 & j \sin \phi_0 \\ j \sin \phi_0 & \cos \phi_0 \end{bmatrix}$$

$$= \begin{bmatrix} \left(\cos \phi_\epsilon \cos \phi_0 \right. & \left(j \sin \phi_0 \cos \phi_\epsilon + \right. \\ \left. -Z \sin \phi_\epsilon \sin \phi_0\right) & \left. jZ \sin \phi_\epsilon \cos \phi_0\right) \\ \left(j \frac{1}{Z} \sin \phi_\epsilon \cos \phi_0 \right. & \left(-\frac{1}{Z} \sin \phi_\epsilon \sin \phi_0 + \right. \\ \left. +j \cos \phi_\epsilon \sin \phi_0\right) & \left. \cos \phi_\epsilon \cos \phi_0 \right) \end{bmatrix} \tag{B-4}$$

If $\phi_\epsilon = \phi_0 = \phi$, the ABCD matrix of the iteration, equation B-4 becomes:

$$\begin{bmatrix} \cos^2 \phi - Z \sin^2 \phi & \frac{j}{2} \sin (2\phi) \left(1 + Z\right) \\ \frac{j}{2} \sin (2\phi) \left(1 + \frac{1}{Z}\right) & \cos^2 \phi - \frac{1}{Z} \sin^2 \phi \end{bmatrix} \tag{B-5}$$

$$= \begin{bmatrix} A_{\epsilon 0} & B_{\epsilon 0} \\ C_{\epsilon 0} & D_{\epsilon 0} \end{bmatrix} = M$$

To find the ABCD matrix (M^n) of n iterations (reference B3):

$$M^n = \begin{bmatrix} P_n A_{\epsilon 0} - P_{n-1} & P_n B_{\epsilon 0} \\ P_n C_{\epsilon 0} & P_n D_{\epsilon 0} - P_{n-1} \end{bmatrix} \tag{B-6}$$

where P_n is a polynominal of the second kind, and:

$$\begin{aligned} P_0 &= 0 \\ P_1 &= 1 \\ P_2 &= Y \\ P_n &= Y P_{n-1} - P_{n-2} \end{aligned} \tag{B-7}$$

where

$$Y = A_{\epsilon 0} + D_{\epsilon 0}$$

Now from Reed and Wheeler, the insertion loss (I.L.) in decibels is:

$$\text{I.L.} = 10 \log \frac{|A + B + C + D|^2}{4} \tag{B-8}$$

Using equation B-6

$$|A + B + C + D|^2 = \left[(P_n Y - 2P_{n-1})^2 + P_n 2 \left(\frac{B_{\epsilon 0}}{j} + \frac{C_{\epsilon 0}}{j} \right)^2 \right] \tag{B-9}$$

Therefore, substituting equation B-9 into B-8, the insertion loss as a function of electrical length is obtained for the general lossless case:

$$\text{I.L.} = 10 \log \frac{\left| P_n^2 Y^2 + 4P_{n-1}^2 \quad 4P_n P_{n-1} Y + P_n^2 X^2 \right|}{4} \text{ db} \qquad \text{(B-10)}$$

where

$$Y = 2 \cos^2 \phi - \left[\sin^2 \phi \right] \left[Z + \frac{1}{Z} \right]$$

$$X = \left[\frac{1}{2} \sin 2\phi \right] \left[2 + Z + \frac{1}{Z} \right]$$

$$Z = \frac{\cos \theta_i}{\sqrt{\epsilon_r} \cos \theta_\epsilon} = \frac{\cos \theta_i}{(\epsilon_r - \sin^2 \theta_i)^{1/2}}$$

since, by Snell's law,

$$\sin \theta_\epsilon = \frac{\sin \theta_i}{\sqrt{\epsilon_r}}$$

where ϕ is the electrical length of each slab, and is $2\pi/\lambda_{air} \cos \theta_i d_0$ for the air slab and $2\pi/\lambda_{air} \sqrt{\epsilon_r} \cos \theta_\epsilon d_\epsilon$ for the other dielectric slab.

APPENDIX C
QUASI-OPTICAL STRIP GRATING CIRCUIT

If the electric field is incident as shown in Figure 27A and the metal strips are in an air dielectric, we have an inductive grating; its equivalent circuit (normalized to the intrinsic impedance of free space) is shown in Figure 27B. Approximate formulas for x and r are given in reference C1; when it is assumed that $\gamma << \lambda$, the formulas are:

$$x = w\,\gamma/\lambda \text{ and } r = \frac{s\,\gamma\,\pi}{u\lambda} \qquad \text{(C-1)}$$

where

$w = \ell n \csc(\pi\, a/\gamma)$

s = Skin depth

u = Strip perimeter = $4a + 2t \approx 4a$ for $a >> t$

a = Strip width

γ = Center to center spacing of strips

It is also convenient to define a Q factor equal to x/r. For a copper grating, $s = 6.62\, f^{-1/2}$ hence

$$Q = \frac{(4a + 2t)\,\ell n \csc(\pi\, a/\gamma)}{6.62\,\pi\, f^{-1/2}} \qquad \text{(C-2)}$$

where a, g, and t are expressed in cm. For our tuner analysis we have chosen b = 2 or x = 1/2. For this case Q simplifies to

$$Q = \frac{(2a + t)\,\lambda}{6.62\,\pi\, f^{-1/2}} \qquad \text{(C-3)}$$

For $\gamma/\lambda = 1/2$ and $f = 3 \times 10^{10}$ Hz, we have for $b = 2$ and $t << 2a$, the condition that $a/\gamma = 1/7$. Substituting these values yields a $Q = 2500$. The normalized shunt resistance is Q or 1250; the theoretical normalized conductance is 8×10^{-4}. In practice the Q factor will be lower due to surface roughness and some diffraction losses; a Q of 1500 is a realistic value.

APPENDIX D

MATCHING BY TWO VARIABLE SUSCEPTANCES SEPARATED BY A FIXED LENGTH

Consider the equivalent circuit of Figure 29. Two variable susceptances b_1 and b_2 are separated by a line of electrical length θ; we wish to determine the range of load admittances, $Y_L = g + jb$, that can be matched. The match condition is to force Y_{aa} (the admittance looking to the left of aa) to equal the conjugate of Y_L.

Using transmission line theory one obtains

$$Y_{aa} = jb_2 + \frac{1 - j(1 - b_1)}{(1 + b_1) - j} = g_{aa} + jb_{aa} \qquad \text{(D-1)}$$

or

$$g_{aa} = \frac{2}{2 + 2b_1 + b_1^2} \qquad \text{(D-2)}$$

and

$$b_{aa} = b_2 + \frac{b_1^2}{2 + 2b_1 + b_1^2} \qquad \text{(D-3)}$$

For a match, $g_{aa} = g = 1/r$ and $b_{aa} = -b$. The first condition is satisfied by

$$b_1^2 + 2b + 2 = 2r = 2/g \tag{D-4}$$

or

$$b_1 = -1 \pm \sqrt{2/g - 1}$$

For realizability, b_1 must be a real quantity. This restricts r to values of 1/2 or greater, or g must be 2 or less. Examination of b_{aa} shows that any real value can be obtained because b_2 can be arbitrarily set.

NASA-Langley, 1969 —— 10 CR-1453